Lyapunov-based Guidance of Underwater Autonomous Vehicles for Real Time Pollutant Source Localization

by

Gabriel Alexis Torres Arosemena

A Thesis

Submitted to the Faculty of the

of the

WORCESTER POLYTECHNIC INSTITUTE

In partial fulfillment of the requirements for the

Degree of Master of Science

in

Mechanical Engineering by

June 28 2021

APPROVED:

Dr. Michael A. Demetriou, Advisor

Dr. David J. Olinger, Committee Member

Dr. John J. Blandino, Committee Member

Dr. Pratap M. Rao, Graduate Committee Representative

Abstract

This work presents a guidance strategy for an autonomous underwater vehicle to localize, in real-time, an underwater oil plume released in the environment as a Gaussian pulse. For this purpose, it is necessary to select a vehicle design to meet the mission requirements. Therefore, after considering multiple vehicles designs, the OUTLAND-1000, due to its specific configuration, has shown to be a suitable fit for the main purpose of this work. Consequently, a reliable dynamical model is developed from physical principles to include the effects of inertial, hydrostatic, hydrodynamic, and control forces. In addition, as a case study, a synthetic oil spill governed by the advection-diffusion partial differential equation is proposed to describe the dispersion of oil in shallow water. Thus, numerical and analytical schemes are studied to generate a concentration spectrum over a given domain. Regarding guidance and control, reference commands are defined as functions of the localized concentration values and their respective localized gradients. Therefore, the problem is simplified to trajectory tracking problem so that a Lyapunov-based control law capable of dealing with the system nonlinearities and performance requirements is designed. The control method is numerically validated through various source trajectories using existing UAUV specifications while accessing local concentration values and gradients throughout a previously measured pollutant concentration field.

Acknowledgements

First of all, I would like to express my deep and sincere gratitude to my research supervisor, professor Michael A. Demetriou, for allowing me to do research and providing invaluable guidance throughout my master's program. His dynamism, vision, sincerity, patience, and motivation have deeply inspired me. In addition, I am incredibly grateful to the Fulbright-LASPAU program for providing me the unique and life-changing opportunity of coming to study in the United States and make my forever dream come true. Furthermore, I would like to express my gratitude to all my evaluation committee members, professors Pratap M. Rao, John J. Blandino, and David J. Olinger, for being part of this process and to all WPI community, faculty, students, and staff for always making me feel at home.

At this point, I would not find the words to thank my family enough, especially my parents Ivette and Marcelino. I have reserved this section of this work for you and your lifetime hard work and sacrifice that allowed me to fulfill all the dreams I ever had and some that I had never thought about. Thank you for all your constant support, prayers, advice, and best wishes, but I especially want to thank you for always believing in me even when I did not believe in myself. I will eternally be grateful to God for giving me the most wonderful and supportive parents that a son could ever want. Additionally, in this section, I would like to mention my grandmother Guillermina and my second mother, Fulvia; thanks for all your prayers and your forever unconditional love. Fulvia, I send you the biggest hug up to heaven, where I know you are always taking care of me.

Finally, I wish to thank my best friend in the world, who has been there in the good and bad moments, the one who has stood there by me, willing to face any

life challenge, my beautiful wife, Claudia. Getting this work done and my master's would have never been possible without your emotional and intellectual support. I am thankful to the life that let us collide in this crazy world, so in this work, I would like to immortalize all the love we have shared so far and the love we will be giving to each other in the upcoming years by saying that I love you and always going to love you for rest of my days and beyond.

Contents

1 Introduction **1**

1.1 Objectives 2

1.2 Background 2

1.2.1 Phoenix and NPS ARIES 3

1.2.2 The C-SCOUT AUV 4

1.2.3 HippoCampus UAV 5

1.2.4 OUTLAND-1000-ROV 6

2 Mathematical Model for Mean Concentration of Species in Turbulence **8**

2.1 General Review on Oil Spills 8

2.2 Advection and turbulent diffusion 9

2.3 Governing Equations of Mean Concentration of Mixing in Rivers Turbulent Diffusion and Dispersion 10

2.4 Problem formulation 13

2.4.1 Gaussian Pulse Analytical Solution 14

2.5 Numerical Schemes for the Solution of the Advection–Diffusion Equation 16

2.5.1 The Forward-Time Centered-Space Scheme 16

2.5.2 The forward-Time Backward-Space Centered-Space Scheme . 18
2.5.3 The Lax–Wendroff Scheme 18
2.5.4 Numerical Models Validation 20

3 UAUV Dynamics and Guidance 24

3.1 Coordinate system 25
3.2 UAUV's Kinematics 26
3.3 UAUV's Dynamics 28
3.3.1 Newton-Euler Equations of Motion (General form) 29
3.3.2 Added Mass and Inertia 30
3.3.3 Hydrodynamic Damping 33
3.3.4 Hydrostatic Forces and Moments 35
3.4 OUTLAND-1000 Dynamics 37
3.4.1 4DOF Reduced Kinematics 39
3.4.2 4DOF Reduced Dynamics 39
3.4.3 Uncertain Dynamics Characterization 40
3.4.4 OUTLAND 1000 Input Dynamics 44

4 Guidance and Control 47

4.1 System Stability of Underwater Vehicles 47
4.1.1 Controls-Fixed Stability 48
4.1.2 Controls-Free Stability 49
4.2 State Feedback Stabilization Based on Backstepping 51
4.3 Hierarchical Backstepping Control Applied to OUTLAND-1000 . . . 53
4.4 Backstepping Trajectory Tracking (Numerical Results) 57
4.4.1 Circular Trajectory Tracking 57
4.4.2 Spiral Trajectory Tracking 64

4.4.3 Backstepping Control Simulation results 70
4.5 Integrated Backstepping and Sliding Mode Tracking Control 71
4.5.1 Sliding Mode Control 72
4.5.2 Bio-inspired Neurodynamics Backstepping Control Model 75
4.5.3 Adaptive Sliding-Mode Control 77
4.5.4 Bio-Inspired Integrated Sliding Mode Control Trajectory Tracking (Numerical Results) 79
4.6 UAUV Source tracking and Guidance 86
4.6.1 Bio-Inspired Integrated Sliding Mode Control for Source Tracking (Numerical Results) 88

5 Conclusions **101**

A **103**

A.1 Dynamics and Control Simulation Parameters 103
A.1.1 OUTLAND-1000 Physical Parameters 103
A.1.2 Circular Trajectory Tracking Control Parameters (Backstepping) 104
A.1.3 Spiral Trajectory Tracking Control Parameters (Backstepping) 104
A.1.4 Circular Trajectory Tracking Simulation Parameters (BIISM control) 104
A.1.5 Concentration Tracking Simulation Parameters (BIISM control) 105

B Control Diagrams **106**

B.1 Hierarchical Backstepping Control 106
B.2 Integrated Bio-Inspired Backstepping and Sliding Mode Tracking Control 107

B.3 BIISM Applied to Pollutant Source Tracking and Localization 107

List of Figures

1.1 NPS-ARIES ©Naval Postgraduate School at Monterrey, California. 3

1.2 C-SCOUT AUV ©Memorial University of Newfoundland. 5

1.3 HippoCampus ©E. Solowjow, D. A. Duecker, A. Hackbarth, V. Rausch, A. R. Geist, and T. Johannink, "HippoCampus - Project", 2018. . . . 6

1.4 OUTLAND-1000 side top view ©2021 Outland Technology, Inc. . . . 7

1.5 OUTLAND-1000 side front side view ©2021 Outland Technology, Inc. 7

2.1 Solute Control Volume 10

2.2 Advection-Diffusion PDE Guassian pulse Exact Solution Horizontal Velocity Field. 15

2.3 Advection-Diffusion PDE Guassian pulse Exact Solution 2-D Velocity Field. 15

2.4 Advection-Diffusion PDE Guassian pulse Aproximated Solution Horizontal Velocity Field. 21

2.5 Root Mean Square Error Horizontal Velocity Field. 21

2.6 Advection-Diffusion PDE Guassian pulse Aproximated Solution 2-Dimensional Velocity Field. 22

2.7 Root Mean Square Error 2-Dimensional Velocity Field. 22

3.1 State Variables Description. 24

3.2 Frames and elementary vehicle's motion [83]. 25
3.3 Hydrostatic stability planes [84]. 38
3.4 Thrusters configuration taken from [34] ©2021 Outland Technology, Inc. 45

4.1 Circular helix trajectory-tracking. 58
4.2 Circular plane trajectory-tracking. 58
4.3 Tracking responses of reference positions for circular trajectory. . . . 59
4.4 Tracking errors with disturbances for circular tracking. 60
4.5 Tracking responses of virtual reference velocities for circular tracking. 61
4.6 Tracking errors of virtual reference velocities for circular trajectory. . 62
4.7 Control signals: Total surge thrust τ_x, sway thrust τ_y, yaw torque τ_N, heave thrust τ_z for circular tracking. 63
4.8 Path Trajectory-Tracking for spiral trajectory. 64
4.9 Tracking responses of reference positions for spiral trajectory. 65
4.10 Tracking errors with disturbances for spiral tracking. 66
4.11 Tracking responses of virtual reference velocities for spiral trajectory. 67
4.12 Tracking responses of virtual reference velocities for spiral trajectory. 68
4.13 Control signals: Total surge thrust τ_x, sway thrust τ_y, yaw torque τ_N, heave thrust τ_z for spiral tracking. 69
4.14 Circular helix trajectory-tracking BIISM. 80
4.15 Circular plane trajectory-tracking BIISM. 80
4.16 Tracking responses of reference positions for circular trajectory BIISM. 81
4.17 Tracking errors with disturbances for circular tracking BIISM. 82
4.18 Tracking responses of virtual reference velocities for circular tracking BIISM. 83

4.19 Tracking errors of virtual reference velocities for circular trajectory BIISM. 84
4.20 Control signals: Total surge thrust τ_x, sway thrust τ_y, yaw torque τ_N, heave thrust τ_z for circular tracking BIISM. 85
4.21 Horizontal Concentration trajectory-tracking BIISM. 89
4.22 Tracking responses of reference positions for horizontal concentration BIISM. 90
4.23 Tracking errors with disturbances for horizontal concentration tracking BIISM. 91
4.24 Tracking responses of virtual reference velocities for horizontal concentration tracking BIISM. 92
4.25 Tracking errors of virtual reference velocities for horizontal concentration tracking BIISM. 93
4.26 Control signals: Total surge thrust τ_x, sway thrust τ_y, yaw torque τ_N, heave thrust τ_z for horizontal concentration BIISM. 94
4.27 2-Dimensional Concentration trajectory-tracking BIISM. 95
4.28 Tracking responses of reference positions for 2-Dimensional concentration BIISM. 96
4.29 Tracking errors with disturbances for 2-Dimensional concentration tracking BIISM. 97
4.30 Tracking responses of virtual reference velocities for 2-Dimensional concentration tracking BIISM. 98
4.31 Tracking errors of virtual reference velocities for 2-Dimensional concentration tracking BIISM. 99
4.32 Control signals: Total surge thrust τ_x, sway thrust τ_y, yaw torque τ_N, heave thrust τ_z for 2-Dimensional concentration BIISM. 100

B.1 Backstepping Trajectory Control. 106
B.2 BIISM Trajectory Control. 107
B.3 BIISM Pollutant Source Tracking and Localization Control. 107

List of Tables

3.1 Nomenclature for marine vehicle's motion [1]. 26

A.1 OUTLAND-1000 Inertia and Hydrodynamic Parameters 103

A.2 Circular Trajectory Tracking Control Parameters (Backstepping). . . 104

A.3 Circular Trajectory Tracking Control Parameters(Backstepping). . . . 104

A.4 Circular Trajectory Tracking Simulation Parameters (BIISM control). 104

A.5 Horizontal Concentration Tracking Simulation Parameters(BIISM control). 105

A.6 2-Dimensional Concentration Tracking Simulation Parameters(BIISM control). 105

Chapter 1

Introduction

Since the ancient Greek era, underwater vehicles have been widely explored, passing through Roberto Valturio, and even Leonardo Da Vinci seemed to have worked on a deadly underwater military vessel [1]. Eventually, these ideas arrived at one of the most intimidating weapons of the whole time, the submarine. As T.I Fossen defines in [4] the submarine as "any naval vessel that is capable of propelling itself beneath the water as well as on the water's surface". However, submarines carry a significant limitation; these vessels are human-crewed operated vehicles. There have been several reports that describe a series of events that involve manned underwater vehicles, unfortunately ending up in tragedy and millions in losses of load and equipment [1]. Remotely operated and autonomous underwater vehicles (ROVs and UAUVs), on the other hand, have shown to be able to achieve the same mission goals as manned vehicles and even more efficiently. These vehicles are currently being used in missions such as ocean and pipeline surveys, the rescue of manned underwater vessels, and off-shore structure maintenance, among large set applications that can be mentioned.

1.1 Objectives

The objectives of this work are:

- To develop a reliable dynamical model that appropriately describes the motion of an autonomous underwater vehicle.
- To generate a robust control law based on hierarchical Lyapunov structures for trajectory tracking and guidance.
- To apply numerical and analytical schemes to generate a realistic unsteady pollutant dispersion in a 2-dimensional domain.
- To localize and track in real-time the source of a pollutant released in marine environments.

1.2 Background

Autonomous underwater vehicles are classified into remotely operated vehicles (ROVs) and unmanned autonomous underwater vehicles (UAUVs). The ROV is an underwater vehicle whose power and control action is given throughout a cable, transmitting information from the user to the vehicle. In contrast, the UAUV relies entirely on the inboard power and control system [1]. This work is exclusively dedicated to deal with the modeling, control, and performance of UAUVs.

A significant amount of research has been done within the field of autonomous underwater vehicles. In general, these vehicles attempt to have a torpedo-shaped body acted by thrusters and hydrodynamic fins (control surface). Nonetheless, this classical configuration could vary depending on design and modeling simplicity, mission and task requirements, or simply the control strategy that could be studying at

the time. Therefore, in sections 1.1,1.2, and 1.3, some current UAUVs are described and studied to make a suitable selection of geometry and actuation configuration that yields the best fit for the proposes of this work.

1.2.1 Phoenix and NPS ARIES

Phoenix is an underwater robot built for student research at the Postgraduate Naval (NPS) School Monterrey, California. Indeed, this vehicle has a torpedo-shaped body but with a rectangular cross-section that simplifies its dynamic and hydrodynamics analysis. In addition, The Phoenix counts with a set of multiple propellers in charge of giving the right amount of thrust to move forward and backward depending on what is required. Moreover, hydrodynamic control surfaces (Fins) are placed on strategic spots around the structure of the vessel to control the six degrees of freedom of the vehicle [11]. Furthermore, the NPS-ARIES, which is the next generation of the Phoenix UAUV developed by the Naval Postgraduate School at Monterrey, California, introduces the implementation of new computer architecture and extended Kalman filter to make the vehicle capable of operating as a network server using acoustic, and radio communication links [12].

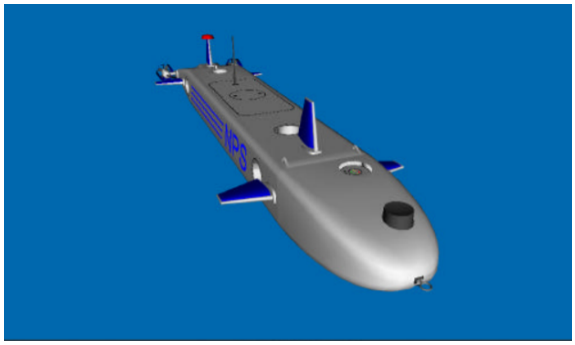

Figure 1.1: NPS-ARIES ©Naval Postgraduate School at Monterrey, California.

1.2.2 The C-SCOUT AUV

Canadian Self-Contained Off-the-shelf Underwater Testbed (C-SCOUT) as it is described in [8] is a UAUV that follows the typical design and actuation as it is described in 1.2. Nonetheless, this particular vessel is designed to be assembled by interchangeable modules as it is shown in [8] and [14]. The versatility of this construction allows the vehicle to reach a good performance in multiple missions since it could be adapted to the mission requirements. In the light of this building approach, two main configurations can be presented regarding the actuation mode, which are the baseline configuration (BC) and the fully actuated configuration (FAC).

The baseline configuration shares with Phoenix and ARIES described in 1.2.1 with the implementation of rear control module based on two horizontal control surfaces coupled with two independent actuators to control their motion.

On the other hand, the FAC adds to the BC a second control module paced at the vehicle's front. In addition, two propulsive modules are also placed through the vessel's body. Each module has two horizontal and one vertical thruster to improve the maneuverability of the vehicle and to make the vehicle capable of hovering in a cross flow [8].

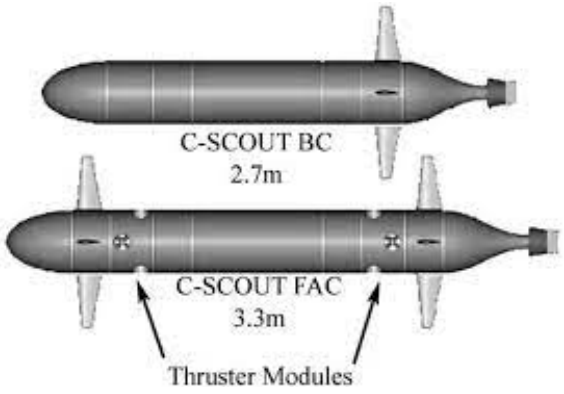

Figure 1.2: C-SCOUT AUV ©Memorial University of Newfoundland.

1.2.3 HippoCampus UAV

The Hippocampus UAV finds its inspiration in the sea animal with the same Greek name, the hippo-campus, better known as a seahorse. In addition, to its animal conception, the Hippocampus UAUV is also an attempt to replicate the performance of one of the most popular air autonomous vehicles, the quadrotor aircraft. Quadrotors are well studied autonomous aircraft that able to achieve complicated tasks and maneuvers by themselves. Likewise, the Hippocampus is capable of impressive acrobatic maneuvers and other autonomous operations due its onboard processing system [7] [10] [15] [16]. Regarding its configuration, the Hippocampus is a streamlined-shaped body with a circular cross area that has coupled four horizontal thrusters disposed in crossed shape at the vehicle's rear. This configuration allows that the turning ratio to be independent of the surge motion providing an advantage over a typical UAUV that is controlled by plane surfaces and propellers §1.2.1,§1.2.2. However, it turns out the fact that this vehicle is highly more energy inefficient than the classical ones due to the number of required motors; therefore, due to its high energy requirements and for some other structural limitations, it is recommended to keep the dimensional and hydrostatics parameters of this vehicle within the range defined for micro UAUV.

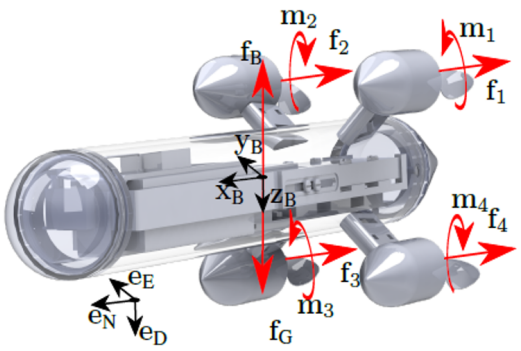

Figure 1.3: HippoCampus ©E. Solowjow, D. A. Duecker, A. Hackbarth, V. Rausch, A. R. Geist, and T. Johannink, "HippoCampus - Project", 2018.

1.2.4 OUTLAND-1000-ROV

OUTLAND-1000 is a four-thruster model manufactured by Outland Technology, capable of reaching 300 m. The Outland ROV 1000 has a two-camera video system. The properties of these cameras are critical for obtaining high-quality photographs for the project's goals. The video signal from the cameras is transmitted through a wire to the Outland ROV 1000's control system for recording purposes [81], [82]. In addition, even though it is conceived as a remotely operated vehicle (ROV), the proposes of this work OUTLAND-1000 is considered a UAUV, so a similar control architecture as the HippoCampus has to be implemented on this particular robot. Base on objectives and modeling simplicity, The OUTLAND-1000 UAUV is the selected UAUV due to its convenient design. Further comments on OUTLAND-1000 configuration and design will be made in Chapter 3.

Figure 1.4: OUTLAND-1000 side top view ©2021 Outland Technology, Inc.

Figure 1.5: OUTLAND-1000 side front side view ©2021 Outland Technology, Inc.

Chapter 2

Mathematical Model for Mean Concentration of Species in Turbulence

2.1 General Review on Oil Spills

Sea oil slicks devastatingly affect marine environments and human culture in the encompassing waterfront regions. The 2010 Deep Water Horizon spill in the Gulf of Mexico endured 87 days and is assessed to have delivered more than 3 million barrels of oil. It affected more than 1,600 miles of coastline, slaughtered more than 8000 marine creatures/seabirds, and caused direct financial misfortune from fishing and visit enterprises assessed at a considerable number of dollars. Likewise, the effects on the long haul general well-being and personal satisfaction of millions of individuals are as yet unclear.

The spreading of oil spilled into the sea is a measure that depends mainly on the flow, wind, temperature, and synthetic structure of the oil and seawater. In addition, Oil spills are genuine natural dangers that regularly show long-term impacts. To control the harms brought about by oil contamination, it is expected that real-time predictions to give an ongoing forecast of the transport and destiny of the spill.

2.2 Advection and turbulent diffusion

The primary processes involved with oil transport on the water surface are the shifts in weather conditions and turbulent dispersion. The shift in weather conditions is basically because of the breeze, surface current, and waves. In this study, a two-dimensional two-phase numerical model is developed to predict the transport and fate of oil slicks in seawater environments.

This work considers a Fickian model, which states that the flux of solute mass, that is, the mass of a solute crossing a unit area per unit time in a given direction, is proportional to the solute concentration gradient in that direction [48]. This generally can be expressed through the total rate of mass transport given by the addition of an advective flux and a diffusive flux.

$$q = [\beta_x, \beta_y, \beta_z]^T C + \left[\alpha_x \frac{\partial C}{\partial x}, \alpha_y \frac{\partial C}{\partial y}, \alpha_z \frac{\partial C}{\partial z}\right]^T \tag{2.1}$$

This equation is referred to as the Advection-Diffusion equation, where α_i and β_i for $i = x, y, z$ are correspondingly the directional diffusivities and flow velocity components defined in Cartesian reference frame.

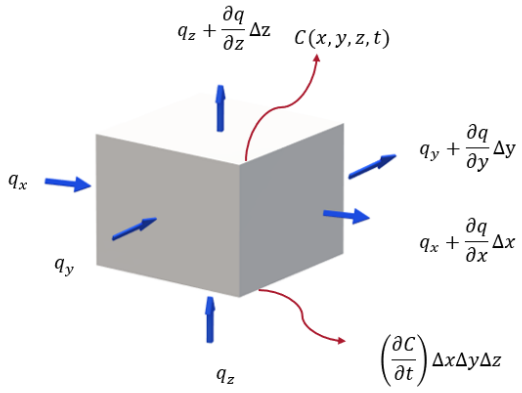

Figure 2.1: Solute Control Volume

Therefore, in order to satisfy the continuity principle the rate of change in concentration per unit volume inside the control volume is given by the following transport equation:

$$\frac{\partial C}{\partial t} + \beta_x \frac{\partial C}{\partial x} + \beta_y \frac{\partial C}{\partial y} + \beta_z \frac{\partial C}{\partial z} = \alpha_x \frac{\partial^2 C}{\partial x^2} + \alpha_y \frac{\partial^2 C}{\partial y^2} + \alpha_z \frac{\partial^2 C}{\partial z^2} \tag{2.2}$$

2.3 Governing Equations of Mean Concentration of Mixing in Rivers Turbulent Diffusion and Dispersion

In the introductory part of this chapter, the advection-diffusion PDE has been defined. However, it is vital to consider that such a formulation only deals with molecular diffusion under laminar flows regimes. Therefore, an analogous Fickian turbulent mixing model is described in [47], and [48] in order to get in count the effects of turbulent components.

Following [46], [47], [48], [49] we present underneath a process model which is addressed by the 3D advection-diffusion under turbulent operation conditions. Think about a wellspring of oil discharge, which is moving along an obscure direction inside a spatial zone defined by $\Omega : x \in [0, Lx], y \in [0, Ly], z \in [0, Lz]$ subject to turbulent flow velocity components U, V, W projected respectively on the x, y, z directions.

In order to study turbulence, let us consider a representation of the fluid velocity consisting of the summation of deterministic and stochastic components as follows [47], [49] :

$$\beta_x = U = \overline{U} + U', \beta_y = V = \overline{V} + V', \beta_z = W = \overline{W} + W' \tag{2.3}$$

Then for convenience proposes:

$$U_i = [U.V, W]^T = \bar{U}_i + U_i' \tag{2.4}$$

This approach is known as the Reynolds decomposition. To derive an advective diffusion condition for disturbance, we substitute the Reynolds decomposition into the typical advection-diffusion PDE and examine the outcomes. However, Before we can do that, we need a Reynolds deterioration similarity for the concentration as follows [50]:

$$C(x_i, t) = \overline{C}(x_i, t) + C'(x_i, t) \tag{2.5}$$

$$\frac{\partial(\overline{C} + C')}{\partial t} + \frac{\partial((\overline{U_i} + u_i')(\overline{C} + C'))}{\partial x_i} = \frac{\partial}{\partial x_i}\left(\alpha_i \frac{\partial(\overline{C} + C')}{\partial x_i}\right) \tag{2.6}$$

In addition, at this point, this work is only focused on the long-term mean behavior of a tracer cloud. Therefore all terms in the resultant Reynolds decomposed

advection-diffusion PDE must be time-averaged:

$$\frac{1}{T}\int_t^{t+T}\left\{\frac{\partial(\overline{C}+C')}{\partial t}+\frac{\partial(\overline{U_i}+u_i')}{\partial x_i}=\frac{\partial}{\partial x_i}\left(\alpha_i\frac{\partial(\overline{C}+C')}{\partial x_i}\right)\right\}d\tau \tag{2.7}$$

Therefore,

$$\frac{\partial(\overline{\overline{C}+\overline{C'}})}{\partial t}+\frac{\partial(\overline{\overline{U_i}\overline{C}}+\overline{\overline{U_i}C'}+\overline{U_i'\overline{C}}+\overline{U_i'C'})}{\partial x_i}=\frac{\partial}{\partial x_i}\left(\alpha_i\frac{\partial(\overline{\overline{C}}+\overline{C'})}{\partial x_i}\right)$$

(2.8)

Now having that $\overline{C'}=0$, hence the terms $\overline{\overline{U_i}C'}=\overline{U_i'\overline{C}}=0$. Thus,

$$\frac{\partial\overline{C}}{\partial t}+\overline{U_i}\frac{\partial\overline{C}}{\overline{x_i}}=-\frac{\partial(\overline{U_i'C'})}{\partial x_i}+\frac{\partial}{\partial x_i}\left(\alpha_i\frac{\overline{C}}{\partial x_i}\right) \tag{2.9}$$

Now, it necessary to deal with the turbulent flux term $\overline{U_i'C'}$, that for this propose Reynolds portrays this turbulent component qualitatively as a form of rapid mixing [50]; hence, it is possible to make a similarity with molecular diffusion. Taylor, in his work, inferred part of this relationship by scientifically following a haze of tracer particles in a turbulent flow and approximating the Lagrangian correlation showing that for times greater than T, the cloud of tracer given $\overline{U_i'C'}$ grows linearly in time. This procedure is used in [48] by Fischer to come up with an analogous model to molecular diffusion to study the uncertain flux term. This is known as the mixing length model, which describes the most extreme distance in the fluid over which the speed variances are related. Then, for turbulent diffusion the length scale is given by $L_D=(K_{ii}T)^{1/2}$ and advective length scale by $L_A=U_iT$, so to assured that the process works under mixing length conditions then $K_{ii}=\frac{(U_iT)^2}{T}$. Thus, for a time

greater than T, Fick's law is used to establish that :

$$\overline{U_i'C'} = K_{ii}\frac{\partial \overline{C}}{\partial x_i} \tag{2.10}$$

Where K_{ii} is the principal eddy diffusivity tensor. Hence, the process model simplifies to :

$$\frac{\partial \overline{C}}{\partial t} + \bar{U}_i\frac{\partial \overline{C}}{\bar{x}_i} = \frac{\partial}{\partial x_i}\left(K_{ii}\frac{\partial \overline{C}}{\partial x_i}\right) + \frac{\partial}{\partial x_i}\left(\alpha_i\frac{\overline{C}}{\partial x_i}\right) \tag{2.11}$$

In addition, it has been proven in most literature [48], [49], [50] that molecular diffusion is negligible compared with the turbulent diffusion. Then the averaged process model end up as follows:

$$\frac{\partial \overline{C}}{\partial t} + \overline{U_i}\frac{\partial \bar{C}}{\overline{x_i}} = \frac{\partial}{\partial x_i}\left(K_{ii}\frac{\partial \overline{C}}{\partial x_i}\right) \tag{2.12}$$

2.4 Problem formulation

Let us consider an instantaneous initial Gaussian pulse released in a 2D domain given constant fluid velocity components U and V and eddy diffusivities K_{xx} and K_{yy}. In addition, it is considered that the UAUV dimensions are small with respect to the size of the concentration spectrum, so the UAUV can be considered a point mass. Therefore, oil droplets propagation and plume deformation due to fluid-structure interaction can be neglected. Then, the resulting advection-diffusion equation is said to be written in a strong conservative form:

$$\frac{\partial \overline{C}}{\partial t} + \overline{U}\frac{\partial \overline{C}}{\partial x} + \overline{V}\frac{\partial \overline{C}}{\partial y} = K_{xx}\frac{\partial^2 \overline{C}}{\partial x^2} + K_{yy}\frac{\partial^2 \overline{C}}{\partial y^2} \tag{2.13}$$

For supplementary Dirichlet and Neuman boundary conditions perform as fol-

lows:

$$\bar{C}(0, y, t) = \overline{C}(x, 0, t) = 0 \tag{2.14}$$

$$\frac{\partial \overline{C}}{\partial x}(L_x, y, t) = \frac{\partial \overline{C}}{\partial x}(x, L_y, t) = 0 \tag{2.15}$$

And for initial Gaussian pulse given such that:

$$\overline{C}(x, y, 0) = exp\left[-\frac{(x - a_x)^2}{K_{xx}} - \frac{(y - a_y)^2}{K_{yy}}\right] \tag{2.16}$$

2.4.1 Gaussian Pulse Analytical Solution

According with most of literature, and specifically [51], [63], [64] and [67] the analytical solution of the two-dimensional advection-diffusion equation, at a given time t for an initial Gaussian pulsed released at point $A(a_x, a_y)$ on the domain $\Omega : x \in [0, L_x], y \in [0, L_y]$ is given by:

$$\overline{C}(x, y, t) = \frac{1}{4t + 1} exp\left[-\frac{(x - a_x - Ut)^2}{K_{xx}(4t + 1)} - \frac{(y - a_y - Vt)^2}{K_{yy}(4t + 1)}\right] \tag{2.17}$$

This solution models a dispersive moving plume on the aforementioned domain. For future application proposes two simulations have been run over a domain defined by $L_x = 1000m$ and $L_y = 1000m$ for time $t = 300sec$, subject firstly to an horizontal velocity field $U = 1.0m/s$, and for equivalent dispersion coefficient $K_{xx} = K_{yy} = 11.68m^2/s$ [48], and secondly to an velocity field $[U, V]^T = [1.0m/s, 1.0m/s]$.

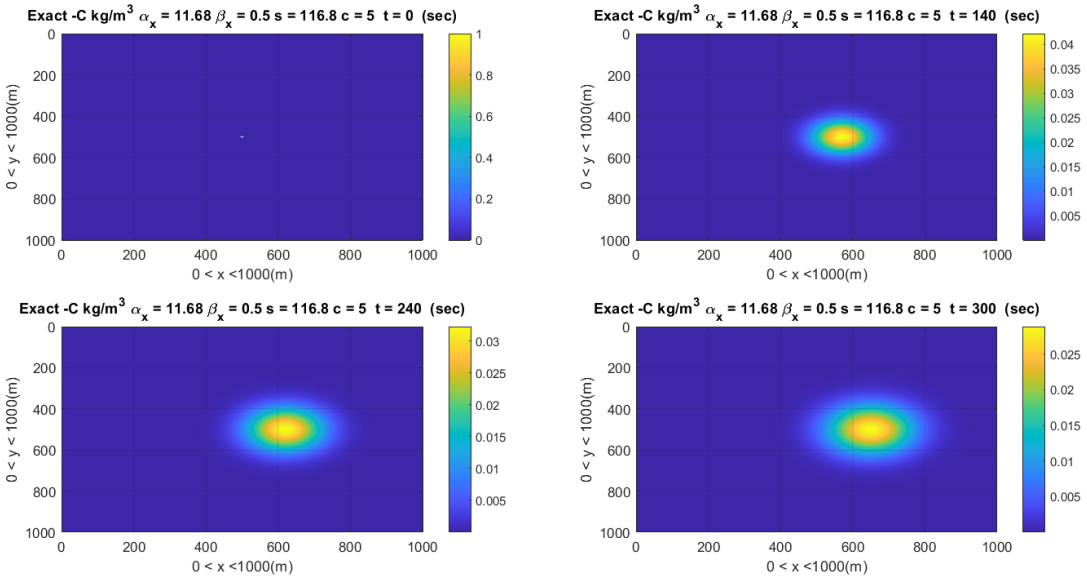

Figure 2.2: Advection-Diffusion PDE Guassian pulse Exact Solution Horizontal Velocity Field.

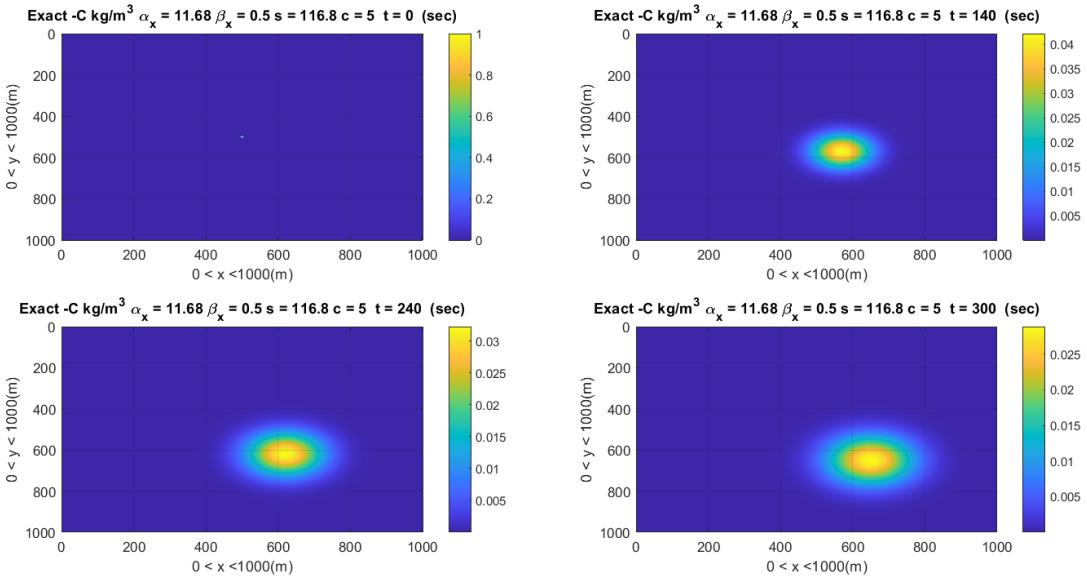

Figure 2.3: Advection-Diffusion PDE Guassian pulse Exact Solution 2-D Velocity Field.

2.5 Numerical Schemes for the Solution of the Advection–Diffusion Equation

Partial differential equations are the basis for numerous numerical models of physical, substance, and biological phenomena. Thus, it is fundamental to approximate the solution of these partial differential equations mathematically in request to explore the forecasts of the numerical models, as the analytical solutions are generally inaccessible.

In this section finite difference schemes are developed based on modified equivalent partial differential equation as described in [51], and [54]. Only explicit numerical schemes will be considered due to the high number of calculations required for the proposed domain, at which implicit schemes could become unfeasible because of the limited computational power available.

2.5.1 The Forward-Time Centered-Space Scheme

This scheme uses the forward-difference form for the time-derivative and centered-difference forms for all spatial derivatives.

$$\left.\frac{\partial \bar{C}}{\partial t}\right|_{i,j}^{n} + \bar{U}\left.\frac{\partial \bar{C}}{\partial x}\right|_{i,j}^{n} + \bar{V}\left.\frac{\partial \bar{C}}{\partial y}\right|_{i,j}^{n} = K_{xx}\left.\frac{\partial^2 \bar{C}}{\partial x^2}\right|_{i,j}^{n} + K_{yy}\left.\frac{\partial^2 \bar{C}}{\partial y^2}\right|_{i,j}^{n} \tag{2.18}$$

Utilizing these approximations for the three-dimensional advection-diffusion equation at the $(i, j)th$ grid point ends up in the following two-level finite difference formula:

$$C_{i,j}^{n+1} = (s_x + c_x/2)C_{i-1,j}^n + (s_y + c_y/2)C_{i,j-1}^n + (s_x - c_x/2)C_{i+1,j}^n + (s_y - c_y/2)C_{i,j+1}^n + (1 - 2s_x - 2s_y)C_{i,j}^n \tag{2.19}$$

where

$$c_x = U\frac{\Delta t}{\Delta x}, c_y = V\frac{\Delta t}{\Delta y} \tag{2.20}$$

and

$$s_x = K_{xx}\frac{\Delta t}{(\Delta x)^2}, s_y = K_{yy}\frac{\Delta t}{(\Delta y)^2} \tag{2.21}$$

The stability criterion of this finite-difference technique is evaluated through the Von Neumann method, which in this case is given by:

$$s_x + s_y \leq \frac{1}{2} \tag{2.22}$$

and

$$\frac{c_x^2}{s_x} + \frac{c_y^2}{s_y} \leq 3 \tag{2.23}$$

The modified partial differential equation (MDE) of this method is given by:

$$\frac{\partial C}{\partial t} + U\frac{\partial C}{\partial x} + V\frac{\partial C}{\partial y} + [-K_{xx} + U\frac{\Delta x c_x}{2}]\frac{\partial^2 C}{\partial x^2} + [-K_{yy} + V\frac{\Delta y c_y}{2}]\frac{\partial^2 C}{\partial y^2} + O[(\Delta x)^2, (\Delta y)^2] = 0 \tag{2.24}$$

From this MDE, it can be seen that this method is only first-order accurate and induces numerical diffusion.

2.5.2 The forward-Time Backward-Space Centered-Space Scheme

This scheme uses forward-difference for the time derivative,centered-difference for the diffusive derivatives, and backward differences for the spatial derivatives in the advective terms. Then the explicit FTBSCS formula is given as follows:

$$\begin{aligned} C_{i,j}^{n+1} = (s_x + C_x)C_{i-1,j}^n + (s_y + c_y)C_{i,j-1}^n + (s_x)C_{i+1,j}^n + (s_y)C_{i,j+1}^n \\ + (1 - 2s_x - 2s_y - c_x - c_y)C_{i,j}^n \end{aligned} \tag{2.25}$$

Similarly, as it was done for the FTCS scheme, a Von Neumann stability analysis is performed. Thus, the stability required for this method is given by:

$$2(s_x + s_y) + c_x + c_y \leq 1 \tag{2.26}$$

Moreover, the correspondent MDE for this method is given as follows:

$$\begin{aligned} \frac{\partial \bar{C}}{\partial t} + \bar{U}\frac{\partial \bar{C}}{\partial x} + \bar{V}\frac{\partial \bar{C}}{\partial y} + [-K_{xx} + U\frac{\Delta x(c_x - 1)}{2}]\frac{\partial^2 \bar{C}}{\partial x^2} + \\ [-K_{yy} + V\frac{\Delta y(c_y - 1)}{2}]\frac{\partial^2 \bar{C}}{\partial y^2} + O[(\Delta x)^2, (\Delta y)^2] = 0 \end{aligned} \tag{2.27}$$

Showing newly that FTBSCS is first order accurate as well as FTCS scheme.

2.5.3 The Lax–Wendroff Scheme

Lax–Wendroff is a weighted scheme that approximates the time and spatial derivatives in the advection-diffusion PDE as follows:

$$\left.\frac{\partial C}{\partial t}\right|_{i,j}^{n} \approx \frac{C_{i,j}^{n+1} - C_{i,j}^n}{\Delta t} \tag{2.28}$$

$$\left.\frac{\partial C}{\partial x}\right|_{i,j}^{n} \approx c_x \frac{C_{i,j}^n - C_{i-1,j}^n}{\Delta x} + (1 - c_x)\frac{C_{i+1,j}^n - C_{i-1,j}^n}{2\Delta x} \tag{2.29}$$

$$\left.\frac{\partial C}{\partial y}\right|_{i,j}^{n} \approx c_y \frac{C_{i,j}^n - C_{i,j-1}^n}{\Delta y} + (1 - c_y)\frac{C_{i,j+1}^n - C_{i,j-1}^n}{2\Delta y} \tag{2.30}$$

$$\left.\frac{\partial^2 C}{\partial x^2}\right|_{i,j}^{n} \approx \frac{C_{i+1,j}^n - 2C_{i,j}^n + C_{i-1,j}}{(\Delta x)^2} \tag{2.31}$$

$$\left.\frac{\partial^2 C}{\partial y^2}\right|_{i,j}^{n} \approx \frac{C_{i,j+1}^n - 2C_{i,j}^n + C_{i,j-1}}{(\Delta y)^2} \tag{2.32}$$

Then, this approximation lead to the following explicit finite difference formula:

$$\begin{aligned} C_{i,j}^{n+1} = {} & \frac{1}{2}(2s_x + c_x(1 + c_x))C_{i-1,j}^n + \frac{1}{2}(2s_x + c_x(c_x - 1))C_{i+1,j}^n + \\ & \frac{1}{2}(2s_y + c_x(1 + c_y))C_{i,j-1}^n + \frac{1}{2}(2s_y + c_y(c_y - 1))C_{i,j+1}^n + \\ & (1 - c_x^2 - c_y^2 - 2s_x - 2s_y)Ci, j^n \end{aligned} \tag{2.33}$$

The stability Von Neumann condition for this method is defined such that:

$$2(s_x + s_y) + c_x^2 + c_y^2 \leq 1 \tag{2.34}$$

and,

$$c_x^2 c_y^2 \leq 8 s_x s_y \tag{2.35}$$

The respective MDE for this scheme yields as follows:

$$\begin{aligned}&\frac{\partial C}{\partial t}+U\frac{\partial C}{\partial x}+V\frac{\partial C}{\partial y}-K_{xx}\frac{\partial^2 C}{\partial x^2}-K_{yy}\frac{\partial^2 C}{\partial y^2}+\\&U\frac{(\Delta x)^2}{6}(1-6s_x-c_x^2)\frac{\partial^3 C}{\partial x^3}+V\frac{(\Delta y)^2}{6}(1-6s_y-c_y^2)\frac{\partial^3 C}{\partial y^3}+\\&O[(\Delta x)^3,(\Delta y)^3]=0\end{aligned} \tag{2.36}$$

From the Lax-Wendroff MDE, it can be concluded that this scheme does not introduce any level of numerical diffusion, which makes out it an interesting choice to come up with an approximate solution of the advection-diffusion PDE.

2.5.4 Numerical Models Validation

It is necessary to compare the model results with analytical solutions, to validate the developed numerical models. Therefore, numerical results for FTCS, FTBSCS, and Lax Wendroff schemes are compared against results obtained in subsection 2.4.1.

For the propose of comparing the accuracy of each scheme, let us define the Root mean square error as the reason between the L_2 norm of the absolute error $E = |C_{aprox} - C_{exact}|$ and the exact solution as follows:

$$RMSE = \frac{(\sum_{i=1}^{N}\sum_{j=1}^{M}E_{i,j}^2)^{1/2}}{(\sum_{i=1}^{N}\sum_{j=1}^{M}C_{exact}{}_{i,j}^2)^{1/2}} \tag{2.37}$$

In addition, in order to achieve stability and make schemes to be feasibly computed, the grid size and time step are $\Delta x = \Delta y = 10m$, and $\Delta t = 0.9s$, so that $c = 0.09$ and $s = 0.1051$ which hold for the three stability conditions defined above for the studied schemes.

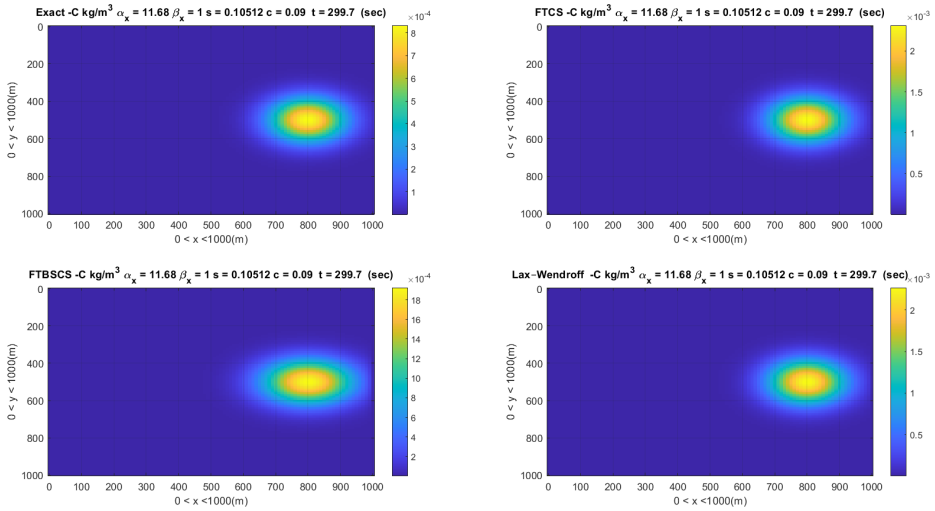

Figure 2.4: Advection-Diffusion PDE Guassian pulse Aproximated Solution Horizontal Velocity Field.

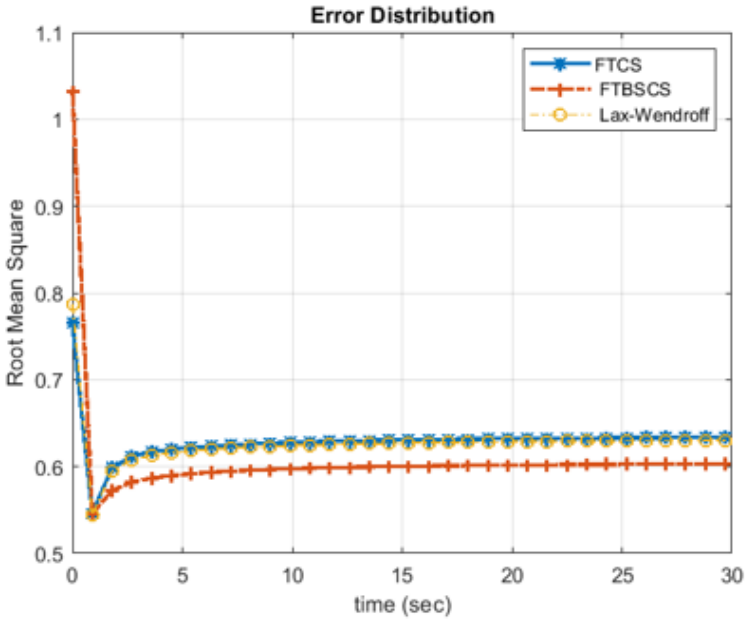

Figure 2.5: Root Mean Square Error Horizontal Velocity Field.

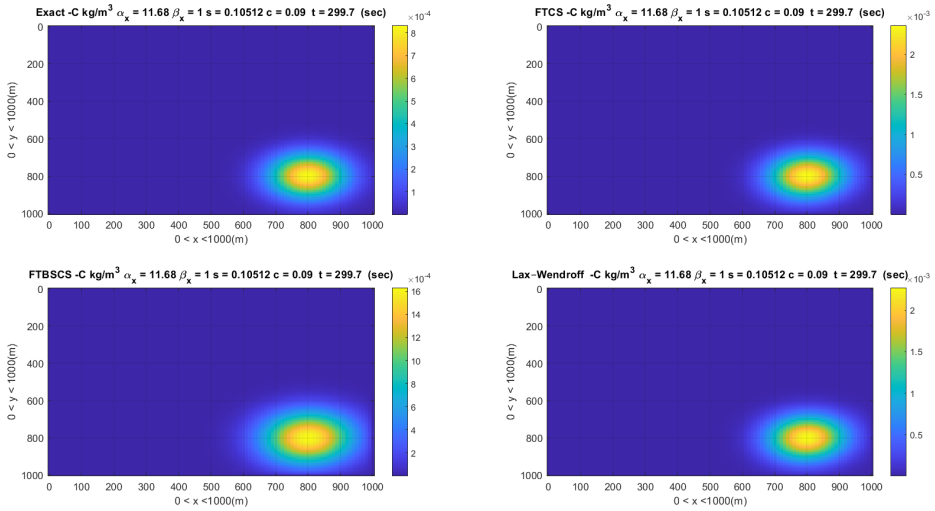

Figure 2.6: Advection-Diffusion PDE Guassian pulse Aproximated Solution 2-Dimensional Velocity Field.

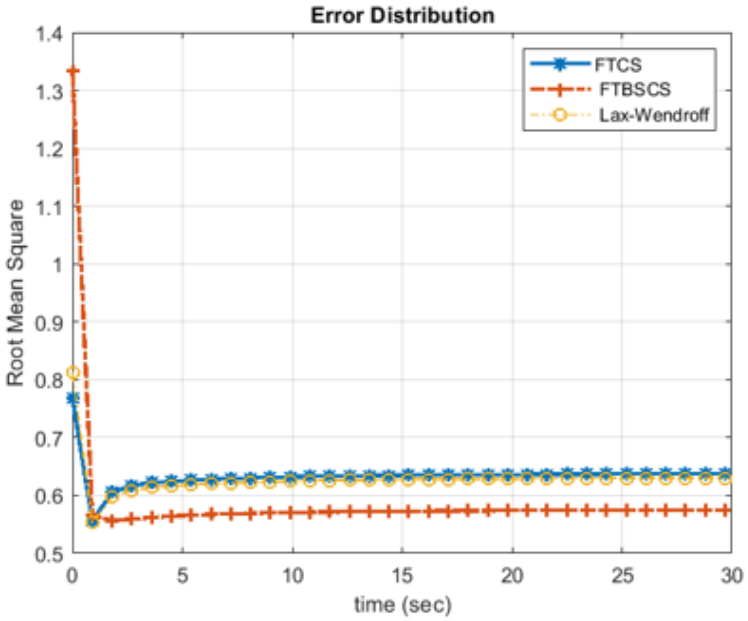

Figure 2.7: Root Mean Square Error 2-Dimensional Velocity Field.

The three schemes seem to produce decent results even though the given large grid size. Showing that proposed explicit methods are straightforward to implement and economical to use, being very efficient and needing less CPU time than the fully implicit finite difference methods. Unfortunately, it can be seen that even for such a big grid size, the number of calculations results to be way too large to run simultaneously with another ODE model to come up with a decent estimation model for guidance and localization. For this work, it is considered that the pollutant concentration field has been measured and estimated a priori by a super-user so that a decent concentration can be produced for purposes of UAUV guidance and localization.

Chapter 3

UAUV Dynamics and Guidance

In this chapter, the respective equations of motions of a general UAUV are derived, which will be represented in terms of a state vector and state-space sets of equations that can be differentiated either from the classical mechanics or Lagrange's formulation. The model that is addressed is given in the form of the general state-space structure $\dot{x} = f(x, t)$ where x is the state vector. The state vector contains the principal variables needed to describe the motion of a UAUV.

Name	Description
X_e	Inertial north position of the MAV
Y_e	Inertial east position of the MAV
Z_e	Inertial down position (negative of altitude) of the MAV
$\dot{X}_e$	
$\dot{Y}_e$	Earth Fixed Relatives Velocities
$\dot{Z}_e$	
u	Body frame velocity measured along e_x^b
v	Body frame velocity measured along e_y^b
w	Body frame velocity measured along e_z^b
ϕ	Roll angle
θ	Pitch angle
ψ	Heading (yaw) angle
p	Roll rate
q	Pitch rate
r	Yaw rate

Figure 3.1: State Variables Description.

The reason for representing the dynamical model in the state-space is that the control approach applied in this work is based on Lyapunov methods defined in terms of state-variable representation.

3.1 Coordinate system

Regardless of the modeling approach to be used to model the system dynamics of the UAUV, it is essential to be able to define a generalized set of coordinates on which acting forces and moments will be described. Similarly, as it is shown in [1], [3], [4], [6] this work defines $E := O_E, X_E, Y_E.Z_E$ as the inertial reference frame which is by definition attached to a reference fixed point in the control volume and $B := O_B, X_B, Y_B.Z_B$ as the body-fixed frame which is usually attached to the center of gravity of the vehicle. In addition, a set of unit vectors pointing respectively in the direction of both reference frames are stated as $e_x^E, e_y^E.e_z^E$ for the inertial reference frame and $e_x^B, e_y^B.e_z^B$ for the body-fixed frame.

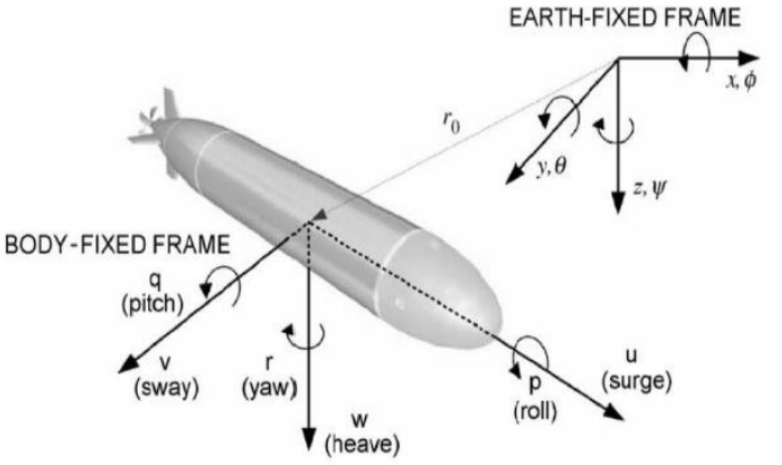

Figure 3.2: Frames and elementary vehicle's motion [83].

		Forces and Moments	ν	η
Motion in the x-body fixed direction	surge	τ_x	u	X_e
Motion in the y-body fixed direction	Sway	τ_y	v	Y_e
Motion in the z-body fixed direction	Heave	τ_z	w	Z_e
Rotation about x-body fixed axis	Roll	τ_K	p	ϕ
Rotation about y-body fixed axis	Pitch	τ_M	q	θ
Rotation about z-body fixed axis	Yaw	τ_N	r	ψ

Table 3.1: Nomenclature for marine vehicle's motion [1].

3.2 UAUV's Kinematics

In general terms, the motion of a vehicle is described by its kinematic variables (position, velocity, and acceleration) concerning a reference frame which either an inertial or noninertial frame. Equation 3.1 is a vector representation of the positions and orientations, including its respective derivatives that respect the inertial. Similarly, 3.2 is the translational and angular velocities vector for the body-fixed frame

$$\eta = \begin{pmatrix} x_e \\ y_e \\ z_e \\ \phi \\ \theta \\ \psi \end{pmatrix} \Rightarrow \dot{\eta} = \begin{pmatrix} \dot{x_e} \\ \dot{y_e} \\ \dot{z_e} \\ \dot{\phi} \\ \dot{\theta} \\ \dot{\psi} \end{pmatrix} \Rightarrow \ddot{\eta} = \begin{pmatrix} \ddot{x_e} \\ \ddot{y_e} \\ \ddot{z_e} \\ \ddot{\phi} \\ \ddot{\theta} \\ \ddot{\psi} \end{pmatrix}, \tag{3.1}$$

$$\nu = \begin{pmatrix} u \\ v \\ w \\ p \\ q \\ r \end{pmatrix} \Rightarrow \dot{\nu} = \begin{pmatrix} \dot{u} \\ \dot{v} \\ \dot{w} \\ \dot{p} \\ \dot{q} \\ \dot{r} \end{pmatrix}. \tag{3.2}$$

In order to define the relation between kinematic variables of both reference frames(inertial and body fixed frame) the η and ν vector are rewritten so that $\eta = [\eta_1, \eta_2]^T$ and $\nu = [\nu_1, \nu_2]^T$ where $\eta_1 = [x_e, y_e, z_e]^T$,$\eta_2 = [\phi, \theta, \psi]^T$,$\nu_1 = [u, v, w]^T$,$\nu_2 = [p, q, r]^T$. Therefore, as it is well developed in most of robot and vehicle dynamics literature the position of an arbitrary point on the vehicle is obtained by only applying a real time transformation of coordinates which is given as follows:

$$\dot{\eta_1} = R_b^e \nu_1 \tag{3.3}$$

$$R_b^e = \begin{pmatrix} c(\psi)\, c(\theta) & c(\psi)\, s(\phi)\, s(\theta) - c(\phi)\, s(\psi) & s(\phi)\, s(\psi) + c(\phi)\, c(\psi)\, s(\theta) \\ c(\theta)\, s(\psi) & c(\phi)\, c(\psi) + s(\phi)\, s(\psi)\, s(\theta) & c(\phi)\, s(\psi)\, s(\theta) - c(\psi)\, s(\phi) \\ -s(\theta) & c(\theta)\, s(\phi) & c(\phi)\, c(\theta) \end{pmatrix} \tag{3.4}$$

Similarly, the vector $\dot{\eta_2}$ is the respective derivative of the η_2 which does not have a physical meaning but it can be indeed studied as a function of the corresponding angular velocities in the body fixed frame and a transformation rule as describe [1], [3], [4], [6]

$$\dot{\eta_2} = J_{k_o}^{-1}(\eta_2)\nu_2 \tag{3.5}$$

where:

$$J_{ko}(\eta_2) = \begin{pmatrix} 1 & 0 & -s(\theta) \\ 0 & c(\phi) & c(\theta)\ s(\phi) \\ 0 & -s(\phi) & c(\phi)\ c(\theta) \end{pmatrix} \Rightarrow J_{k_o}^{-1} = \begin{pmatrix} 1 & \frac{s(\phi)\,s(\theta)}{c(\theta)} & \frac{c(\phi)\,s(\theta)}{c(\theta)} \\ 0 & c(\phi) & -s(\phi) \\ 0 & \frac{s(\phi)}{c(\theta)} & \frac{c(\phi)}{c(\theta)} \end{pmatrix} \tag{3.6}$$

By collecting both kinematic analysis in one 6-dimensional vector, it can be shown that:

$$\dot{\eta} = J_e(R_b^e)\nu \tag{3.7}$$

where:

$$J_e(R_b^e) = \begin{pmatrix} R_b^e & O_{3x3} \\ O_{3x3} & Jko^{-1} \end{pmatrix} \tag{3.8}$$

In fact, the reader may notice that(3.6)is not invertible for every angular position specifically when $\theta = (2n+1)\pi/2$ for $n = 1, 2, 3, ...$ at which $Jko^{-1}(\eta_2)$ is singular. This can be prevented if quaternion representations are applied. However, in this work, it will be shown that for the chosen UAUV (OUTLAND1000), this will not represent a problem, so the Euler angle attitude representation can still be applied.

3.3 UAUV's Dynamics

As it was shown in Section 3.2 the kinematics problem tackles the description of motion regardless of what causes the motion itself. Thus, a complementary analysis that includes a description of what phenomena cause the motion is required to get an entire picture of how and why the motion is occurring. In literature, this procedure is called dynamical formulation. Multiple approaches might be considered when it comes to generating a reliable dynamical model. For instance, the classi-

cal mechanics' approach is based on Newtonian and Eulerian formulations, and the variational approach is based on Lagrangian and energy formulations. To summarize, regardless of the formulation method, the main goal of the dynamical analysis of a generic system is to characterize the resultant forces and moments acting over the system. I this section, external forces and moments acting over an underwater vehicle will be defined and written as a function of η and ν to derive the governing equations of motion of a General marine vehicle.

3.3.1 Newton-Euler Equations of Motion (General form)

As it is specifically developed in [1] and [2] Newton-Euler equations of motion can be written in matrix form as follows:

$$M_{RB}\dot{\nu} + C_{RB}(\nu)\nu = \tau_{\nu}$$

where:

M_{RB} = inertial matrix (constant, symmetric, and positive definite)

C_{RB} = Coriolis matrix

$\tau = [\tau_1, \tau_2]^T$ = total 6-Dimensional external forces and moments vector(3.9)

M_{RB} and C_{RB} are given by:

$$\mathrm{M}_{RB} = \begin{pmatrix} mI & -mS(r_c^b \\ mS(r_c^b & Jo \end{pmatrix}$$

$$\mathrm{C}_{RB} = \begin{pmatrix} O_{33} & -mS(\nu_1) - mS(\nu_2)S(r_c^b) \\ -mS(\nu_1) + mS(\nu_2)S(r_c^b) & S(J_o\nu_2) \end{pmatrix} \quad (3.10)$$

where m is the total mass of the vehicle, $I = diag[I_{xx}, I_{yy}, I_{zz}]$ is the moment of inertia respect the principal axes of inertia (longitudinal, lateral and normal symmetry axes of the vehicle), I_3 is the 3-dimensional identity matrix and, $S(x)$ is the skew symmetric operator matrix performing the cross product of two (3x1) vectors which is given as follows:

$$S(x) = \begin{pmatrix} 0 & -x_3 & x_2 \\ x_3 & 0 & -x_1 \\ -x_2 & x_1 & 0 \end{pmatrix} \quad (3.11)$$

An expanded version of (3.9), and (3.10) is found at [2].

3.3.2 Added Mass and Inertia

When a rigid body is moving in a fluid, the additional inertia of the fluid surrounding the body that is accelerated by the movement of the body has to be considered hence the force required to accelerate the body increases. This phenomenon is defined as added mass and inertial effect.

For simplicity, consider the classic one-dimensional second-order system, which contains inertia, damping, and stiff forces effects to describe motion in general terms.

$$m\ddot{x} + b\dot{x} + kx = f(t) \quad (3.12)$$

where m is the system mass, b is the linear damping, k is the system stiffness, and $f(t)$ is the force acting on the mass, while x is the displacement of the mass.

In a physical sense, added mass is the weight added to a system because an accelerating or decelerating body must move some volume of surrounding fluid with it as it moves. It can prove that he added mass force opposes the motion and can be included in the model as it is shown below:

$$m\ddot{x} + b\dot{x} + kx = f(t) - m_a\ddot{x} \tag{3.13}$$

In addition, added mass forces depend on the motion; hence these forces can arise in more than just one direction; therefore, in a three-degree of freedom system, the term m_a will become a 3x3 matrix or, in the most general case for spatial motion (six-degree of freedom) will end 6x6 added mass coefficients matrix. Thus, the added forces moments written in matrix form are presented as follows:

$$F_A = \begin{pmatrix} m_{11} & m_{12} & m_{13} & m_{14} & m_{15} & m_{16} \\ m_{21} & m_{22} & m_{23} & m_{24} & m_{25} & m_{26} \\ m_{31} & m_{31} & m_{33} & m_{34} & m_{35} & m_{36} \\ m_{41} & m_{42} & m_{43} & m_{44} & m_{45} & m_{46} \\ m_{51} & m_{52} & m_{53} & m_{54} & m_{55} & m_{56} \\ m_{61} & m_{62} & m_{63} & m_{64} & m_{65} & m_{66} \end{pmatrix} \begin{pmatrix} \dot{u_1} \\ \dot{u_2} \\ \dot{u_3} \\ \dot{u_4} \\ \dot{u_5} \\ \dot{u_6} \end{pmatrix} \tag{3.14}$$

$$M_A = \begin{pmatrix} m_{11} & m_{12} & m_{13} & m_{14} & m_{15} & m_{16} \\ m_{21} & m_{22} & m_{23} & m_{24} & m_{25} & m_{26} \\ m_{31} & m_{31} & m_{33} & m_{34} & m_{35} & m_{36} \\ m_{41} & m_{42} & m_{43} & m_{44} & m_{45} & m_{46} \\ m_{51} & m_{52} & m_{53} & m_{54} & m_{55} & m_{56} \\ m_{61} & m_{62} & m_{63} & m_{64} & m_{65} & m_{66} \end{pmatrix} \tag{3.15}$$

Extrapolating a similar approach to the submarine vessel problem, it can be shown that hydrodynamic added forces and moments along body-fixed frame axes are defined by the structure given in [1].

$$X_A = -X_{\dot{u}}\dot{u} \Rightarrow X_{\dot{u}} = \frac{\partial \tau_x}{\partial \dot{u}} \tag{3.16}$$

Following this particular procedure all other 35 elements of M_A matrix are approximated. In fact, This coefficients can be also estimated experimentally as it was done in [16] where parameter identification for the UAUV Hippocampus was developed. For futher analysis in added mass effects formulation, calculations and properties the reader may take look into [1], [2], [4], [17], and [18].

To summarize, added mass effects over UAUVs have been demonstrated in [1], [2], and most of the literature in underwater vehicle dynamics that inertial added mass effects can be modeled if and only if the velocity is low, the three planes of symmetry are considered within the design phase of the vehicle.

$$M_A = -\text{diag}[X_{\dot{u}}, Y_{\dot{v}}, Z_{\dot{w}}, K_{\dot{p}}, M_{\dot{q}}, N_{\dot{r}}] \tag{3.17}$$

Not only inertial forces and moments are affected by added mass, but also Coriolis and centripetal forces are also influenced by the motion of a rigid body through an ideal fluid. In fact, Coriolis forces and centripetal matrix $C_A(\nu)$ can be characterized by affirming that $C_A(\nu)$ is skew symmetrical [2]:

$$C_A(\nu) = -C_A^T(\nu) \tag{3.18}$$

$$C_A = \begin{pmatrix} 0 & 0 & 0 & 0 & -Z_{\dot{w}}w & Y_{\dot{v}}v \\ 0 & 0 & 0 & Z_{\dot{w}}w & 0 & -X_{\dot{u}}u \\ 0 & 0 & 0 & -Y_{\dot{v}}v & X_{\dot{u}}u & 0 \\ 0 & -Z_{\dot{w}}w & Y_{\dot{v}}v & 0 & -N_{\dot{r}}r & M_{\dot{q}}q \\ Z_{\dot{w}}w & 0 & -X_{\dot{u}}u & N_{\dot{r}}r & 0 & -K_{\dot{p}}p \\ -Y_{\dot{v}}v & X_{\dot{u}}u & 0 & -M_{\dot{q}}q & K_{\dot{p}}p & 0 \end{pmatrix} \tag{3.19}$$

3.3.3 Hydrodynamic Damping

At the end end of subsection 3.3.2 implies that (3.9) becomes :

$$M_{RV}\dot{\nu} + C_{RB}(\nu)\nu = \tau_\nu - M_A\dot{\nu} - C_A(\nu)\nu \tag{3.20}$$

Similarly, in order to consider the effects of hydrodynamic forces and moments, an additional term is added to (3.20) RHS such that:

$$M_{RB}\dot{\nu} + C_{RB}(\nu)\nu = \tau_\nu - M_A\dot{\nu} - C_A(\nu)\nu - D(\nu)\nu \tag{3.21}$$

where the term $D(\nu)\nu$ represents the hydrodynamic damping forces due to fluid viscous dissipative effects. As it is mentioned in [2] multiple causes of hydrodynamic dissipation can be described so that the hydrodynamic damping matrix can be

decoupled as a function of different hydrodynamic phenomena as follows:

$$D(\nu) = D_P(\nu) + D_S(\nu) + D_W(\nu) + D_M(\nu) \tag{3.22}$$

$D_P(\nu)$: is the radiation-induced potential damping due to forced body oscillations.

$D_s(\nu)$: is the linear skin friction due to boundary layers effects.

$D_W(\nu)$: is the wave drift damping.

$D_M(\nu)$: is the damping ratio due to vortex shedding

In addition, further commentaries and analysis regarding the drag and lift forces and moments as functions of the angle of attack, side-slip angle, and the geometry of the vehicle are developed in [19] for further revisions of literature on hydrodynamic damping effects. However, the proper development of these specific external perturbations goes beyond the scope of this work; therefore, applying a typical simplification of the model considering only linear and quadratic damping terms according to what is done in [1], [2], [6], [16], [19] would represent a representation reliable enough to proof the objectives of this work. Therefore hydrodynamic damping components yield to:

$$\begin{aligned} D_{RB}(\nu) = &-\text{diag}[X_u, Y_v, Z_w, Kp, M_q, N_r] \\ &- \text{diag}[X_{uu}|u|, Y_{vv}|v|, Z_w|w|, K_{pp}|p|, M_{qq}|q|, N_{rr}|r|] \end{aligned} \tag{3.23}$$

where $D_{RB}(\nu)$ elements are a function of drag and lift forces and moments. Moreover, drag depends on the fluid density ρ, submarine vehicle frontal area A_f

and lies in the direction of the fluid velocity whereas lift forces action point is on the center of pressure of the vehicle acting in a perpendicular orientation with respect to the flow [19].

3.3.4 Hydrostatic Forces and Moments

Better known in marine and ocean engineering as restoring or alignment forces and moments since usually watercraft is designed to hold a stable position in the transversal(y-z) and longitudinal(x-z) body frame. In fact, the problem of keeping a fixed roll ($\phi \cong \phi_1$) and ($\theta \cong \theta_1$) by only applying hydrostatic components represents by itself a whole study field within the naval architecture and marine engineering sciences. Further in this work, this property applied to the chosen vehicle (OUTLAND-1000) will be substantially helpful for the development of the mathematical and control model.

In general, hydrostatic effects can be regarded to one of the most basic principles of physics, which is the Archimedes' principle which states " any body completely or partially submerged in a fluid (gas or liquid) at rest is acted upon by an upward, or buoyant, force, the magnitude of which is equal to the weight of the fluid displaced by the body. The volume of displaced fluid is equivalent to the volume of an object fully immersed in a fluid or to that fraction of the volume below the surface for an object partially submerged in a liquid. The weight of the displaced portion of the fluid is equivalent to the magnitude of the buoyant force. The buoyant force on a body floating in a liquid or gas is also equivalent in magnitude to the weight of the floating object and is opposite in direction"

Following a similar approach as [1] let us define $g = 9.81m/s^2$ as the magnitude of the earth's gravity field, $W = mg$ to be the weight of the body, and Δ as the volume of fluid displaced by the body so that the Buoyancy force is given by $B = \rho g \Delta$. In addition, it necessary to define $r_G^B = [x_g, y_g, z_g]^T$ and $r_B^B = [x_B, y_B, z_B]^T$ which are the position of the center of gravity and center of buoyancy, respectively, which are the locations over the vehicle where gravitational forces are acting. For design and stability proposes, the center of mass and the center of gravity are said to coincide so that $r_C^B = r_G^B$

From these definitions the vector form of the forces mentioned above are given as follows:

$$g(\eta) = \begin{pmatrix} -(W-B)\,sin\,(\theta) \\ (W-B)\,cos\,(\theta)\,sin\,(\phi) \\ (W-B)\,cos\,(\theta)\,cos\,(\phi) \\ -(y_g W - y_B B)cos(\theta)cos(\phi) + (z_g W - Z_B B)cos(\theta)sin(\phi) \\ (z_g W - Z_B)sin(\theta) + (x_g W - x_B B)cos(\theta)cos(\phi) \\ -(x_g W - x_B B)cos(\theta)sin(\phi) - (y_g W - y_B B)sin(\theta) \end{pmatrix} \tag{3.24}$$

Correspondingly, the effect of these hydrostatic external forces and moments vector is added to model (3.21) to obtain:

$$M_{RB}\dot{\nu} + C_{RB}(\nu)\nu = \tau_\nu - M_A\dot{\nu} - C_A(\nu)\nu - D(\nu)\nu - g(\eta) \tag{3.25}$$

Hence:

$$(M_{RB} + M_A)\dot{\nu} + (C_{RB} + C_A)(\nu)\nu + D(\nu)\nu + g(\eta) = \tau_\nu \tag{3.26}$$

where: $\tau_\nu = \tau + \Delta\tau$ being τ recognized as the input dynamics vector and $\Delta\tau$ a quantity that further in this work will be considered as an equivalent uncertainty that gathers the effects of different external perturbations due to random physical processes or non considered uncertainties on the dynamical formulation itself. The definition of these two last components depends on the time, geometry, architecture, and actual state values of the vehicle and will be studied later in this chapter.

Let us consider $M = M_{RB} + M_A$ and $C = C_{RB} + C_A$ as the total inertia and Coriolis matrices so that (3.26) finally becomes into the vector representation of the dynamical equations of motion of the general underwater vessel, which is presented as follows:

$$M\dot{\nu} + C(\nu)\nu + D(\nu)\nu + g(\eta) = \tau_\nu \tag{3.27}$$

where parameter matrices M, C and D must hold for the following properties [1], [2], [6], [7] [17] [18]:

- the inertia matrix is symmetric and positive definite, i.e., $M = M^T > 0$
- the damping matrix is positive definite, i.e., $D(\nu) > O$
- the damping matrix is positive definite, i.e., $D(\nu) > O$ the matrix $C(\nu)$ is skew-symmetric, i.e.,$C(\nu) = C(\nu)^T, \forall\nu \in R^6$

3.4 OUTLAND-1000 Dynamics

Up to this point, the reader may infer that the analysis is moving towards to state the actual control problem, so it is important to mention that the mentioned control problem for underwater autonomous vessels can be analyzed either in the

body-fixed or earth-fixed representation. In [1], [2] particular rules of transformation are applied to project the UAUV dynamics between both coordinate systems while [21], [22] are good examples of how to tackle the UAUV earth-fixed dynamics and control problem.

As mentioned above in previous sections, most marine vehicles(surface or underwater) are usually designed based on transverse and longitudinal stability, as can be respectively seen in Figure 3.3. The main goal of this analysis is essentially defined by the ship hydrostatics with the unique objective to maintain a static position in both planes. Therefore, it can be concluded that aligning moments and symmetrical design over the three planes ensure hydrostatic stability, so that roll and pitch moments are neglected, i.e.,$\phi = \theta \approx 0$ and consequently $p = q \approx 0$ to finally arrive to the assumption that OUTLAND-1000 can be treated as a 4 degrees of freedom

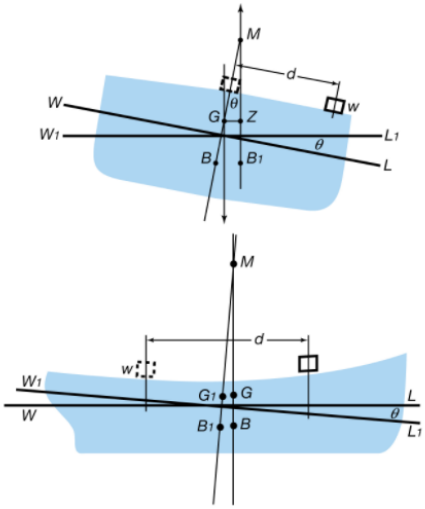

Figure 3.3: Hydrostatic stability planes [84].

In this section the 4DOF kinematics and dynamics of OUTLAND-1000 are described as it is done in [20]-[30] and [34].

3.4.1 4DOF Reduced Kinematics

From the assumptions above regarding roll and pitch motion, the new position and orientation vector, as well as the translational and angular velocities vector, are now given as follows:

$$\eta = \begin{pmatrix} x_e \\ y_e \\ z_e \\ \psi \end{pmatrix} \Rightarrow \nu = \begin{pmatrix} u \\ v \\ w \\ r \end{pmatrix} \tag{3.28}$$

In addition, the spatial transformation matrix $J_e(R_b^e)$ is also simplified into:

$$J = \begin{pmatrix} \cos(\psi) & -\sin(\psi) & 0 & 0 \\ \sin(\psi) & \cos(\psi) & 0 & 0 \\ 0 & 0 & 1 & 0 \\ 0 & 0 & 0 & 1 \end{pmatrix} \tag{3.29}$$

Thus, the kinematic model is represented as:

$$\dot{\eta} = J(\eta)\nu \tag{3.30}$$

3.4.2 4DOF Reduced Dynamics

The reduced form of total matrices $M, C, D \in R^{4x4}$ and $g \in R^4$ are expressed as follows:

$$M = \begin{pmatrix} m_{11} & 0 & 0 & 0 \\ 0 & m_{22} & 0 & 0 \\ 0 & 0 & m_{33} & 0 \\ 0 & 0 & 0 & m_{44} \end{pmatrix}, \tag{3.31}$$

$$m_{11} = m - X_{\dot{u}}, m_{22} = m - Y_{\dot{v}}, m_{33} = m - Z_{\dot{w}}, m_{44} = I_z - N_{\dot{r}} \tag{3.32}$$

$$C = \begin{pmatrix} 0 & c_{12} & 0 & 0 \\ c_{21} & 0 & 0 & 0 \\ 0 & 0 & 0 & 0 \\ c_{41} & 0 & 0 & c_{44} \end{pmatrix}, \tag{3.33}$$

$$c_{12} = -mr, c_{21} = -mr, c_{41} = mv, c_{44} = -mu \tag{3.34}$$

$$D = \begin{pmatrix} d_{11} & 0 & 0 & 0 \\ 0 & d_{22} & 0 & 0 \\ 0 & 0 & d_{33} & 0 \\ 0 & 0 & 0 & d_{44} \end{pmatrix}, \tag{3.35}$$

$$d_{11} = -X_u, d_{22} = -Y_v, d_{33} = -Z_w, d_{44} = -N_r \tag{3.36}$$

$$g = \begin{pmatrix} g_{11} \\ g_{21} \\ g_{31} \\ g_{41} \end{pmatrix}, \tag{3.37}$$

$$g_{11} = -X_{uu}u|u|; g_{21} = -Y_{vv}v|v|; g_{31} = -Z_{ww}w|w|; g_{41} = -N_{rr}r|r| \tag{3.38}$$

3.4.3 Uncertain Dynamics Characterization

At the end of Section 3.3 equation (3.26) introduces the vector $\tau_\nu = \tau + \Delta\tau$ which is basically a representation of the interaction of system control inputs and system uncertainties.

In real life, a vehicle operates under the effects of unknown environmental conditions and estimation error of actual dynamical parameters and states due to noisy hardware components such as sensors that generate an external perturbation that has to be handled by the control inputs. These perturbations are usually called in literature as uncertain dynamics. For example, in [20], and [34] uncertain components associated with each acting force on the vehicle and the vehicle kinematics are defined such that the overall magnitude of the $\Delta\tau$ vector is less or equal than the 20% of the magnitude of τ. In addition, uncertain kinematics must also hold for some other requirements regarding the control approach that is applied in this work which is going to be described further in Chapter 4.

In order to come up with an uncertain dynamics mathematical model that holds for the description above [20] and [34] have chosen to go with a set of perturbations given as follows:

Uncertain Equivalent Kinematic Matrix

$$\Delta J = \begin{pmatrix} \Delta \mathrm{J}_{11} & \Delta \mathrm{J}_{12} & 0 & 0 \\ \Delta \mathrm{J}_{21} & \Delta \mathrm{J}_{22} & 0 & 0 \\ 0 & 0 & \Delta \mathrm{J}_{33} & 0 \\ 0 & 0 & 0 & \Delta \mathrm{J}_{44} \end{pmatrix} \tag{3.39}$$

$$
\begin{aligned}
\Delta J_{11} &= J_{11}(0.02\cos(10t) - 0.3\sin(100tx_e)),\\
\Delta J_{12} &= J_{12}(0.02\cos(10t) - 0.3\sin(100tx_e)),\\
\Delta J_{21} &= J_{21}(-0.03\cos(2t) + 0.4\sin(200t)),\\
\Delta J_{22} &= J_{22}(-0.03\cos(2t) + 0.4\sin(200t)),\\
\Delta J_{33} &= J_{33}(-0.5\sin(300t)),\\
\Delta J_{44} &= J_{44}(0.04\cos(0.1t))
\end{aligned}
\tag{3.40}
$$

Uncertain Equivalent Inertia Matrix

$$
\Delta M = \begin{pmatrix}
\Delta \mathrm{m}_{11} & 0 & 0 & 0\\
0 & \Delta \mathrm{m}_{22} & 0 & 0\\
0 & 0 & \Delta \mathrm{m}_{33} & 0\\
0 & 0 & 0 & \Delta \mathrm{m}_{44}
\end{pmatrix}
\tag{3.41}
$$

$$
\begin{aligned}
\Delta m_{11} &= M_{11}(-0.02\cos(5t) + 0.2\sin(50tu)),\\
\Delta m_{22} &= M_{22}(0.02\sin(t) - 0.3\sin(40t)),\\
\Delta m_{33} &= M_{33}(0.03\cos(0.1t) - 0.4\cos(60w)),\\
\Delta m_{44} &= M_{44}(-0.02\sin(0.5tr) + 0.3\cos(80t))
\end{aligned}
\tag{3.42}
$$

Uncertain Equivalent Coriolis Matrix

$$
\Delta C = \begin{pmatrix}
0 & \Delta \mathrm{c}_{12} & 0 & 0\\
\Delta \mathrm{c}_{21} & 0 & 0 & 0\\
0 & 0 & 0 & 0\\
\Delta \mathrm{c}_{41} & 0 & 0 & \Delta \mathrm{c}_{44}
\end{pmatrix}
\tag{3.43}
$$

$$
\begin{aligned}
\Delta c_{12} &= C_{12}(-0.02\cos(5t) + 0.2\sin(50tu)),\\
\Delta c_{21} &= C_{21}(0.02\sin(5t) - 0.3\cos(40t)),\\
\Delta c_{41} &= C_{41}(0.03\cos(0.1t) - 0.4\cos(60w)),\\
\Delta c_{44} &= C_{44}(-0.02\sin(0.5tr) + 0.3\cos(80t))
\end{aligned}
\tag{3.44}
$$

Uncertain Equivalent Hydrodynamic Damping Matrix

$$
\Delta D = \begin{pmatrix}
\Delta \mathrm{d}_{11} & 0 & 0 & 0\\
0 & \Delta \mathrm{d}_{22} & 0 & 0\\
0 & 0 & \Delta \mathrm{d}_{33} & 0\\
0 & 0 & 0 & \Delta \mathrm{d}_{44}
\end{pmatrix}
\tag{3.45}
$$

$$
\begin{aligned}
\Delta d_{11} &= D_{11}(-0.02\cos(5t) + 0.2\sin(50tu)),\\
\Delta d_{22} &= D_{22}(-0.02\cos(5t) + 0.2\sin(50tu)),\\
\Delta d_{33} &= D_{33}(0.03\cos(0.1t) - 0.4\cos(60w)),\\
\Delta d_{44} &= D_{44}(-0.02\sin(0.5tr) + 0.3\cos(80t))
\end{aligned}
\tag{3.46}
$$

Uncertain Equivalent Hydrodynamic Hydrostatic Vector

$$
\Delta g = \begin{pmatrix}
\Delta \mathrm{g}_{11}\\
\Delta \mathrm{g}_{21}\\
\Delta \mathrm{g}_{31}\\
\Delta \mathrm{g}_{41}
\end{pmatrix}
\tag{3.47}
$$

$$
\begin{aligned}
\Delta g_{11} &= g_{11}(-0.02\cos(5t) + 0.2\sin(50tu)),\\
\Delta g_{21} &= g_{21}(0.02\sin(t) - 0.3\cos(40t)),\\
\Delta g_{31} &= g_{31}(0.03\cos(0.1t) - 0.4\cos(60w)),\\
\Delta g_{41} &= g_{41}(-0.02\sin(0.5tr) + 0.3\cos(80t))
\end{aligned}
\tag{3.48}
$$

Hence, the composed nominal and uncertain dynamics is given now given by:

$$\dot{\eta} = (J + \Delta J)\nu$$

$$(\mathrm{M} + \Delta M)\dot{\nu} + (C(\nu) + \Delta C)\nu + (D(\nu) + \Delta D)\nu + (g(\eta) + \Delta g) = \tau \tag{3.49}$$

For convinience let us define $M_c = M + \Delta M, C_c = C(\nu) + \Delta C, D_c = D(\nu) + \Delta D, g_c = g(\eta) + \Delta g$.

3.4.4 OUTLAND 1000 Input Dynamics

Coming up to the last section of this chapter, let us recall comments done in chapter 1 and section 3.3 about input dynamics, which stated and described the influence of the vehicle geometry, architecture, and installed hardware over the relation of actuators control inputs and the desired forces and torques. The OUTLAND-1000 is designed such that the actual dynamics and kinematics of the robot can be reduced from a 6DOF to a 4DOF; therefore, the control problem of the OUTLAND-1000 is also simplified from an underacted to a fully acted control problem. In figure 3.1 it can be observed the actuator (thrusters) configuration of the studied robot.

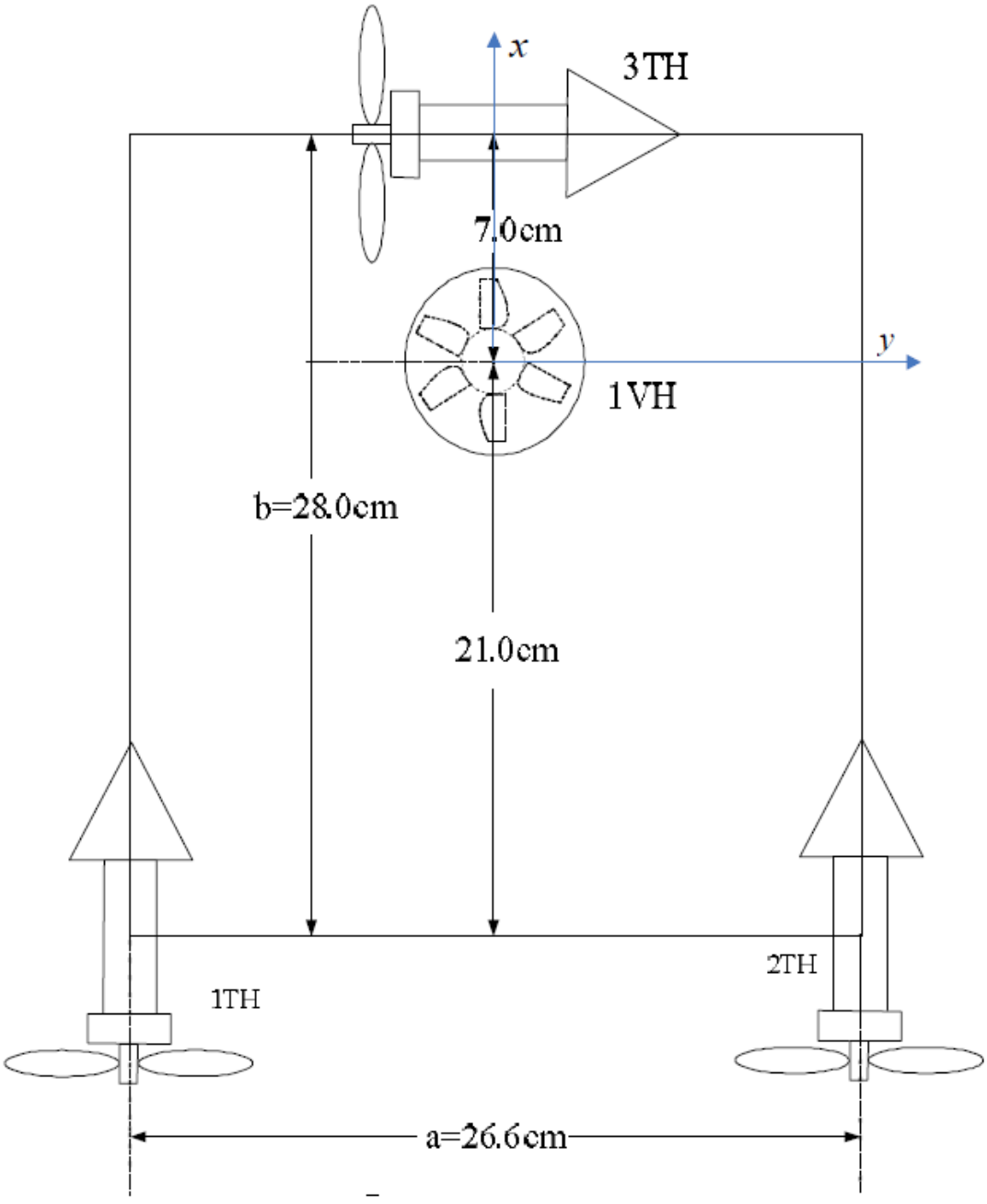

Figure 3.4: Thrusters configuration taken from [34] ©2021 Outland Technology, Inc.

In [1] it is mentioned that thrusters inputs (voltage) and thrust force given by the actuators are highly nonlinear. This relation is usually needed to be estimated experimentally and then modeled by applying data analysis and model approximation techniques. However, for the proposes of this work, according to [34] the generated force F_T is directly proportional to the square of motor rotational speed(ω). Moreover, generated moments by thrusters are given are said to be $M_T = r \times F_T$ where $r = [r_x, r_y, r_z]^T$ is the position of the actuator respect the origin of the body-fixed reference frame. Therefore the i_{th} forces and moments are given by:

$$F_{Ti} = k_1 \omega_i^2 = k u_i^2 \Rightarrow \omega_i = k_2 u_i \Rightarrow \lambda = k_1 k_2^2 \Rightarrow M_{Ti} = r_i \times k u_i^2 \tag{3.50}$$

Therefore the total input vector adapted to given OUTLAND-1000 configuration presented above is given as follows:

$$\tau = \begin{pmatrix} \tau_X \\ \tau_Y \\ \tau_Z \\ \tau_N \end{pmatrix} = \begin{pmatrix} \lambda & \lambda & 0 & 0 \\ 0 & 0 & \lambda & 0 \\ 0 & 0 & 0 & \lambda \\ \frac{a\lambda}{2} & -\frac{a\lambda}{2} & \lambda\ (b-21) & 0 \end{pmatrix} \begin{pmatrix} {u_1}^2 \\ {u_2}^2 \\ {u_3}^2 \\ {u_4}^2 \end{pmatrix} \equiv Bu \tag{3.51}$$

In order to give a conclusive remark to this chapter, the nonlinear state-space model that is going to be used later in this work for control proposes is finally presented as follows:

$$\dot{\eta} = J_c \nu \tag{3.52}$$

$$\dot{\nu} = M_c^{-1}(-C_c \nu - D_c \nu - g_c + \tau + \Delta\tau) \tag{3.53}$$

Chapter 4

Guidance and Control

In Chapter 3 it was developed the dynamical model of a UAUV.In fact, from work done in this chapter, the reader may already have an idea of what are the challenges to be addressed by the control scheme that will be proposed in this chapter 4. The chosen control strategies must be advanced enough to handle the highly nonlinear UAUV dynamics and robust enough to deal with unpredictable external disturbances. Such as the one produced by ocean currents, waves, wind, and vortex shedding.

In this chapter, further comments on guidance and control of UAUV's will be stated, and suitable control strategies for trajectory and source tracking will be studied for them to be implemented on the dynamics of the OUTLAND-1000.

4.1 System Stability of Underwater Vehicles

There exists some kind of confusion when marine vehicle stability is on the table. For instance, a naval architect is asked to give some notions on ships stability which with a high level of certainty, he/she will come up with concepts, such as stability plane, healing angles, and aligning moments which are all associated with the ships

hydrostatics. In contrast, a mechanical engineer would give up some comments on the boundedness of the kinematics and dynamics of the vehicle. Indeed both approaches are right depending on the study area; however, both are complementary to each other. Therefore, for nomenclature convenience for now on in this work, stability will be accepted as the ability of the vehicle to return to an equilibrium state of motion after a disturbance without any corrective action; whereas the capability to carry out specific maneuvers will be defined as maneuverability, [2] [3].

A more general study would be to study the system behavior under two specific conditions defined as controls-fixed stability and controls-free stability.

4.1.1 Controls-Fixed Stability

This stability study, also known as open-loop stability analysis considers the response of the vehicle when actuators (thrusters and surfaces) set in a constant position. Since the dynamics of a UAUV is nonlinear, a stability analysis based on Lyapunov's direct method is applied.

In order to study open-loop stability for marine vehicles, the total mechanical energy is said to be a suitable Lyapunov candidate to define the region under the system as stable at a constant input condition.

$$V(\eta, \dot{\eta}) = \frac{1}{2}\dot{\eta}^T M_\eta \dot{\eta} + \int_0^\eta g_\eta^T(z)\, dz \tag{4.1}$$

for $\tau_\eta = \tau(\eta) + \Delta\tau(\eta, t) = 0$, and $M_\eta, g_\eta(z)$ are the inertia matrix and hydrostatic vector represented in the earth fixed coordinate system.

An extensive and detailed analysis and manipulations regarding open-loop stability are made in [2] to end up with the following conditions for the system to achieve open-loop stability:

- $V = 0$ for $\dot{\eta} = \eta = 0$
- For $V > 0, \forall \dot{\eta}, \eta \in R^n$ the inertia matrix is symmetric and positive definite, i.e., $M = M^T > 0$
- $\dot{V} < 0, \forall \nu \in R^n$ if and onlu if the damping matrix is positive definite, i.e., $D(\nu) > O$
- $V \to \infty$ as $||\eta|| \to \infty$ and $||\dot{\eta}|| \to \infty$

4.1.2 Controls-Free Stability

Also known as closed-loop stability considers the dynamics of the control inputs have to be considered in the stability analysis. A typical way to come up with a description of this analysis is to consider a tracking problem.

Let us define $e_\nu = \nu(t) - \nu_d(t)$ as the kinematic tracking error function where $\nu_d(t)$ is the desired state vector.Moreover, the following Lyapunov function is proposed:

$$V(e,t) = \frac{1}{2} e^T M e \tag{4.2}$$

Taking the first time derivative of equation (4.2)

$$\dot{V} = e^T M \dot{e} \tag{4.3}$$

substitute equation (3.53) into (4.3) , so that:

$$\dot{V} = e^T[\tau - M\dot{\nu_d} - C(\nu)\nu_d - D(\nu)\nu_d - g(\eta] - e^T D(\nu)e \tag{4.4}$$

By invoking Coriolis matrix skew-symmetric property, then, $e^T C(\nu)e = 0, \forall e \in R^n$ can be also concluded. Therefore, in order to meet Lyapunov's stability criteria, the control law can be primarily suggested as follows:

$$\tau = M\dot{\nu_d} + C(\nu)\nu_d + D(\nu)\nu_d + g(\eta) - K_d e \tag{4.5}$$

where K_d is non negative gain matrix. Hence,

$$\dot{V} = -e^T[D(\nu) + K_d]e \leq 0 \tag{4.6}$$

where $K_d > 0$ is known as the "Slotine and Li algorithm" regulator gain matrix.

This Lyapunov-based analysis shows a typical structure for the control input τ that handles to linearize the dynamics of the vehicle since the velocity gives the reference commands and angular velocity vector $\nu = [\nu_1, \nu_2]^T$. However, the main interest of this work is to control the variables inside the position vector $\eta = [\eta_1, \eta_2]^T$. Therefore, the control strategies to be presented in this work will be based on a combination of exact linearization and backstepping techniques.

4.2 State Feedback Stabilization Based on Backstepping

In this section, theoretical background on backstepping is presented to summarize the foundations and structures required to formulate a backstepping feedback stabilization control so that for this proposal, the same nomenclature that is used by Khalil in [36] is implemented for consistency interests. Yet, in further sections of this work, every control formulation will be adapted to the notation used up to this point.

Consider a cascade nonlinear dynamical system which form definition is said to be the system that one of its states is the control input of the following state in the subsequent dynamical system. In other words, consider the following system:

$$\dot{\eta} = f_a(\eta) + g_a(\eta)\xi \tag{4.7}$$

$$\dot{\xi} = f_b(\eta, \xi) + g_b(\eta, \xi)u \tag{4.8}$$

where $\eta \in R^n$, $\xi \in R^1$ is the virtual input and $u \in R^1$ is the actual control input. Moreover, it is assumed the ξ is stabilized by a smooth state feedback control $\xi = \phi(\eta)$ with $\phi(0) = 0$ which allows the origin of 4.9 to be asymptotically stable.

$$\dot{\eta} = f_a(\eta) + g_a\phi(\eta), f_a(0) = 0 \tag{4.9}$$

To prove that the statement above is true, suppose that there exists a smooth and positive definite Lyapunov function $V_a(\eta)$ that satisfies:

$$\frac{\partial V_a}{\partial \eta}\dot{\eta} = \frac{\partial V_a}{\partial \eta}[f_a(\eta) + g_a(\eta)\phi(\eta)] \leq -W(\eta) \tag{4.10}$$

where $W(\eta)$ is positive definite. Futhermore, applying some algebraic manipulations in (4.7) by adding and subtracting $g_a(\eta)\phi(\eta)$ on the RHS of (4.7) results in:

$$\dot{\eta} = f_a(\eta) + g_a(\eta)\phi(\eta) + g_a(\eta)[\xi - \phi(\eta)] \tag{4.11}$$

Now consider the following a new error variable $z = \xi - \phi(\eta)$ which arrives in the system:

$$\dot{\eta} = f_a(\eta) + g_a(\eta)\phi(\eta) + g_a(\eta)z \tag{4.12}$$

$$\dot{z} = f_b(\eta, \xi) - \frac{\partial \phi}{\partial \eta}[f_a(\eta) + g_a(\eta)\phi(\eta) + g_a(\eta)z] + g_b(\eta, \xi)u \tag{4.13}$$

Up to this point, in order to study the overall stability of the system, let us define the following Lyapunov function candidate:

$$V(\eta, \xi) = V_a + \frac{1}{2}z^2 \tag{4.14}$$

Hence:

$$\begin{aligned}\dot{V} = &\frac{\partial V_a}{\partial \eta}[f_a(\eta) + g_a(\eta)\phi(\eta)] + \frac{\partial V_a}{\partial \eta}g_a(\eta)z \\ &+ z[f_b(\eta, \xi) - \frac{\partial \phi}{\partial \eta}[f_a(\eta) + g_a(\eta)\phi(\eta) + g_a(\eta)z]] + zg_b(\eta, \xi)u \leq \\ &- W(\eta) + z[\frac{\partial V_a}{\partial \eta}g_a(\eta) + f_b(\eta, \xi) - \frac{\partial \phi}{\partial \eta}[f_a(\eta) + g_a(\eta)\phi(\eta) + g_a(\eta)z] + g_b(\eta, \xi)u]\end{aligned} \tag{4.15}$$

In order to stabilize the system, u is chosen so that $\dot{V}$ is negative definite in η and ψ

$$u = -\frac{1}{g_b(\eta, \xi)}[\frac{\partial V_a}{\partial \eta}g_a(\eta) + f_b(\eta, \xi) - \frac{\partial \phi}{\partial \eta}[f_a(\eta) + g_a(\eta)\phi(\eta) + g_a(\eta)z] + Kz], \tag{4.16}$$

for $K \geq 0$ that yields:

$$\dot{V} \leq -W(\eta) - Kz^2 \tag{4.17}$$

Therefore, if such a $V_a(\eta)$ and $V(\eta, \xi)$ can be defined, then the origin $(\eta = 0, z = 0)$ is asymptotically stable and since $\phi(0) = 0$, it can be implied that the origin of the original system $(\eta = 0, \xi = 0)$ is also asymptotically stable. Additionally, if it is able to proof that $V_a(\eta)$ is radially unbounded, then the global origin of the system is globally asymptotically stable.

4.3 Hierarchical Backstepping Control Applied to OUTLAND-1000

In this section, it is embraced the fact that the implementation sometimes is unfeasible for some control design purposes, especially for those systems where input coupling cannot be neglected [37]. This fact is indeed one of the main reasons that most of the literature states the restriction that the UAUV must be fully actuated by either control surfaces or thrusters or a combination of both.

In 4.2 the central notions of backstepping Lyapunov-based control are formulated. The reader may have noticed that input "u" is defined as a scalar which for our system, which at least has 4-DOF, is not enough. Nonetheless, plenty of work has been done in [19] to [37] to evaluate the effectiveness of backstepping approaches on underwater vehicles showing some promising results in trajectory tracking and formation maneuvers of multiple UAUV's.

Control Problem Formulation for OUTLAND-1000

As it was mentioned in previous sections, all nomenclature exposed by Khalil in [36] will be updated and adapted to the convention used during most of this work, and similarly, since the control formulation in this section is based on [20], its nomenclature and variables will be adjusted as well.

According to the reduced dynamics of the OUTLAND-1000 described in 3 let us define $\eta_d = [x_d, y_d, z_d, \psi_d]^T$ as the reference or desired position vector and its respective error tracking function $e = [e_x, e_y, e_z, e_\psi]^T$. In addition, based on kinematics a desired body-fixed velocity vector ν_d can be approach from η_d and its derivative as it can be seen:

$$\begin{gathered} u_d = \dot{x_d}\cos(\psi_d) + \dot{y_d}\sin(\psi_d) \\ \mathrm{v}_d = -\dot{x_d}\sin(\psi_d) + \dot{y_d}\cos(\psi_d) \\ \mathrm{w}_d = \dot{z_d} \\ \mathrm{r}_d = \dot{\psi_d} \end{gathered} \tag{4.18}$$

However, velocities tracking error will be defined as the difference of the actual velocities of the UAUV respect a virtual control input given as follows:

$$\nu_c = J^{-1}(\dot{\eta_d} + Ke) \tag{4.19}$$

Then, the velocity control is said to be $e_\nu = \nu_c - \nu$ so that $e_\nu = [e_u, e_v, e_w, e_\psi]^T$.

Notice that at this stage of the problem formulation the uncertain kinematic term ΔJ has been ignored. In addition, due to OUTLAND-1000 reduced kinematics it can be concluded the $J \in R^{4\times4}$ is a positive, always ivertible matrix and K a positive definite diagonal Matrix.

Looking at the system exposed in (3.52) and (3.53) it can be observed that the dynamics and the dynamics of OUTLAND-1000 fits the main structure requirement of the backstepping control approach. Therefore, to prove that this method can be applied for this UAUV, the following Lyapunov candidate function is defined for the system kinematics.

$$V_a = \frac{1}{2} e^T e \tag{4.20}$$

Then, by taking the derivative of V_a it is obtained:

$$\begin{aligned}
\dot{V_a} &= e^T(\dot{\eta_d} - J_c\nu) \\
\dot{V_a} &= e^T[\dot{\eta_d} - (J + \Delta J)J^{-1}(\dot{\eta_d} + Ke)] \\
\dot{V_a} &= e^T[-Ke - \Delta J J^{-1}(\dot{\eta_d} + Ke)] \\
\dot{V_a} &= -e^T Ke - e^T \Delta J J^{-1}(\dot{\eta_d} + Ke) \leq -\alpha||e||^2 + \beta||e|| = -\alpha||e||(||e|| - \frac{\beta}{\alpha})
\end{aligned} \tag{4.21}$$

where $\alpha = \lambda_{min}[K + \Delta J J^{-1} K] > 0$ and $\beta = max||\Delta J J^{-1}\dot{\eta_d}||$. Therefore, since $||e|| \geq \frac{\beta}{\alpha}$ then, $\dot{V_a} \leq 0$ as $t \to \infty$ [20], so it can be shown that V_a is bounded as well it can be implied that e is ultimately unbounded.Hence, this virtual control input ν_c can be implemented as the virtual reference velocity input similarly as it is work out in [20], [34], [37].

Now moving forward, the control input τ in system dynamics (3.53) is designed to stabilize the virtual reference velocity ν_c based on the backstepping method as

follows:

$$\tau = M(\dot{\nu_c} + K_1 e_\nu) + C(\nu)\nu + D(\nu)\nu + g(\eta) \tag{4.22}$$

where K_1 is a properly dimensioned positive diagonal matrix, to further proceed with the stability analysis, the overall Lyapunov function is also defined as the backstepping method described, then:

$$V(\eta, \nu) = V_a + \frac{1}{2} e_\nu^T e_\nu \tag{4.23}$$

To continue the analysis the first time derivative of V is taken:

$$\begin{aligned}
\dot{V}(\eta, \nu) &= \dot{V_a} + e_\nu^T [\dot{\nu_c} - (M + \Delta M)^{-1} [M(\dot{\nu_c} + K1 e_\nu) - \Delta C\nu - \Delta D\nu - \Delta g] \\
&= \dot{V_a} + e_\nu^T [\dot{\nu_c} - (M^{-1} + X)[M(\dot{\nu_c} + K_1 e\nu) - \Delta C\nu - \Delta D\nu - \Delta g]] \\
&= \dot{V_a} + e_\nu^T [-(K_1 + XMK_1)e_\nu - XM\dot{\nu_c} + (M^{-1} + X)(\Delta C\nu + \Delta D\nu \Delta g)] \\
&\leq \dot{V_a} - \Gamma_1 ||e_\nu||^2 + \Gamma_2 ||e_\nu|| \leq -\alpha ||e|| (||e|| - \frac{\beta}{\alpha}) - \Gamma_1 ||e_\nu|| (||e_\nu|| - \frac{\Gamma_2}{\Gamma_1})
\end{aligned} \tag{4.24}$$

where $X = -(I + M^{-1}\Delta M)^{-1} M^{-1} \Delta M M^{-1}$. $\Gamma_1 = \lambda_{min}[K_1 + XMK_1]$ and $\Gamma_2 = \max[||-XM\dot{\nu_c} + (M^{-1} + X)(\Delta C\nu + \Delta D\nu + \Delta g)||]$. Hence, since $||e|| \geq \frac{\beta}{\alpha}$ is satisfied and $||e_\nu|| \geq \frac{\Gamma_2}{\Gamma_1}$ implies that $V(\dot{\eta}, \nu) \leq 0$ as $t \to \infty$ then it can be finally concluded that $V(\eta, \nu)$ is bounded.

4.4 Backstepping Trajectory Tracking (Numerical Results)

4.4.1 Circular Trajectory Tracking

In this section, to study the performance and robustness, the proposed Dynamical model and its control law are simulated. In this section, it can be seen how the system performs for tracking a circular helical trajectory with disturbances given by :

$$\eta_d(circle) = \left[a\sin\left(\frac{2\pi t}{T_{circle}}\right), -a\cos\left(\frac{2\pi t}{T_{circle}}\right), z_d(t), \psi_d(t)\right]^T \tag{4.25}$$

Where a is the radius of the circle,T_{circle} is the circular period,z_d is the desired water depth which for the proposed of following a helical trajectory it should be defined as a linear function $z_d(t) = m_1 t + b_1$ and, ψ_d is desired yaw angle which for seeking of stability will be given as linear function as well $\psi_d = m_2 t + b_2$

Results that are shown up are gotten from using simulations parameters in Appendix A.1.2

Let the initial position and orientation of the vehicle to be $\eta(0) = [10, 10, 1, 0]$ and the reference desired trajectory and orientation to be chosen as:

$$\eta_d = [2\sin(0.5t), -2\cos(0.5t), 0.1t, 0.5t] \tag{4.26}$$

The tracking responses of trajectory and virtual velocity for the AUV system are shown in the following set of figures.

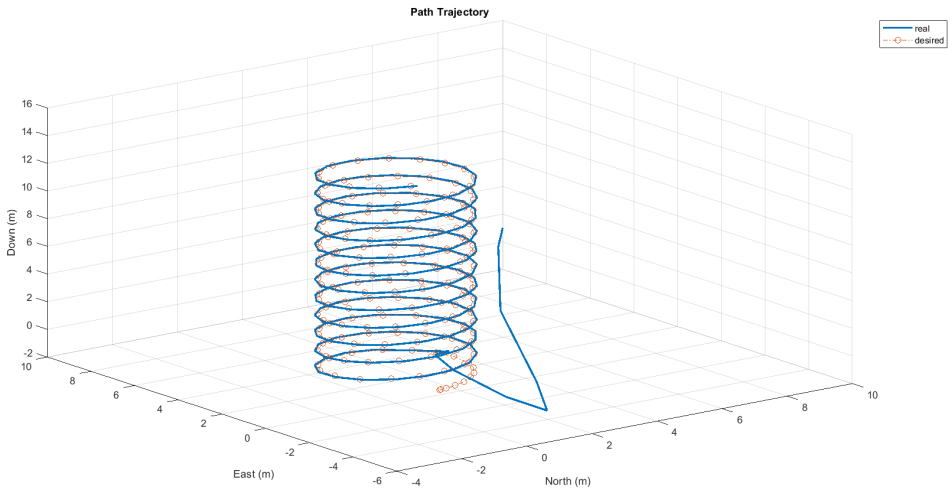

Figure 4.1: Circular helix trajectory-tracking.

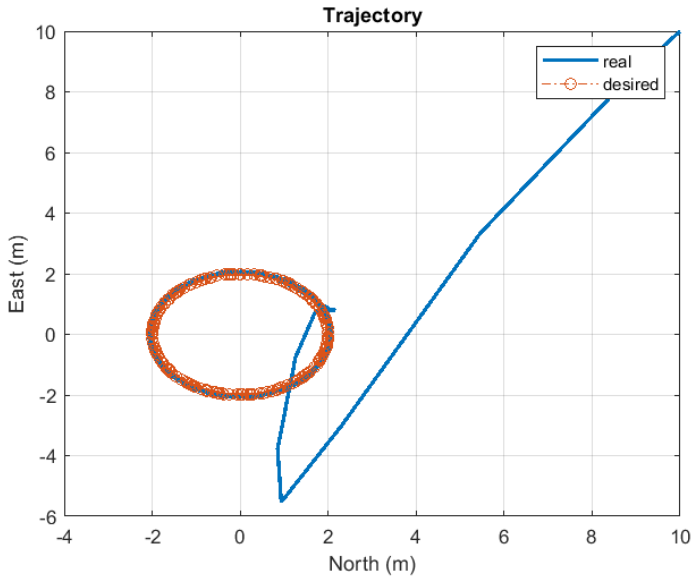

Figure 4.2: Circular plane trajectory-tracking.

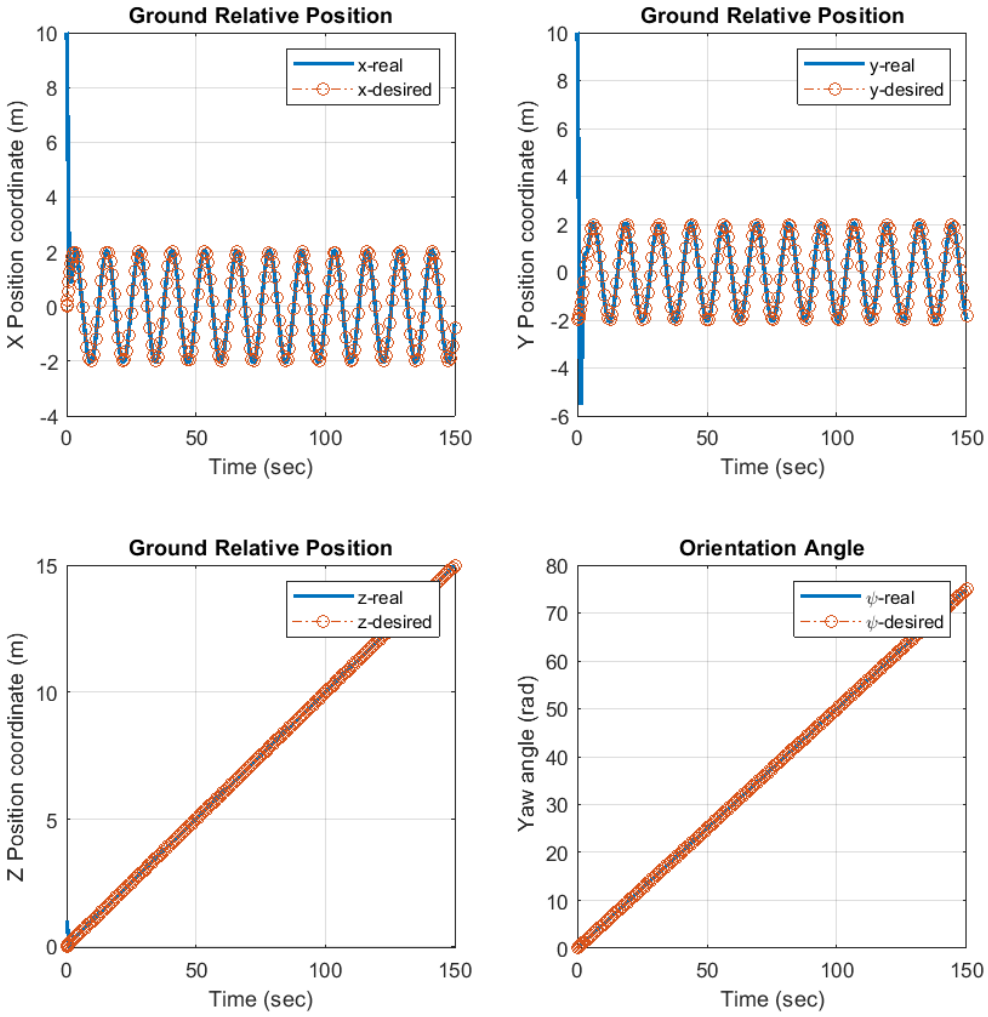

Figure 4.3: Tracking responses of reference positions for circular trajectory.

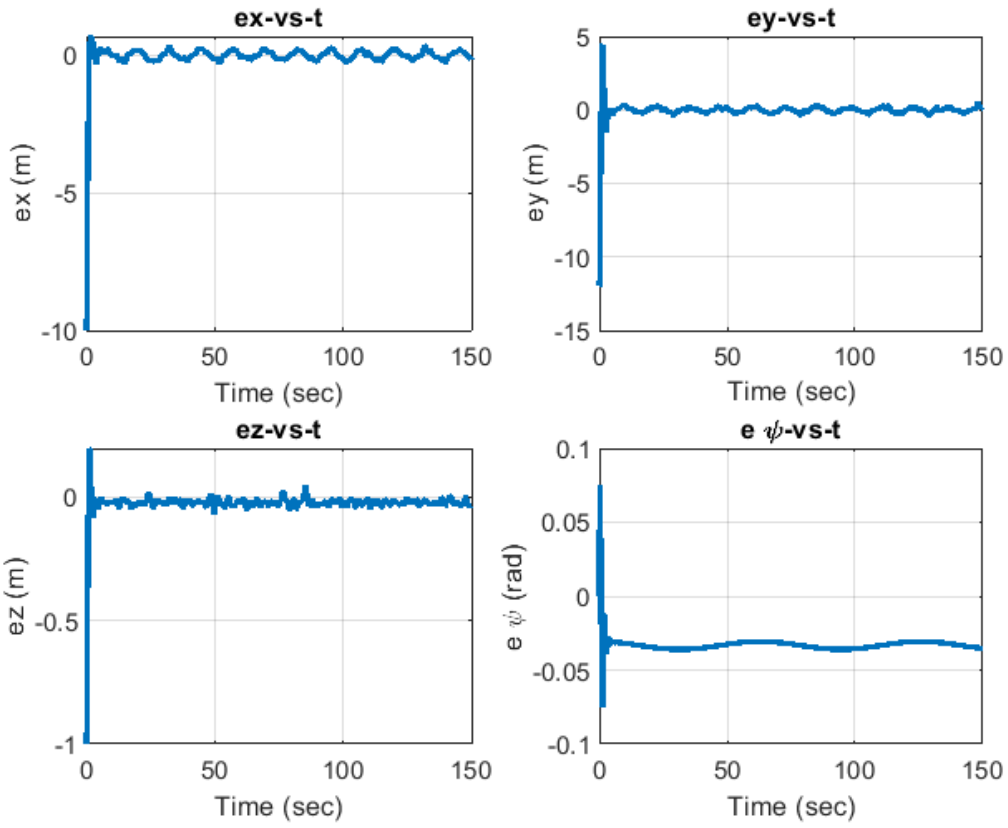

Figure 4.4: Tracking errors with disturbances for circular tracking.

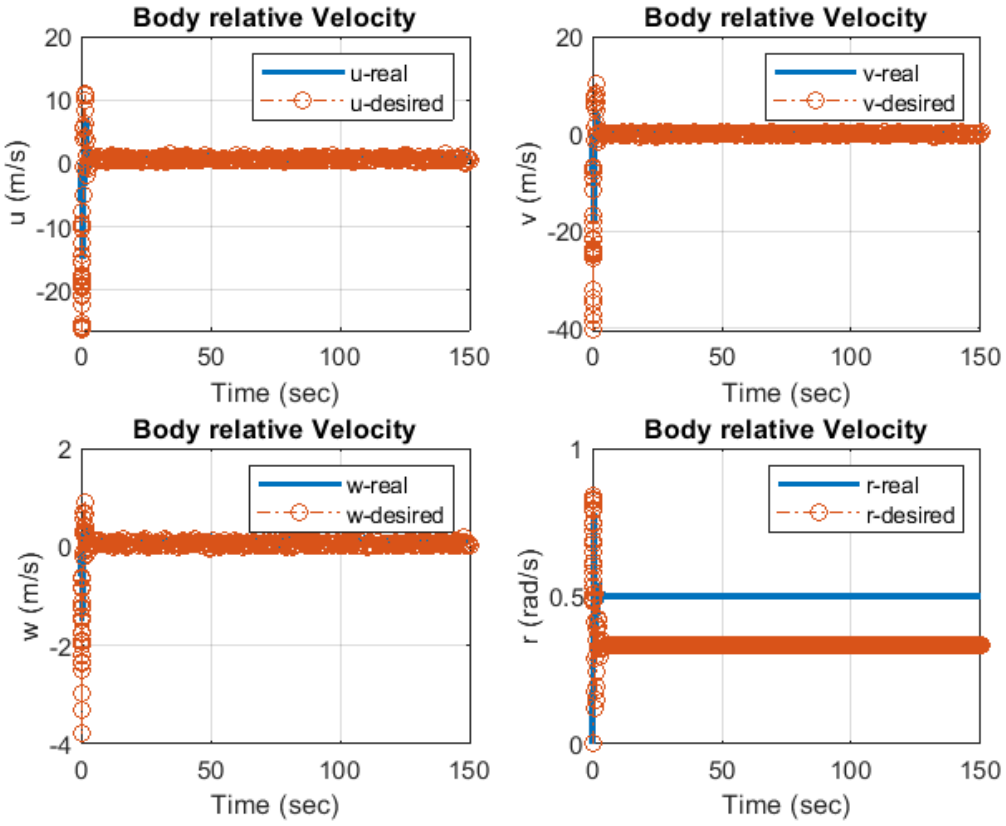

Figure 4.5: Tracking responses of virtual reference velocities for circular tracking.

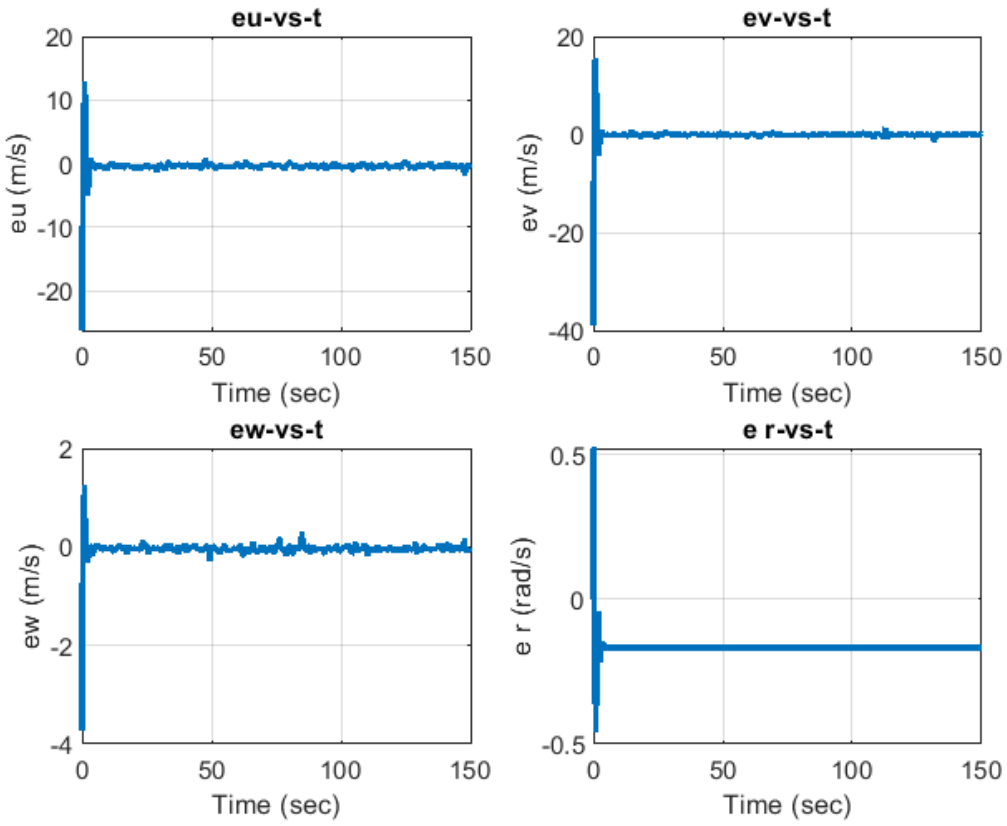

Figure 4.6: Tracking errors of virtual reference velocities for circular trajectory.

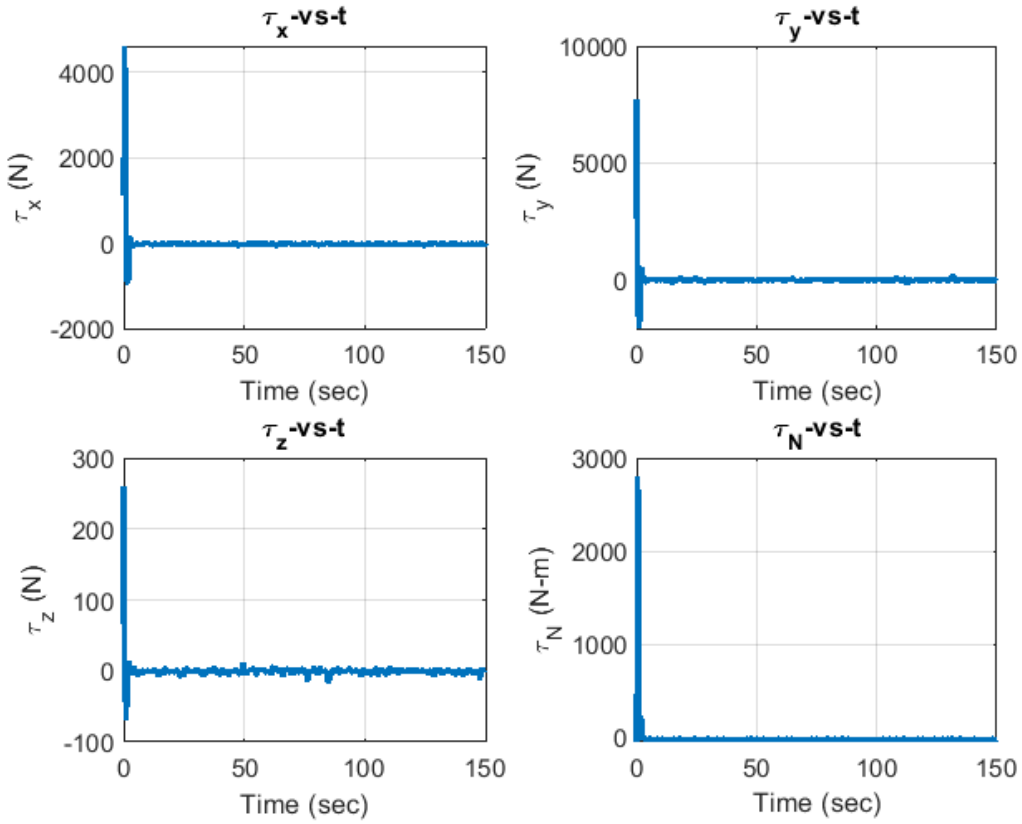

Figure 4.7: Control signals: Total surge thrust τ_x, sway thrust τ_y, yaw torque τ_N, heave thrust τ_z for circular tracking.

4.4.2 Spiral Trajectory Tracking

A little more complex spiral trajectory is being tracked in this study to demonstrate that the control scheme applied in this work produces a well-behaved, smooth transient response and quick convergence of tracking errors near the origin.

The spiral trajectory that is desired to track in this section is given by:

$$\eta_d = [t\sin(0.1t), -t\cos(0.1t), 0.1t, 0.5t] \tag{4.27}$$

For the exact same set of initial conditions studied in the circular trajectory tracking in the last section.

The reader should notice that control gains must be modified to get a feasible performance of system state variables for the system to follow this new trajectory. Simulation parameters can be found in Appendix A.1.3

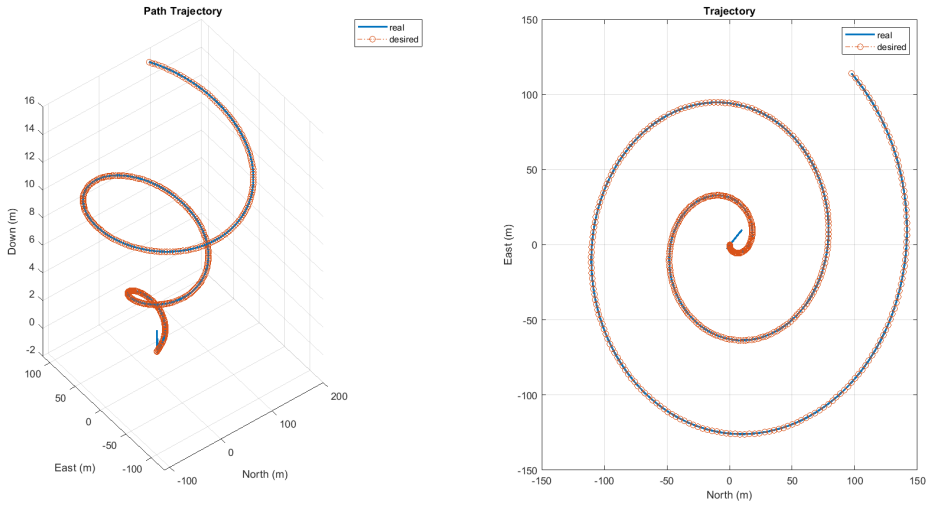

Figure 4.8: Path Trajectory-Tracking for spiral trajectory.

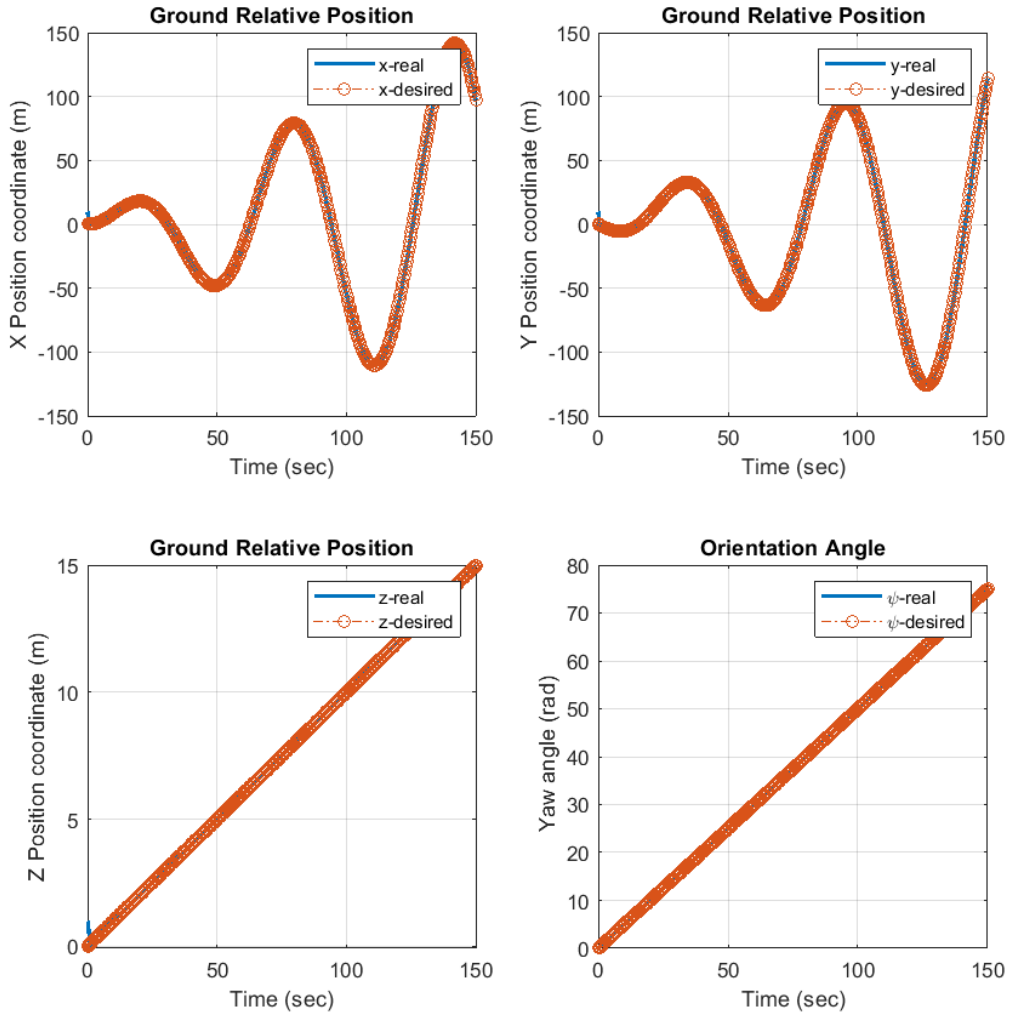

Figure 4.9: Tracking responses of reference positions for spiral trajectory.

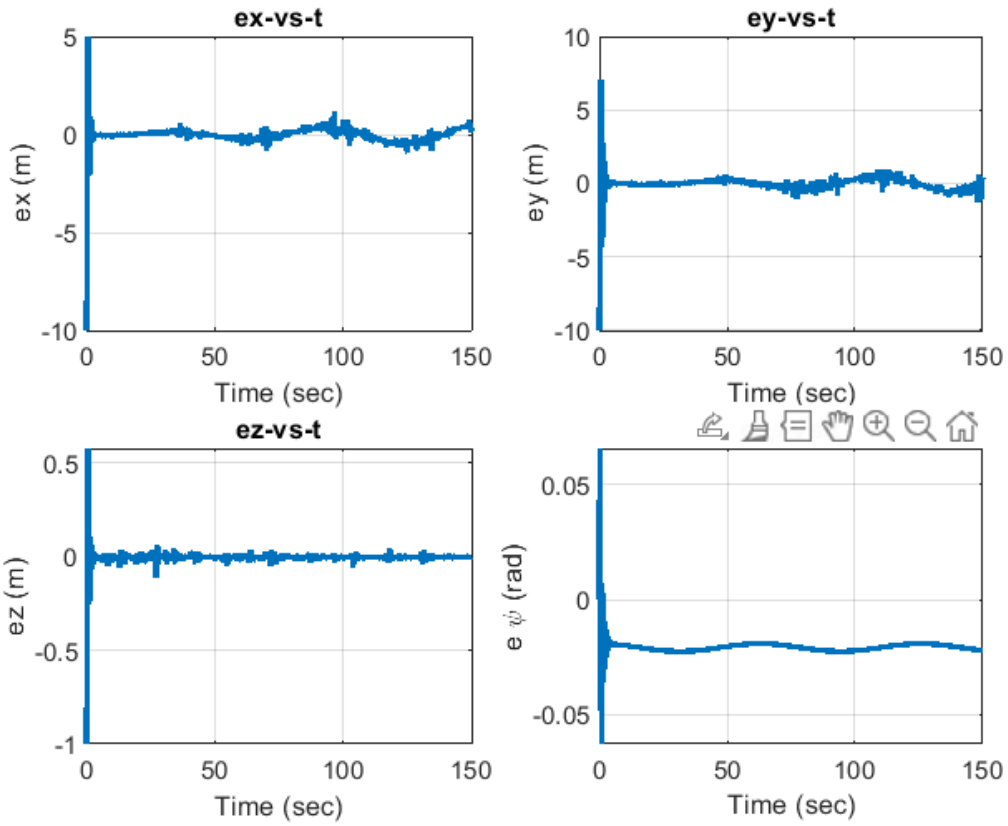

Figure 4.10: Tracking errors with disturbances for spiral tracking.

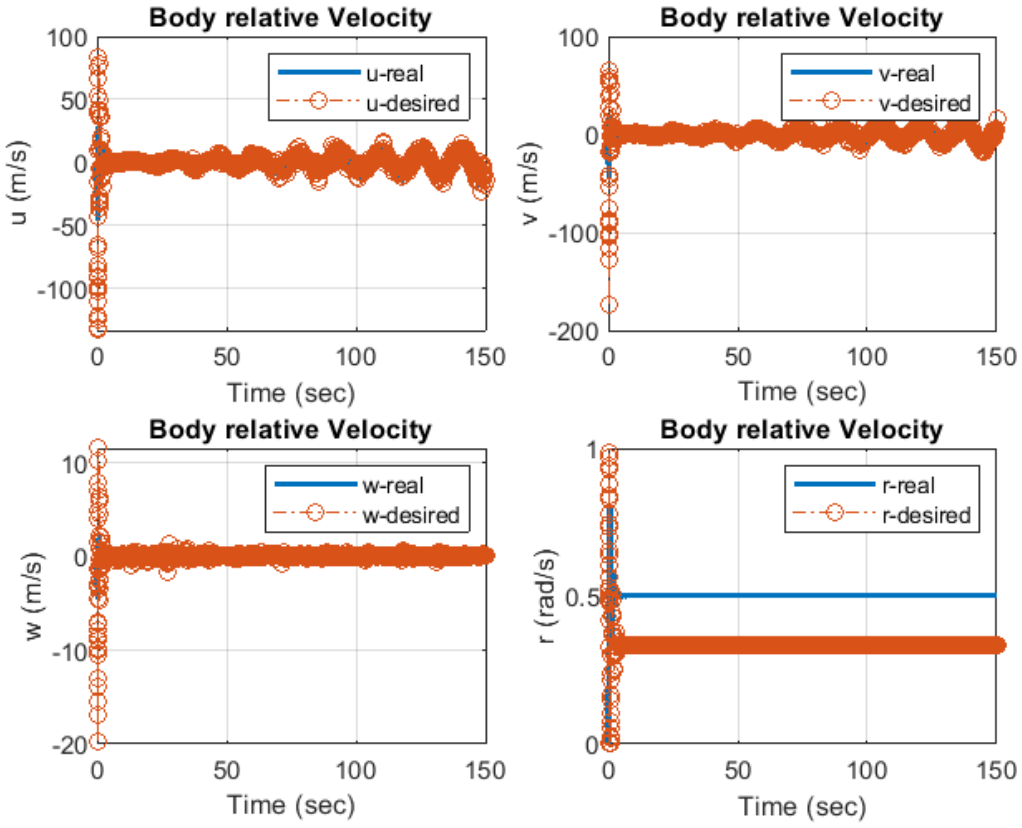

Figure 4.11: Tracking responses of virtual reference velocities for spiral trajectory.

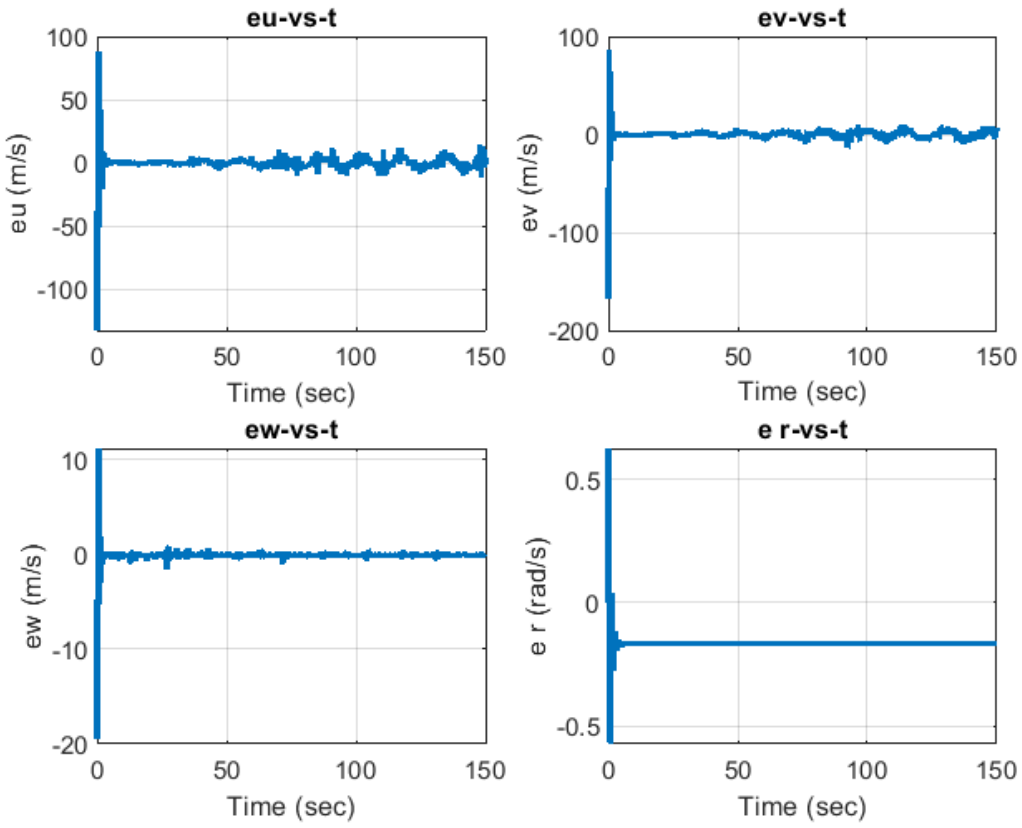

Figure 4.12: Tracking responses of virtual reference velocities for spiral trajectory.

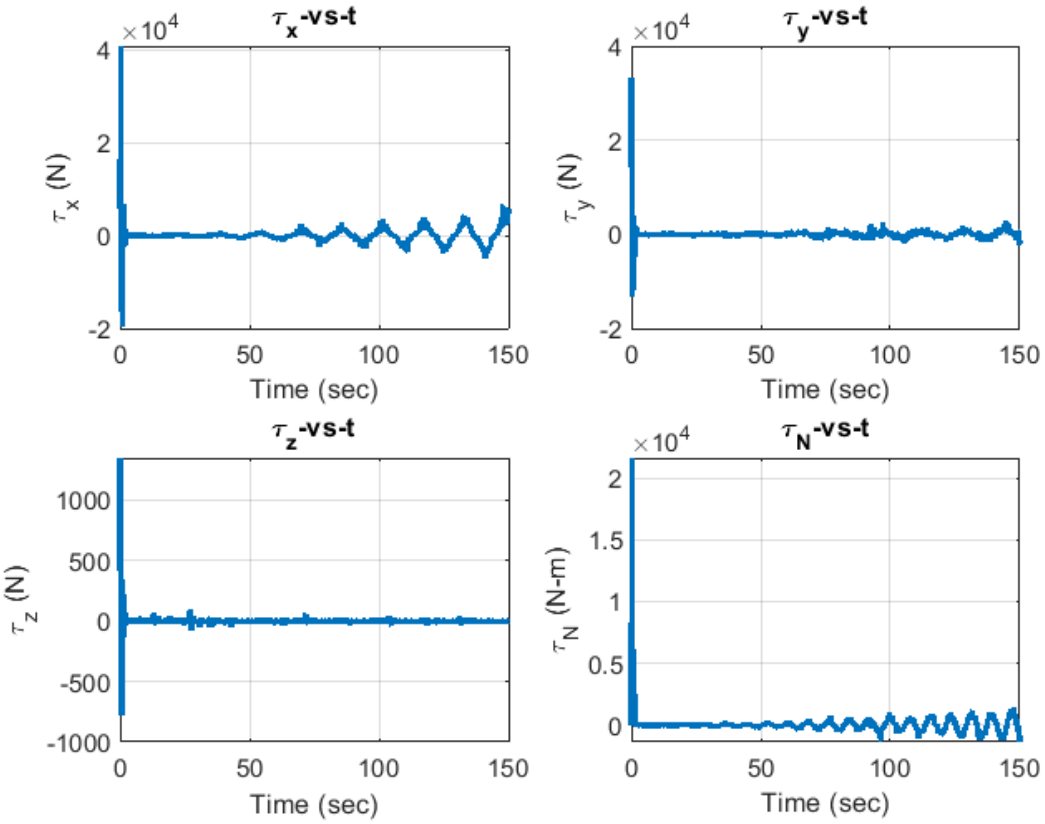

Figure 4.13: Control signals: Total surge thrust τ_x, sway thrust τ_y, yaw torque τ_N, heave thrust τ_z for spiral tracking.

4.4.3 Backstepping Control Simulation results

From figures 4.1,4.2, and 4.8, it can observed the effectiveness of the control strategy proposed. In addition,regarding system robustness, in Figures 4.3,4.4,4.5,4.6,4.9,4.10, 4.11, and 4.12 it can be also seen that not only the trajectory tracking responses, but also virtual reference velocities are demonstrated to be satisfactory in terms of convergence. The system's performance and stability can be improved by modifying the control parameters in the respective gains K and K_1. However, the main drawback of this backstepping control approach becomes evident newly in Figures 4.5, and 4.11 where it can be implied the instantaneous high energy demand imposed on the actuators for the system to meet the desired virtual reference velocity values. Therefore, this side effect could yield the system simulation to reach physically unfeasible values depending on the control gains proposed and path trajectory complexity. Furthermore, an interesting comparison on how the control inputs behave with respect to the complexity of the trajectory is shown in Figures 4.7 and 4.13. In fact, in this study, it can be appreciated that control efforts tend to be larger for the spiral trajectory than circular trajectory tracking since control grain are required to be larger for the system to track a spiral trajectory properly.

To provide a closure to this section, it has to be said that if a Hierarchical-Backstepping control structure is applied, a compromise must be set up for acceptable ranges of performance and stability due to its robustness and fast convergence. Further in this work, input and output variables responses under this control approach will be studied for source tracking and estimation duties.

4.5 Integrated Backstepping and Sliding Mode Tracking Control

For the propose of trajectory tracking, backstepping techniques are widely used; however, numerical experiments made in the previous section and most of the literature are agreed when they state the most apparent disadvantage of this kind of algorithm, which is the fact that the relationship of the velocity control with state errors generates, physically unfeasible large velocities for significant initial state errors as well as sharp speed jumps for sudden tracking errors. Thus, one can say that the best feature of the backstepping method is also its principal flaw depending on the application.

Since the main objective of this work is that our vehicle can track and follow a moving oil plume on the surface of an open channel, then the probability that the system encounters significant initial tracking errors and sudden disturbances are high. Therefore, finding a suitable solution to overcome those impractical speed jumps result from the backstepping method becomes essential for the proposes of this work. Throughout the years multiple approaches have been suggested, some of them in the field of fuzzy logic algorithms, and most recently, neural networks algorithm [34]. [38], [39], [40], [41]. However, in order to tackle this drawback an integrated cascaded control for the kinematics and dynamics based on a bio-inspired backstepping model and sliding mode control is presented for the 4-DOF tacking control of the OUTLAND-1000.

4.5.1 Sliding Mode Control

Before going any further, this section will be focused on defining the foundations of sliding mode control methods. Similarly, as it was done in section4.2 the same nomenclature utilized by Khalil in [36] is taken to introduce the sliding mode control method, then it will be adapted to the nomenclature currently used in this work.

In [36] the sliding mode control is motivated through the following example:

Let us consider:

$$\dot{x_1} = x_2 \tag{4.28}$$

$$\dot{x_2} = h(x) + g(x)u \tag{4.29}$$

where h and g are unknown locally Lipschitz function and $g(x) \geq g_0 > 0 \forall x$. In this case, a state feedback controller is desired to stabilize the origin. This proposal assumes that a controller that constrains the trajectory within a manifold $s(t)$ can be designed. The manifold or time-varying surface is given as follows:

$$s = ax_1 + x_2 = 0 \tag{4.30}$$

Thus, the motion is governed by $\dot{x_1} = -ax_1$ which by choosing $a > 0$, then $x(t) \to 0$ is guaranteed as $t \to \infty$. Additionally, the rate of convergence can be controlled by the right choice of a. In fact, it can be seen that the motion on the manifold $s = 0$ is independent of h and g.Now, the objective that is needed to follow is to keep the trajectory within the manifold. Hence, the first derivative of the manifold is studied.

$$\dot{s} = a\dot{x_1} + \dot{x_2} = a_x 2 + h(x) + g(x)u \tag{4.31}$$

where h and g are said to satisfy:

$$|\frac{ax_2 + h(x)}{g(x)}| \leq \rho(x), \forall x \in R^2 \tag{4.32}$$

for some known function $\rho(x)$

Now let us define the following Lyapunov function candidate:

$$V(s) = \frac{1}{2}s^2 \tag{4.33}$$

Hence,

$$\begin{aligned} \dot{V} &= s\dot{s} \\ &= sax_2 + sh(x) + sg(x)u = s\frac{ax_2 + h(x)}{g(x)}g(x) + sg(x)u \\ &\leq |s||\frac{ax_2 + h(x)}{g(x)}|g(x) + sg(x)u \leq |s|\rho(x)g(x) + sg(x)u \end{aligned} \tag{4.34}$$

Consequently, control u is chosen such that the term $sg(x)u$ is negative and dominates $|s|\rho(x)g(x)$ whenever $|s| \neq 0$, so stability is achieved. In addition, the net negative term to force $|s|$ to zero is wanted to do so in a finite time. This can be achieved by taking:

$$u = -\beta(x)\,\mathrm{sign}(s) \tag{4.35}$$

Where function $\beta(x) : \beta(x) \geq \rho(x) + \beta_0$ for $\beta_0 > 0$ Therefore, whenever $|s| \neq 0$, we have:

$$\begin{aligned} \dot{V} \leq |s|\rho(x)g(x) + sg(x)u &= |s|\rho(x)g(x) - g(x)\beta(x)\,\mathrm{sign}(s) \\ &\leq |s|\rho(x)g(x) - g(x)s(\rho(x) + \beta_0)\,\mathrm{sign}(s) \\ &= g(x)\beta_0|s| \leq -g_0\beta_0|s| \end{aligned} \tag{4.36}$$

Thus, $W = \sqrt{2V} = |s|$ satisfies the differential inequality $\dot{W} \leq -g_0\beta_0$. By integration, it can be seen that:

$$|s(t)| \leq |s(0)| - g_0\beta_0 t \tag{4.37}$$

Therefore, it is shown that once the trajectory reaches the manifold in finite time and once on the manifold, trajectory cannot leave letting $u = -\beta(x)\,\text{sign}(s)$ is the sliding mode control.

Khalil, in his work presented in [36] describes how the motion consists of the reaching phase during which the trajectories starting off the manifold $s = 0$ move toward it and reach it in a finite time, followed by a sliding phase during which the motion is confined to the manifold $s = 0$ and the dynamics of the system are represented by the reduced-order model $\dot{x_1} = -ax_1$.

A commonly used sliding mode controller is when $\beta(x) = k$, then inequality (4.32) and control (4.35) simplify to :

$$|\frac{ax_2 + h(x)}{g(x)}| \leq k_1 \tag{4.38}$$

and,

$$u = -k\,\text{sign}(s), k > k_1 \tag{4.39}$$

This simplified form of the sliding mode controller is known as the simple relay form. Nonetheless, this control structure usually leads to a finite region of attraction;the condition $s\dot{s} \leq 0$ within the set $|s| \leq c$ makes it positively invariant.

To estimate the region of attraction consider:

$$\dot{x_1} = x_2 = -ax_1 + s, V_0 = \frac{1}{2}x_1^2 \tag{4.40}$$

Then,

$$\dot{V_0} = x_1\dot{x_1} = ax_1^2 + sx_1 \leq -ax_1^2 + |x_1|c = -|x_1|(a|x_1| - c) \leq 0, \forall |x_1| \geq \frac{c}{a} \quad (4.41)$$

Therefore, since $|x_1(0)| \leq \frac{c}{a} \Rightarrow |x_1(t)| \leq \frac{c}{a}, \forall t \geq 0$, the set $\Omega = |x_1| \leq \frac{c}{a}, |s| \leq c$ is positively invariant if inequality (4.38) holds for all $x \in \Omega$. Thus, if k is chosen arbitrarily large, the subsequent control law is able to achieve semi-global stability. However, for this ideal setup sliding mode control requires the control input to oscillate with a very high (ideally infinite) frequency which is physically unfeasible for most actuators. Furthermore, due to imperfections in switching devices/delays sliding mode control presented in (4.39) may cause the trajectory to oscillate around the sliding surface instead of staying identically on it. This effect is named chattering which some basic notions on how this could be handled are developed in [36]. In this work, chattering effects are considered and managed by implementing an adaptive control law that replaces the discontinuous term. In further sections, the work done in [34] and [38] will be presented and integrated into the source tracking problem.

4.5.2 Bio-inspired Neurodynamics Backstepping Control Model

To overcome the high-speed jump and control constraint problem carried by backstepping based control laws, a bio-inspired neurodynamics model developed by Grossberg in [44] is implemented within the design of virtual control velocity controller. The main characteristic of this model is that it provides shunting features that make its output bounded to a finite interval and hold a smooth and sharpless behavior when inputs change suddenly.

This bio-inspired neurodynamics model was initially derived based on the membrane model developed by Hodgkin and Huxley in [45] for a path of the membrane using electrical elements. The following state-space model shows the voltage dynamics through the membrane:

$$C_m \frac{dV_m}{dt} = -(Ep + V_m)g_p + (E_{Na} - V_m)g_{Na} - (E_k + V_m)g_k \tag{4.42}$$

where C_m is the membrane capacitance and the Parameters E_k, E_{Na} and E_p are said to be the Nernst potentials for potassium, sodium, and passive current leaks across the membrane while g_k, g_p and g_{Na} are the respective conductance of potassium and sodium, the passive channels are functions of time-varying inputs. This modeled equation is further manipulated by Sun in [34] and [43];, in his work, Sun how this model can be used to describe an online adaptive behavior of tracking errors. After the manipulations, it has been able to produce an adjusted model given as follows:

$$\dot{V_i} = -AV_i + (B - V_i)f(e_i) - (D + v_i)g(e_i) \tag{4.43}$$

where parameters A, B and D are positive constants that define respectively the passive decay rate. In fact, it can be proven that the dynamics describe by equation (4.43) is restricted to a bounded range $[-D, B]$ for any external input. In addition, excitatory and inhibitory inputs (external input) are given respectively, such as $f(e_i) = max(e_i, 0)$ and $g(e_i) = max(-e_i, 0)$ where e is the tracking error function defined previously in section 4.3.

Now the original virtual velocity control law is updated by implementing the bio-inspired neurodynamic model such that the new virtual velocity control is given by:

$$\nu_c = J^{-1}(\dot{\eta_d} + KV) \tag{4.44}$$

Consequently, due to the shunting characteristics of V, now the output of ν_c is bounded in a finite and smooth within a finite interval. Hence, the backstepping controller proposed in section 4.2 has significantly been improved.

4.5.3 Adaptive Sliding-Mode Control

Since velocity has been enhanced, the control forces and moments will now be generated by the integration of a nonchattering sliding mode controller following the knowledge presented in [34], [38], and [43]. This control structure has been chosen because it has shown excellent handling of external disturbances and uncertain dynamics. In fact, in Section 4.5.1 it has been proven that this control is entirely independent of the system dynamics and could produce a well-behaved output as long as a suitable way to keep the trajectory within the sliding manifold is conceived. In this section, the formulation of an adaptive, free chattering sliding mode control law is presented as follows:

Firstly, it is necessary to define the sliding mode manifold and consequently design a control law that moves the state trajectory towards the given sliding surface:

$$s = \dot{e_\nu} + 2\Lambda e_\nu + \Lambda^2 \int e_\nu dt \tag{4.45}$$

where $\nu = \nu_c - \nu$ is the virtual velocity tracking, error while Λ is a positive constant.

Taking the derivative of s:

$$\dot{s} = \ddot{e_\nu} + 2\Lambda \dot{e_\nu} + \Lambda^2 e_\nu = \ddot{e_\nu} + 2\Lambda(\dot{\nu_c} - \dot{\nu}) + \Lambda^2 e_\nu \tag{4.46}$$

When the system is operation on the sliding surface then $\dot{s} = 0$. Thus,

$$\ddot{e_\nu} + 2\Lambda(\dot{\nu_c} - \dot{\nu}) + \Lambda^2 e_\nu = 0 \tag{4.47}$$

Substituting in (3.53) into (4.47), we obtain:

$$\ddot{e_\nu} + 2\Lambda(\dot{\nu_c} - M^{-1}(\tau - C\nu - D\nu - g)) + \Lambda^2 e_\nu = 0 \tag{4.48}$$

Then the equivalent control law is given by:

$$\tau_{eq} = M(\dot{\nu_c} + \frac{\ddot{e_\nu}}{2\Lambda} + \frac{\Lambda}{2} e_\nu) + C\nu + D\nu + g \tag{4.49}$$

where M, C, D, and g are the average inertia, Coriolis, hydrodynamic matrices and hydrostatic vector defined in Chapter 3.

A naive conventional sliding mode control can be proposed such that

$$\tau = \tau_{eq} + k\,\mathrm{sign}(s) \tag{4.50}$$

Nonetheless, in previous sections, it was shown that the $k\,\mathrm{sign}(s)$ leads the control inputs to oscillate at high frequency, generating chattering then and a adaptive term is added as it is proposed in [38].

$$\tau_{ad} = \tilde{\tau}_{est} - (K + \frac{C}{2\Lambda})s \tag{4.51}$$

where $\tilde{\tau}_{est}$ is the adaptive term that estimates the effects of lumped uncertainties while K is a positive constant intimately related with the convergence rate of the controller. In addition, the estimation of the lumped uncertainty vector is proposed

to be given as follows:

$$\dot{\tilde{\tau}}_{est} = -\Gamma s \tag{4.52}$$

where Γ is is a positive definite diagonal constant design matrix that determines the rate of adaptation. This adaptive term relates the error metric s function to the dynamic uncertainties and acts on the controller in such a way that the estimated dynamics reflect the unknown dynamics more closely to the actual dynamics [38].

Finally the total control can be stated as it is shown

$$\tau = \tau_{eq} + \tilde{\tau}_{est} - (K + \frac{C}{2\Lambda})s \tag{4.53}$$

Notice that the presented control variables are a function of tracking errors and corresponding derivatives, which are difficult to compute. For this work, it will be considered acceptable the numerical derivatives are computed as follow:

$$\frac{d^n x}{dt^n} = -k_c \frac{d^{n-1} x}{dt^{n-1}} \tag{4.54}$$

4.5.4 Bio-Inspired Integrated Sliding Mode Control Trajectory Tracking (Numerical Results)

Similarly, as it was done for the pure backstepping control defined in section 4.2 a numerical experiment is run to show this new bio-inspired integrated sliding Mode Control (BIISM). In this case, the system is newly asked to track the same circular trajectory for the same initial values presented in section 4.4.1. In addition, simulation parameters for this study, case are presented in appendix A.1.4.

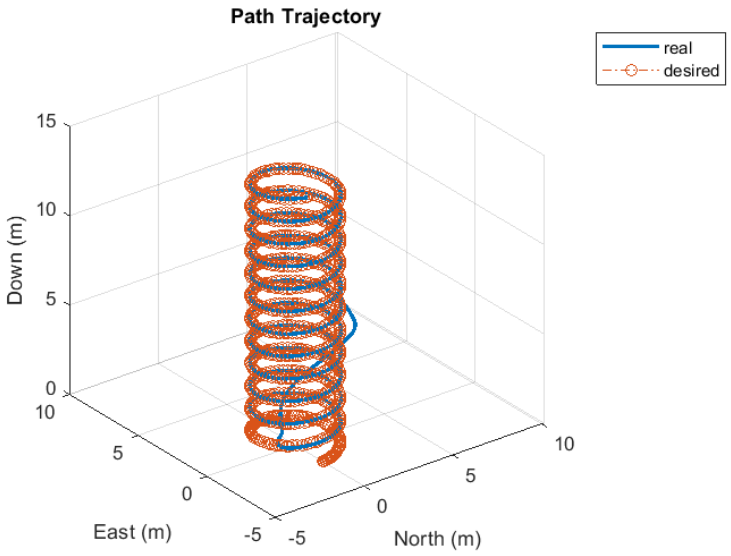

Figure 4.14: Circular helix trajectory-tracking BIISM.

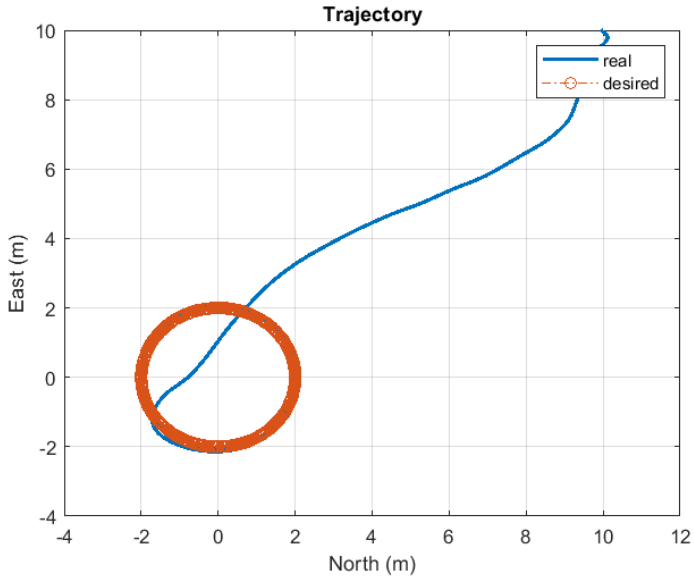

Figure 4.15: Circular plane trajectory-tracking BIISM.

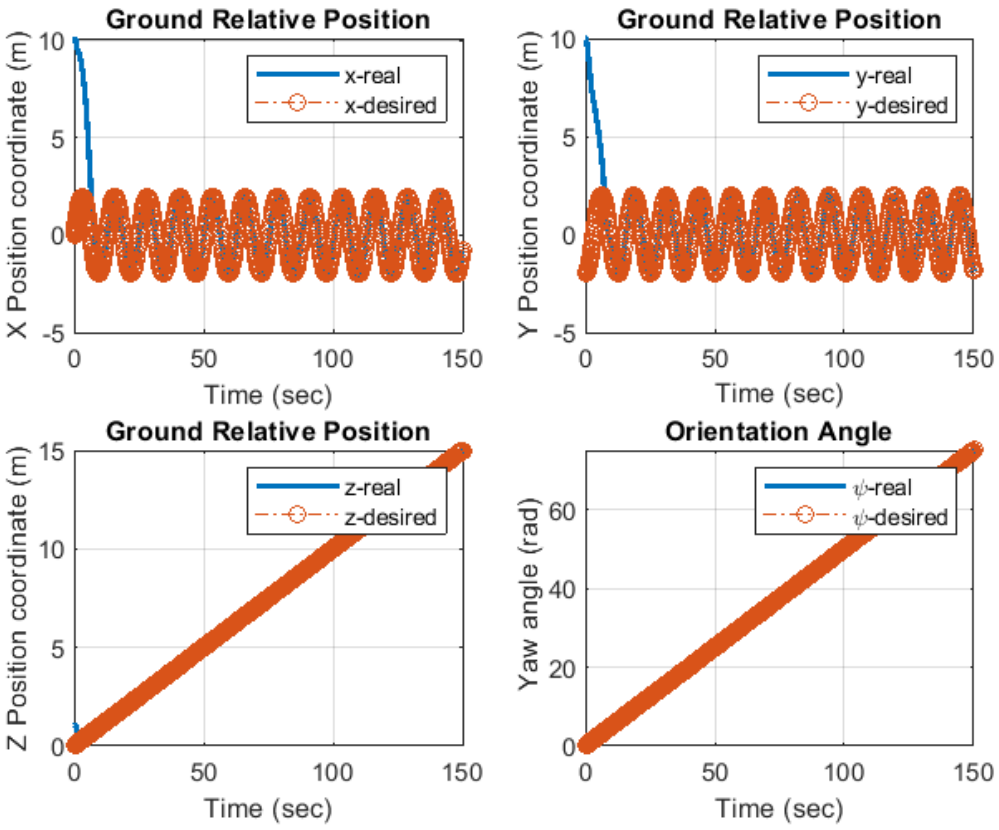

Figure 4.16: Tracking responses of reference positions for circular trajectory BIISM.

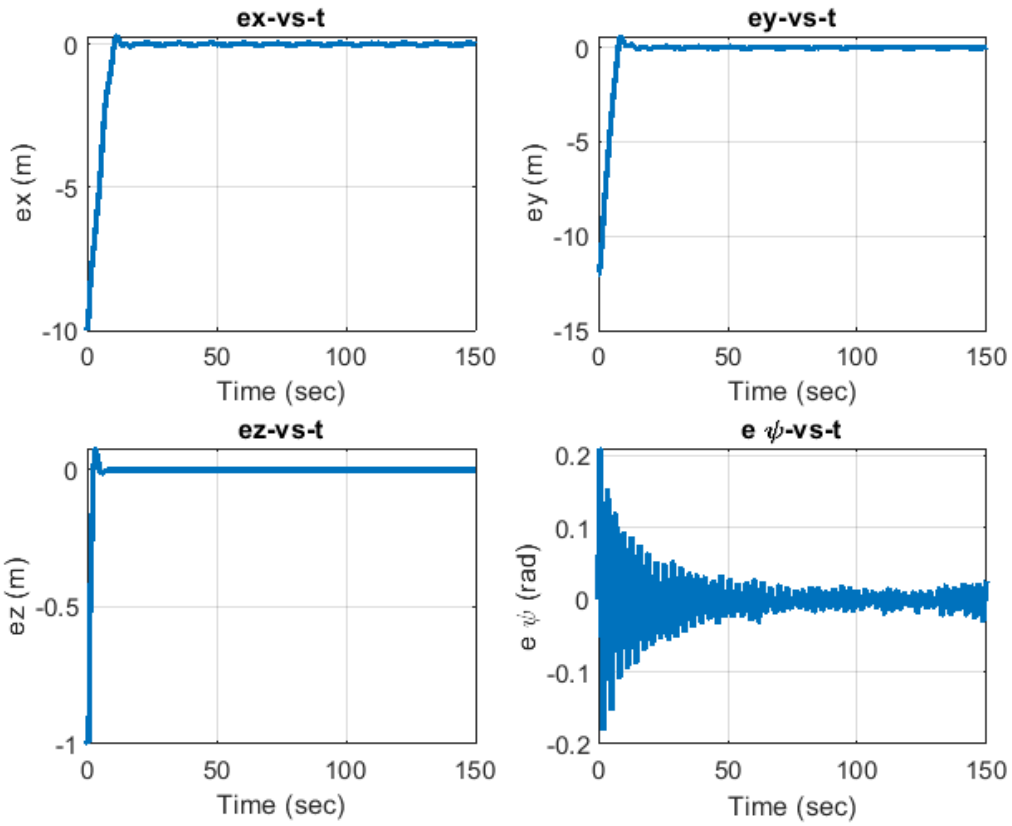

Figure 4.17: Tracking errors with disturbances for circular tracking BIISM.

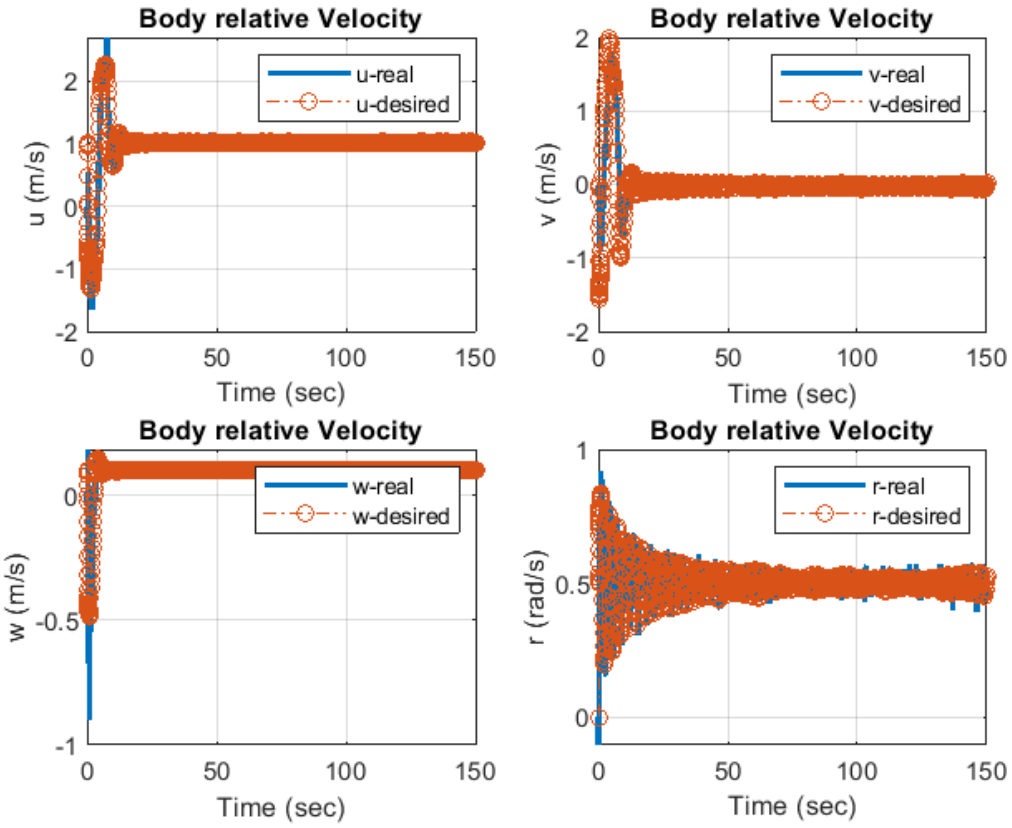

Figure 4.18: Tracking responses of virtual reference velocities for circular tracking BIISM.

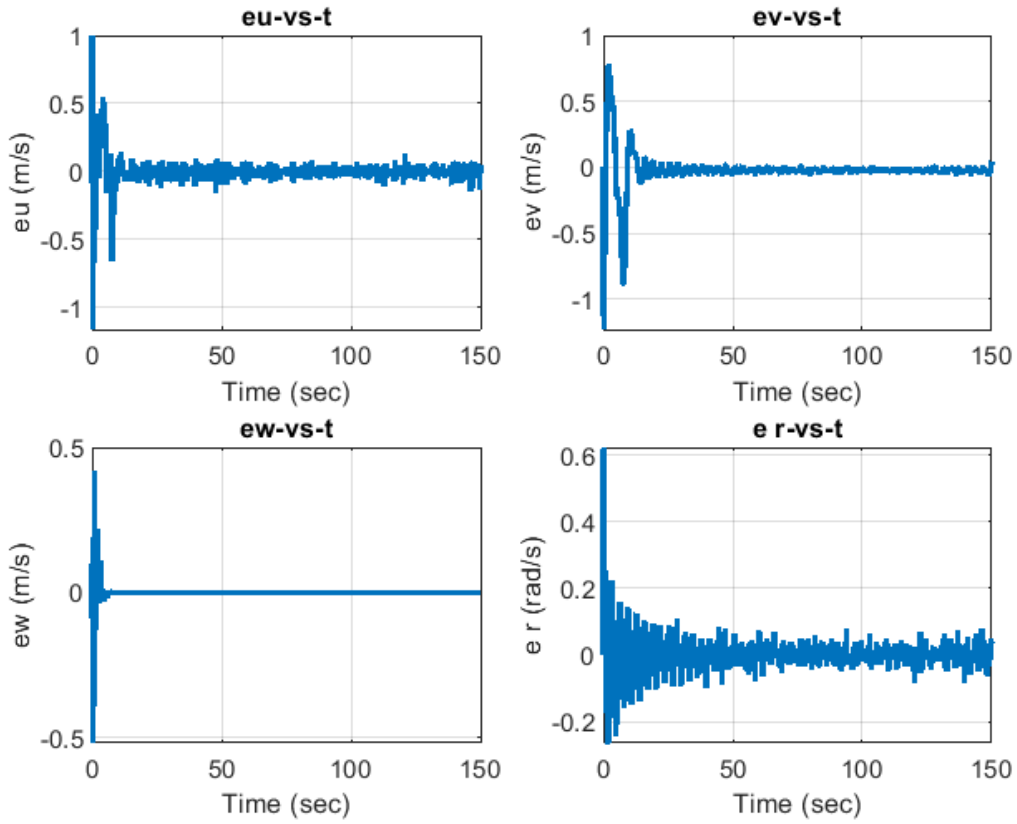

Figure 4.19: Tracking errors of virtual reference velocities for circular trajectory BIISM.

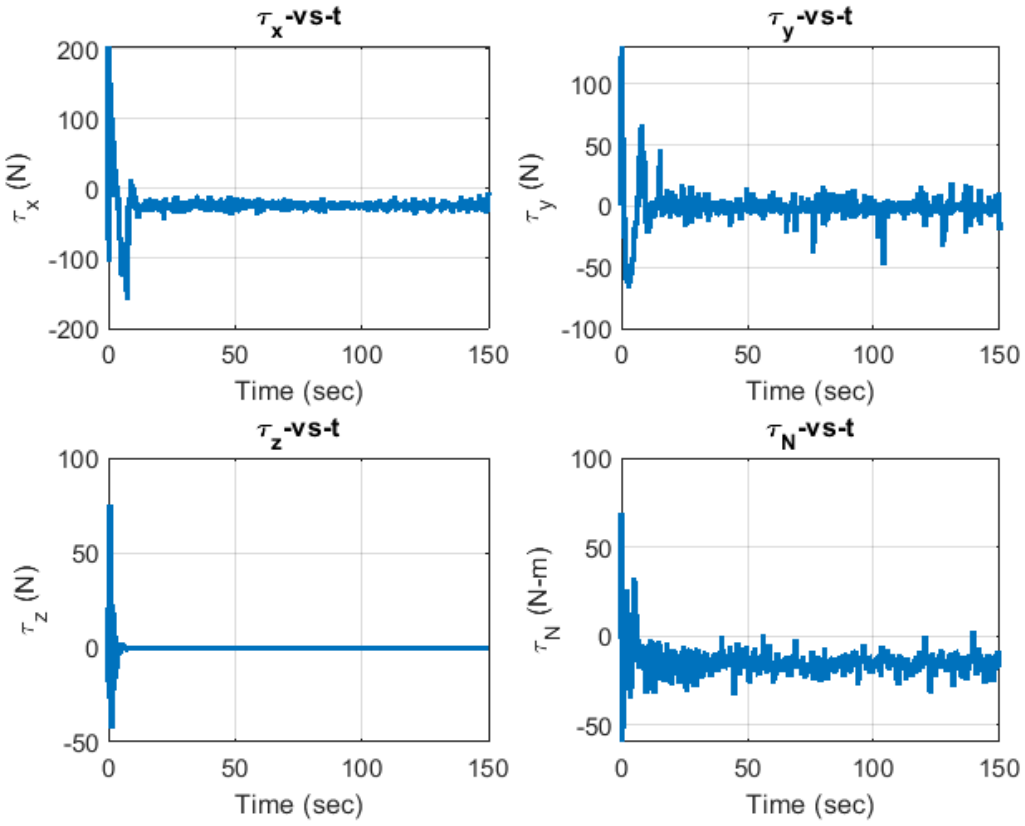

Figure 4.20: Control signals: Total surge thrust τ_x, sway thrust τ_y, yaw torque τ_N, heave thrust τ_z for circular tracking BIISM.

Giving some remarks on BIISM control, it can be seen that main issues such as high velocity jumps due to either high initial errors or sudden disturbances have been corrected due to the boundedness provided by the shunting property of the bio-inspired velocity control. Additionally, the control input is shown to have been improved significantly by dropping its order magnitude due to non-chattered sliding mode control action.

4.6 UAUV Source tracking and Guidance

The concentration field will be defined such that it can serve as reference values to be tracked by our UAUV. In [46] Tian developed a domain decomposition algorithm to model a moving plume generated by a moving aerial source. The primary purpose of this work is to implement a concentration estimator that allows a follower aircraft to estimate and track the concentration spectrum carried by the moving source in real-time. Moreover, The guidance strategy presented in [46] is based on two components. One of them is provided by a concentration sensor mounted on the aircraft, and the second is given by a PDE estimator of the concentration field. One may guess the goal is to propose a guidance law to minimize the difference between the values obtained from the process-state estimator and concentration sensor. Thus, the following state estimation error function is defined:

$$\varepsilon(t) = e(x_e(t), y_e(t), z_e(t), t) = C(x_e(t), y_e(t), z_e(t), t) - \hat{C}(x_e(t), y_e(t), z_e(t), t) \tag{4.55}$$

Therefore control inputs given as function of desired Cartesian velocities are said

to be as [46] follows:

$$U_d \equiv \dot{x_d} = k_X \,\text{sign}(\varepsilon(t)) \,\text{sign}\left(\frac{\partial \varepsilon(t)}{\partial(x)}\right) \tag{4.56}$$

$$V_d \equiv \dot{y_d} = k_Y \,\text{sign}(\varepsilon(t)) \,\text{sign}\left(\frac{\partial \varepsilon(t)}{\partial(y)}\right) \tag{4.57}$$

$$W_d \equiv \dot{z_d} = k_Z \,\text{sign}(\varepsilon(t)) \,\text{sign}\left(\frac{\partial \varepsilon(t)}{\partial(z)}\right) \tag{4.58}$$

Therefore, desired positions the vehicle are obtain by integrating functions (4.60),(4.61), and (4.62) such that:

$$x_d = \int U_d dt, \qquad y_d = \int V_d dt, \qquad z_d = \int W_d dt \tag{4.59}$$

In [46], the PDE Luenberger estimator is solved using an adaptive parallel processing upwinding finite volume method based on domain decomposition. However, in this work, the concentration field will be known a priori by a super-user, and its historical data is uploaded and implemented in the dynamical model. Consequently, modified control velocity commands are proposed as follows:

$$U_d \equiv \dot{x_d} = k_X \,\text{sign}\left(C(x_e(t), y_e(t), z_e(t), t)\right) \text{sign}\left(\frac{\partial C(x_e(t), y_e(t), z_e(t), t)}{\partial x}\right) \tag{4.60}$$

$$V_d \equiv \dot{y_d} = k_Y \,\text{sign}\left(C(x_e(t), y_e(t), z_e(t), t)\right) \text{sign}\left(\frac{\partial C(x_e(t), y_e(t), z_e(t), t)}{\partial y}\right) \tag{4.61}$$

$$W_d \equiv \dot{z_d} = k_Z \,\text{sign}\left(C(x_e(t), y_e(t), z_e(t), t)\right) \text{sign}\left(\frac{\partial C(x_e(t), y_e(t), z_e(t), t)}{\partial z}\right) \tag{4.62}$$

where k_X, k_Y, k_Z are positive defined by the user. Desired positions remain as they were given in equation (4.59).

4.6.1 Bio-Inspired Integrated Sliding Mode Control for Source Tracking (Numerical Results)

A 2-dimensional concentration process (moving plume) is modeled. in a domain $L_X = 1000m \times L_Y = 1000m$ as an instantaneous Gaussian pulse released in given point $a = (500, 500)m$. In this section, the performance of the UAUV is studied under high-demand initial error conditions, and as it can be expected in a real-life operation with high-order disturbances. Therefore, only BIISM control will be tested out in the following numerical experiment since it has been proven that it is the most suitable strategy available to handle the requirements of the experiment. Multiple test runs were done in this section, but for representation proposes, two runs are presented to compare the effects on the system behavior of 1-D and 2-D concentration advective components.

1-D advective velocity component

For this study case initial position is set up to be $\eta(0) = [900, 900, 10, 0]$, and an horizontal uniform flow velocity is given by $u_w = U_\infty = \beta_x = 0.5m/s$. Further control and simulation parameters can be found in Appendix A.1.5

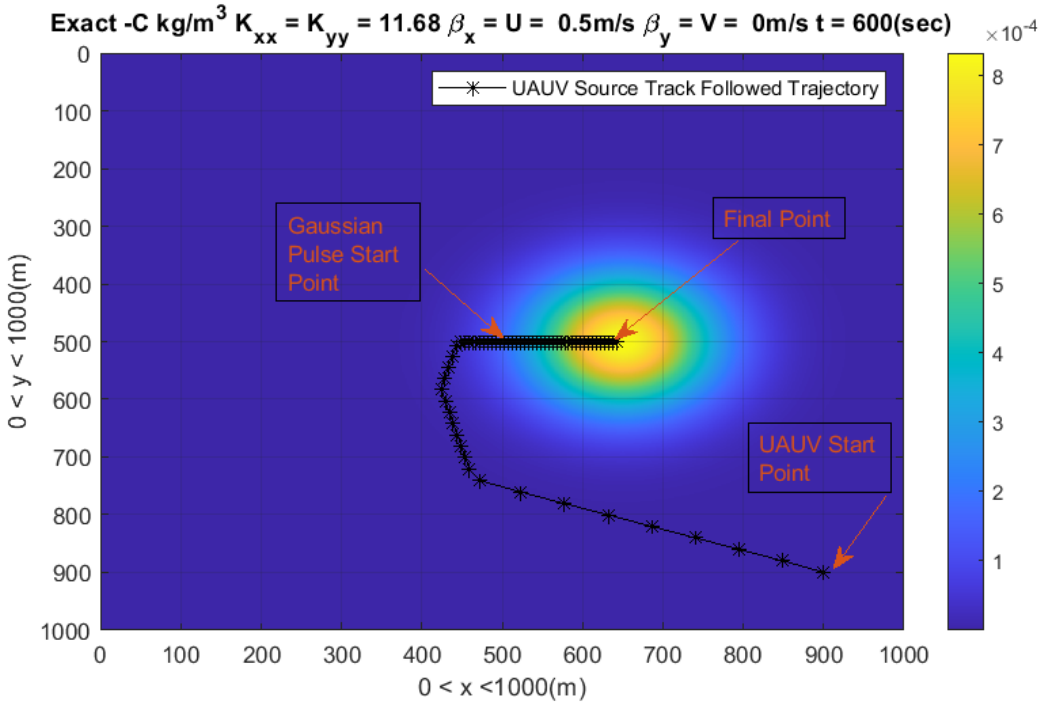

Figure 4.21: Horizontal Concentration trajectory-tracking BIISM.

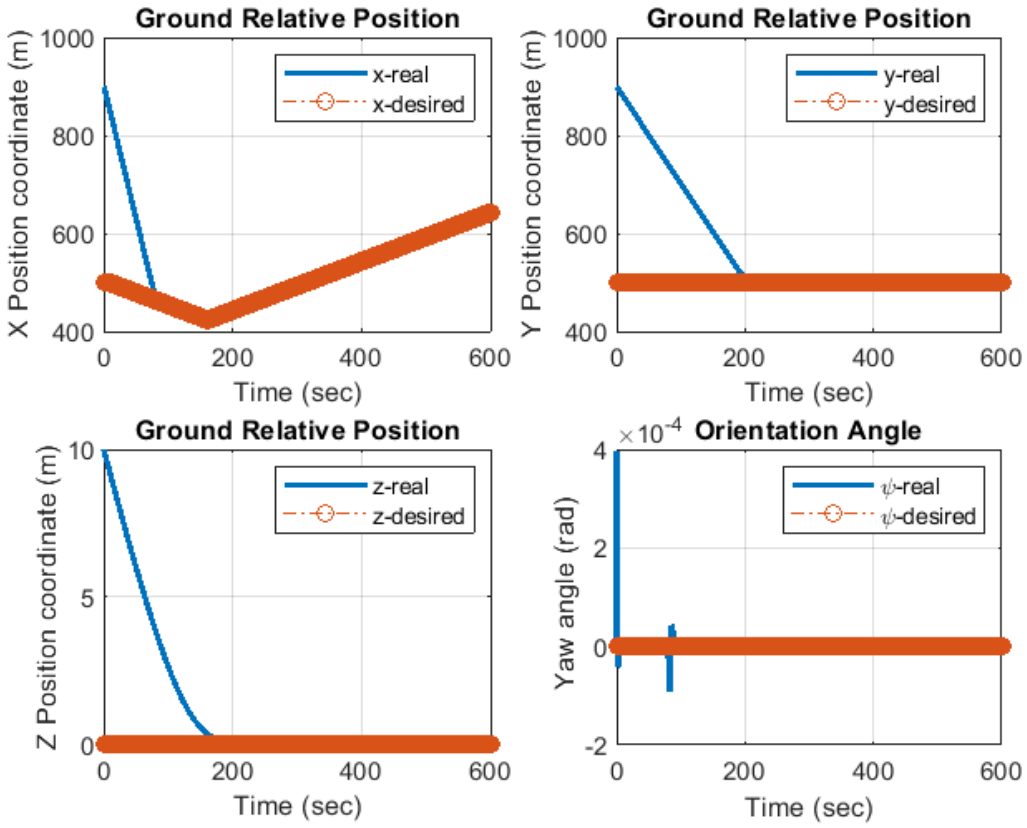

Figure 4.22: Tracking responses of reference positions for horizontal concentration BIISM.

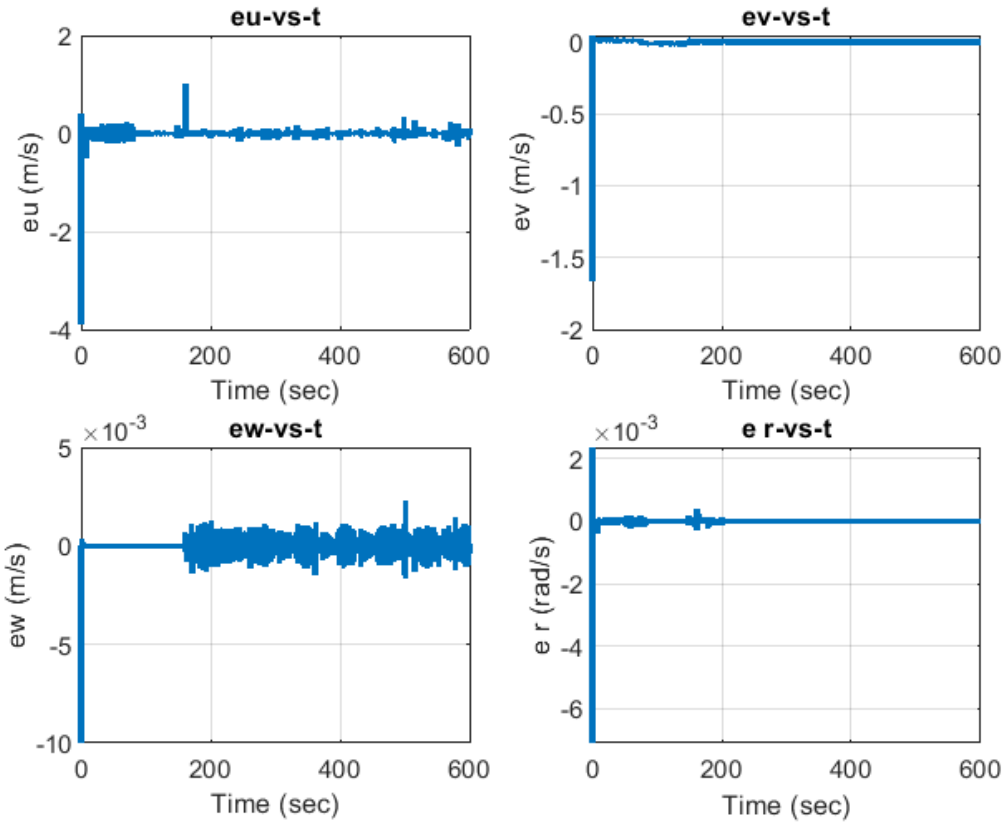

Figure 4.23: Tracking errors with disturbances for horizontal concentration tracking BIISM.

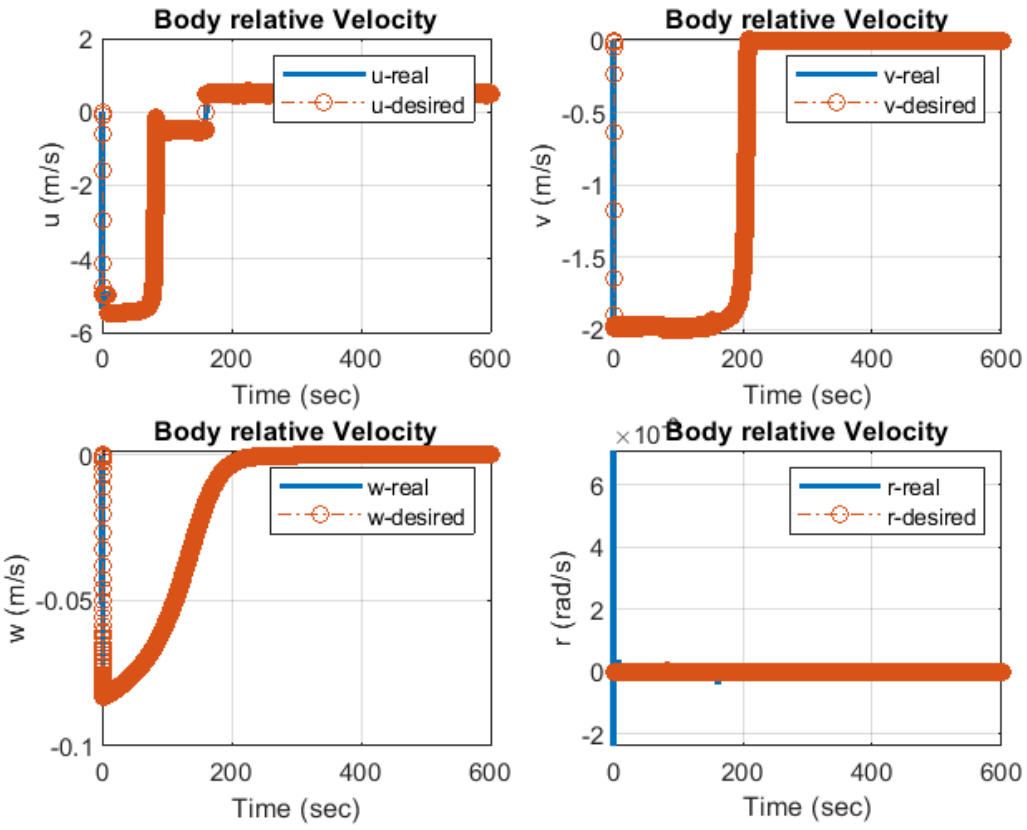

Figure 4.24: Tracking responses of virtual reference velocities for horizontal concentration tracking BIISM.

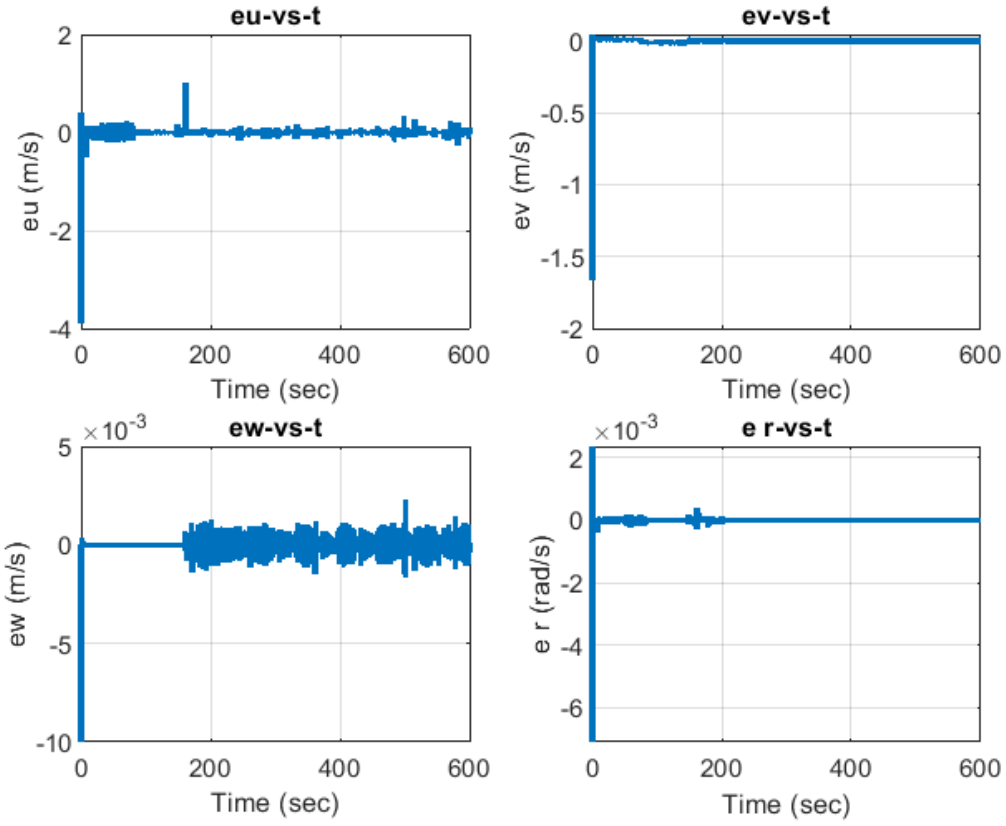

Figure 4.25: Tracking errors of virtual reference velocities for horizontal concentration tracking BIISM.

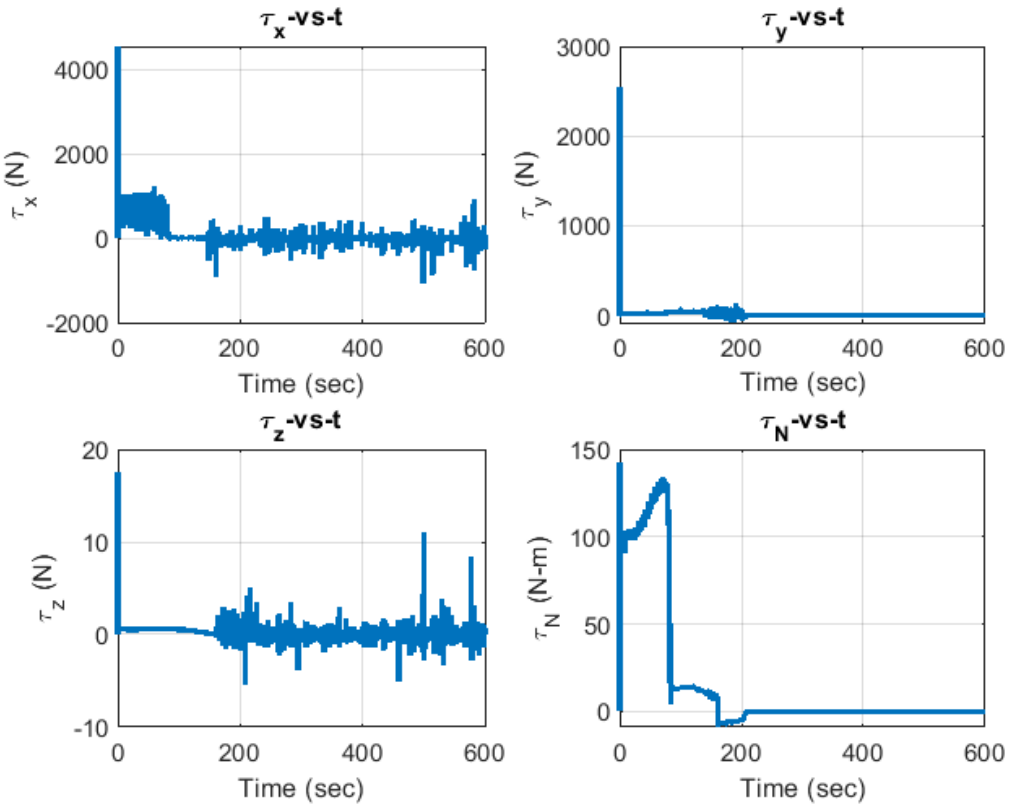

Figure 4.26: Control signals: Total surge thrust τ_x, sway thrust τ_y, yaw torque τ_N, heave thrust τ_z for horizontal concentration BIISM.

2-D advective velocity component

For this study case initial position is set up to be $\eta(0) = [100, 900, 10, 0]$, and an horizontal uniform flow velocity is given by $u_w = U_\infty = \beta_x = 0.5m/s$,$v_w = V_\infty = \beta_y = 0.5m/s$. Further control and simulation parameters can be found in Appendix A.1.5

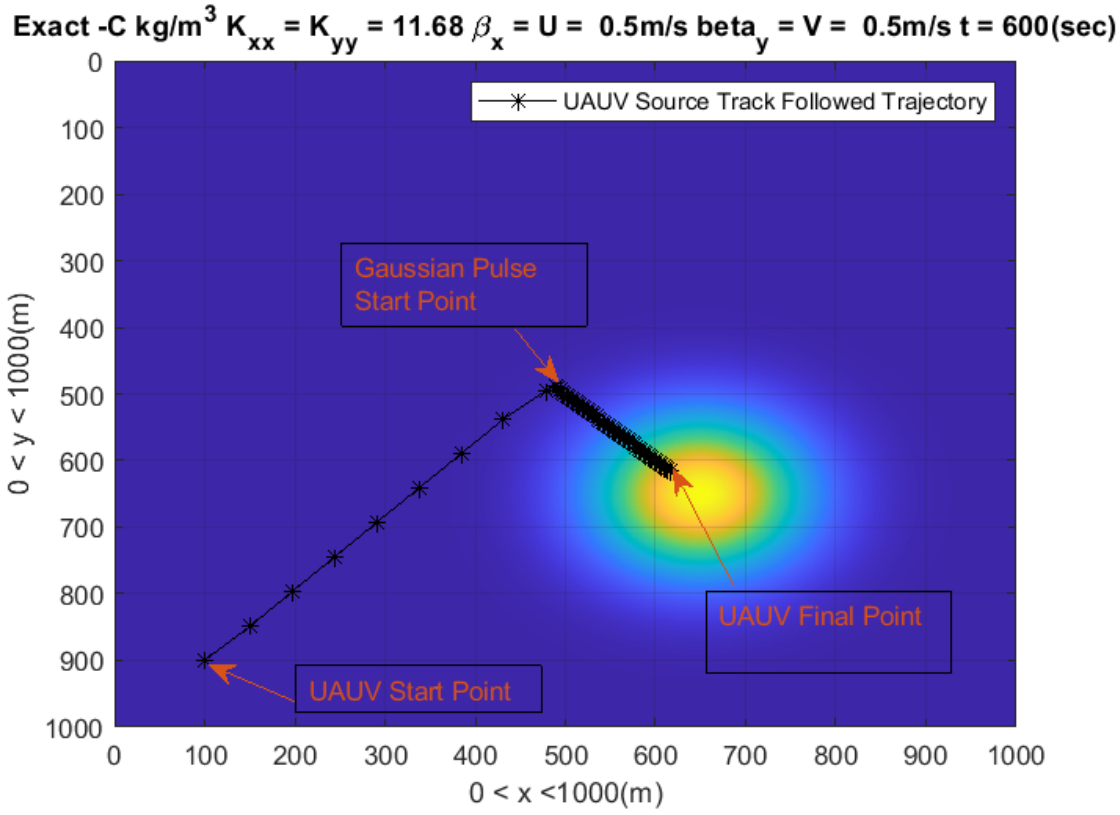

Figure 4.27: 2-Dimensional Concentration trajectory-tracking BIISM.

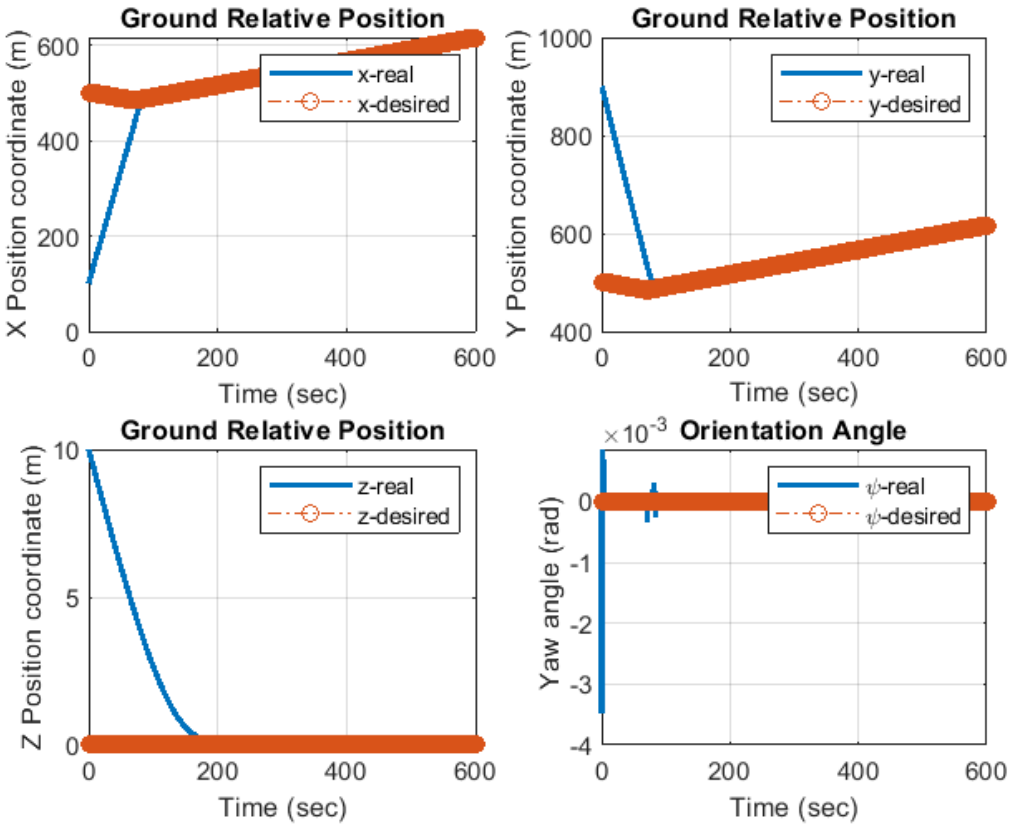

Figure 4.28: Tracking responses of reference positions for 2-Dimensional concentration BIISM.

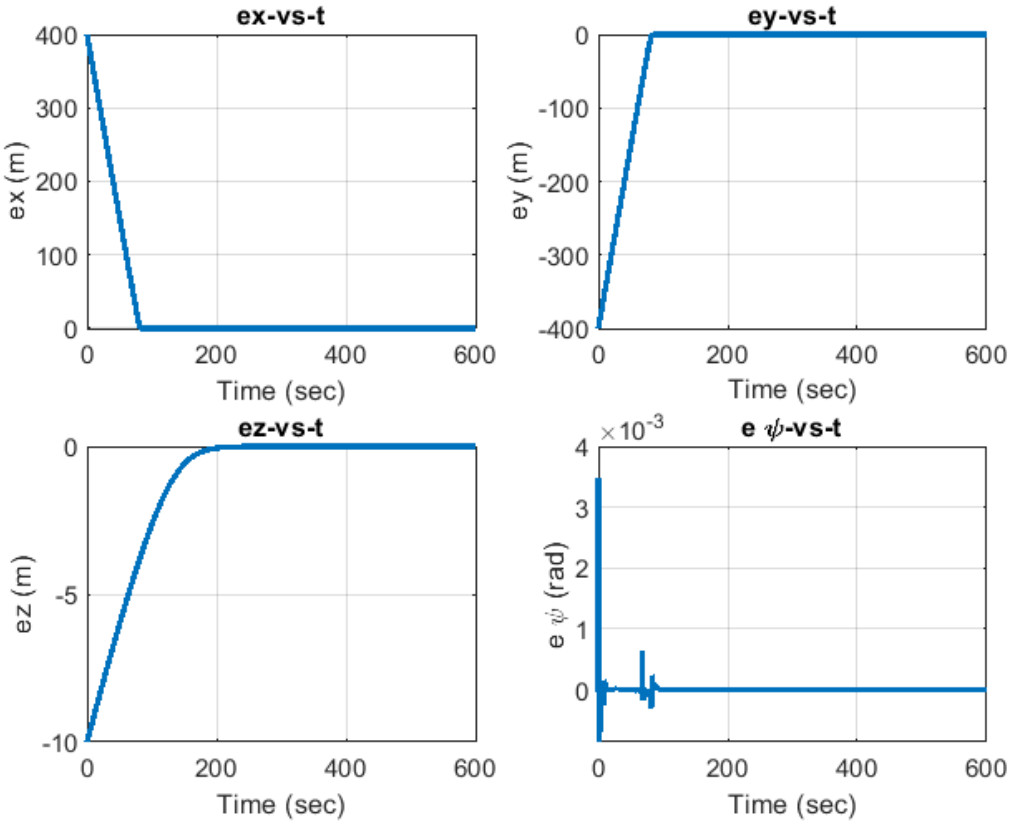

Figure 4.29: Tracking errors with disturbances for 2-Dimensional concentration tracking BIISM.

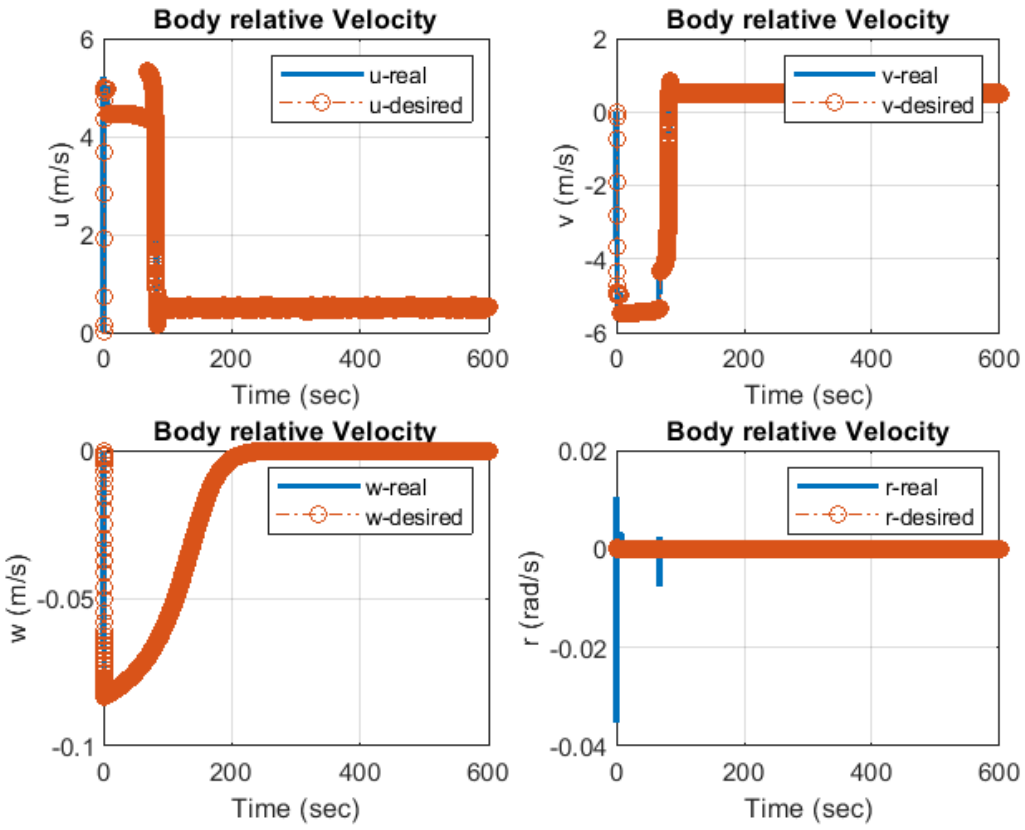

Figure 4.30: Tracking responses of virtual reference velocities for 2-Dimensional concentration tracking BIISM.

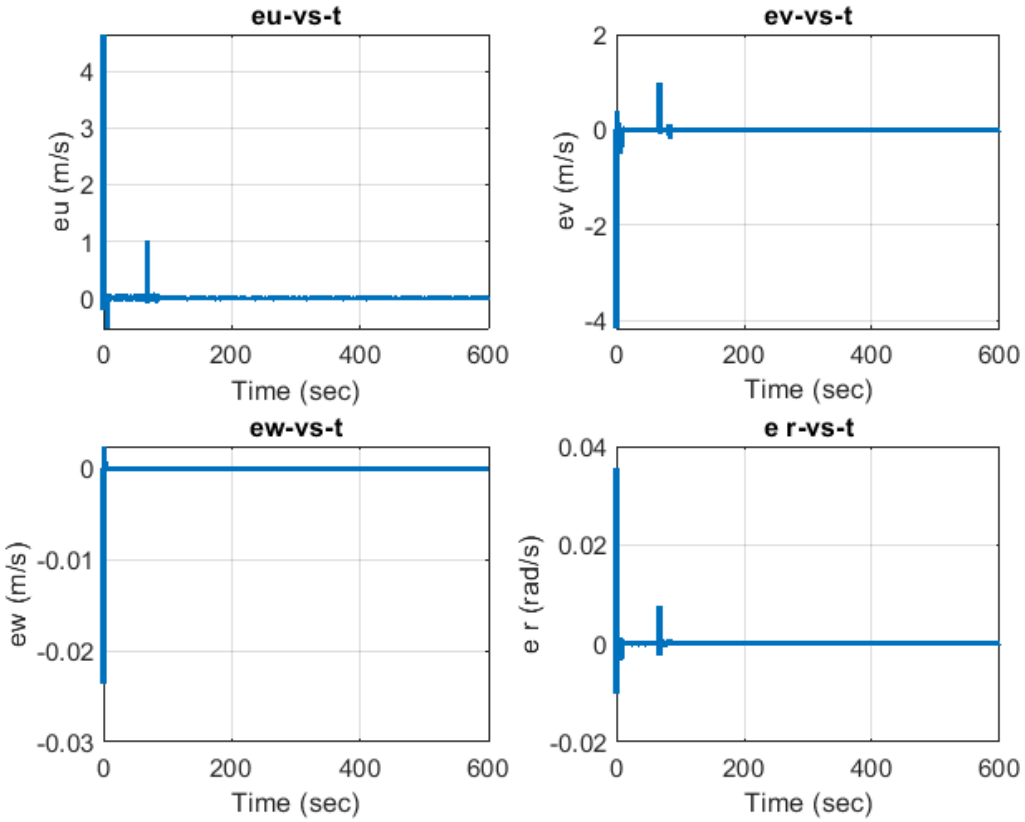

Figure 4.31: Tracking errors of virtual reference velocities for 2-Dimensional concentration tracking BIISM.

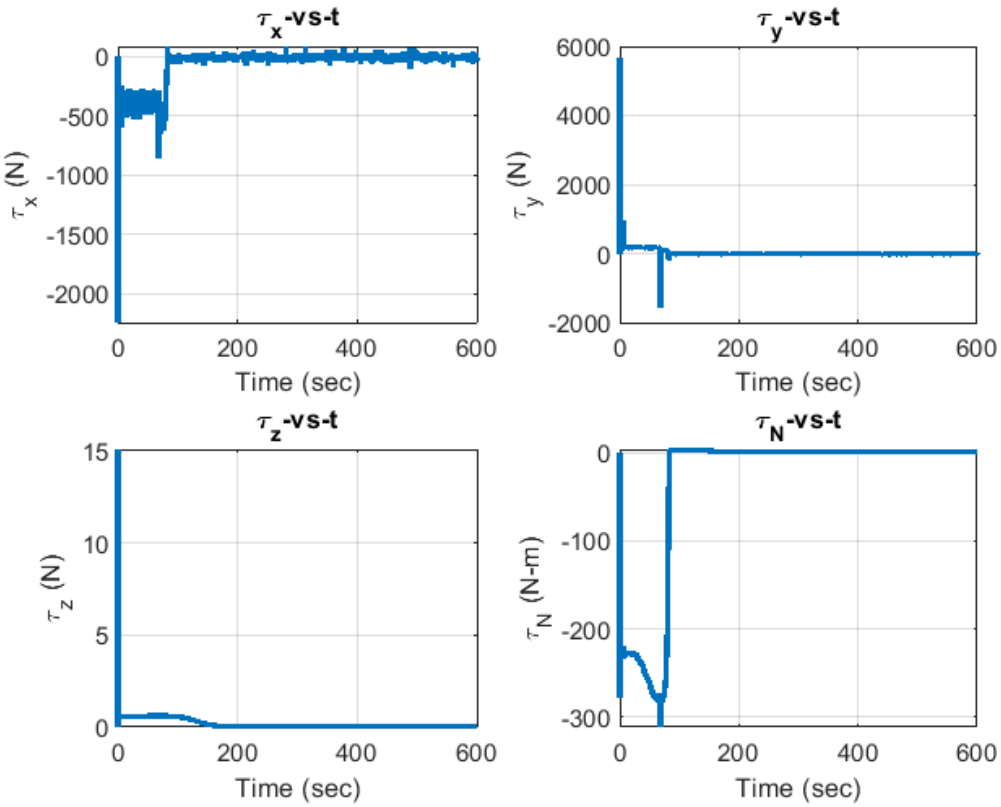

Figure 4.32: Control signals: Total surge thrust τ_x, sway thrust τ_y, yaw torque τ_N, heave thrust τ_z for 2-Dimensional concentration BIISM.

Chapter 5

Conclusions

The interaction between the UAUV's communication system and pollutant concentration data represents the piece of resistance of this work. Therefore, mean oil concentration for dispersion of species on coastal zones has been developed and supplemented with analytical and explicit numerical schemes to describe a pollutant moving plume on coastal zones. The numerical schemes work throughout a fixed computational grid size to achieve stability and computational economy since this is said to be accessed by the UAUV to generate commanded reference values. Hence, The control system subsequently interprets these commanded reference values as actual control forces and moments. This work focused its effort on developing a robust guidance strategy based on Lyapunov structures that can provide a suitable system dynamical response for pollutant source localization, so that desired commands can be reached out properly. The guidance technique applied is the bio-inspired integrated sliding mode control. The bio-inspired component of this strategy found its basis on the backstepping Lyapunov transformation to produce virtual control velocities and provide a certain level of relaxation to the tracking errors so that unfeasible initial velocity jumps can be prevented (virtual kinematic

control). At the same time, the adaptive sliding mode takes care of tracking velocity errors while providing a robust component able to handle uncertain dynamics and external disturbances due to turbulence.Results shown in the previous Section 4.6.1 show that the BIISM control provides a feasible control strategy for localization and tracking of the pollutant source as it can be observed in Figures 4.21 through 4.32. By applying the analytical and numerical schemes mentioned above on the advection-diffusion model, a super-user has been able to process, estimate, and upload a suitable concentration field description into the UAUV system to compute in real-time localized concentration values with its respective gradients. However, in realistic operation conditions, accessing such a precise model is usually not available. Therefore, to come up with realistic input velocity commands, it becomes imperative the implementation of an estimator model that can compare in real-time actual concentration localized values against a time-dependent PDE observer as it is done in [46], [47], [68], and [70]. Nonetheless, this procedure requires that the UAUV ODE model, the turbulent advection-diffusion time-dependent PDE, and an output error injection observer PDE have to be solved simultaneously in the same simulation environment which computationally speaking is extremely demanding. In fact, in Chapter 2 it is mentioned that not only for stability proposes, but also for computational feasibility grid size resolution has been set to be large to generate an approximated scheme that can model a realistically large domain, but somehow compromising the accuracy of the scheme itself. Therefore, due to computational limitations, this work only presents a preliminary source localization Lyapunov-based control law which in future works will be supplemented with a PDE state estimator by the implementation of more computational power or a certain level of computational process parallelization.

Appendix A

A.1 Dynamics and Control Simulation Parameters

A.1.1 OUTLAND-1000 Physical Parameters

m	I_{zz}	$X_{\dot{u}}$
10 kg	30 kg-m$\hat{2}$	34
$Y_{\dot{v}}$	$Z_{\dot{w}}$	$N_{\dot{r}}$
75	33	62
X_u	Y_v	Z_w
6	6	7
N_r	X_{uu}	Y_{vv}
14	18	4
Z_{ww}	N_{rr}	
4	14	

Table A.1: OUTLAND-1000 Inertia and Hydrodynamic Parameters

A.1.2 Circular Trajectory Tracking Control Parameters (Backstepping)

K_x	K_y	K_z	K_ψ	K_u	K_v	K_w	K_r
2	2	2	5	2	2	2	2

Table A.2: Circular Trajectory Tracking Control Parameters (Backstepping).

A.1.3 Spiral Trajectory Tracking Control Parameters (Backstepping)

K_x	K_y	K_z	K_ψ	K_u	K_v	K_w	K_r
10	10	10	8	2	2	2	2

Table A.3: Circular Trajectory Tracking Control Parameters(Backstepping).

A.1.4 Circular Trajectory Tracking Simulation Parameters (BIISM control)

K_x	K_y	K_z	K_ψ	k_c	Γ	Λ	K	A	B	D
2	2	2	5	10	5	3	100	2	1	1

Table A.4: Circular Trajectory Tracking Simulation Parameters (BIISM control).

A.1.5 Concentration Tracking Simulation Parameters (BIISM control)

K_x	K_y	K_z	K_ψ	k_c	Γ	Λ	K	A	B	D
5	2	0.1	0.5	80	50	40	100	2	1	1

Table A.5: Horizontal Concentration Tracking Simulation Parameters(BIISM control).

K_x	K_y	K_z	K_ψ	k_c	Γ	Λ	K	A	B	D
5	5	0.1	0.5	80	50	30	50	2	1	1

Table A.6: 2-Dimensional Concentration Tracking Simulation Parameters(BIISM control).

Appendix B

Control Diagrams

B.1 Hierarchical Backstepping Control

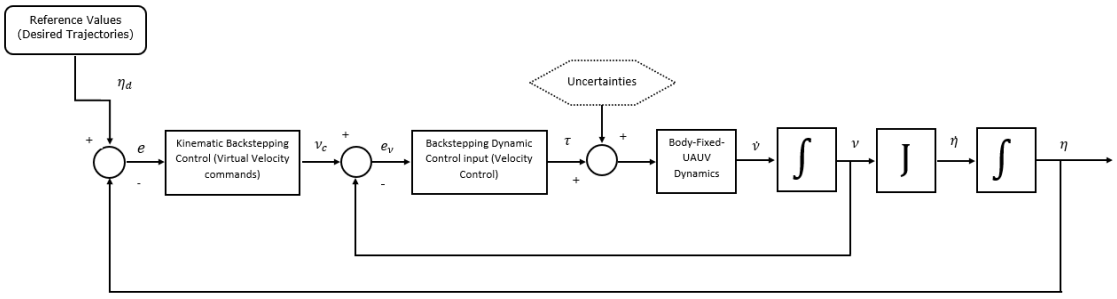

Figure B.1: Backstepping Trajectory Control.

B.2 Integrated Bio-Inspired Backstepping and Sliding Mode Tracking Control

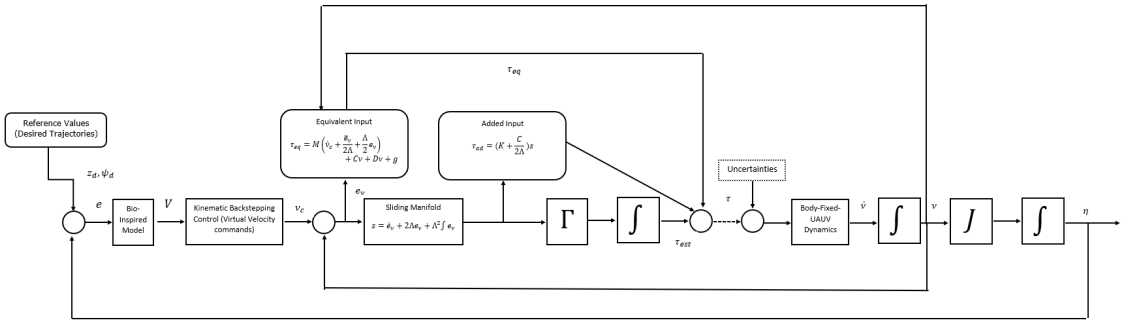

Figure B.2: BIISM Trajectory Control.

B.3 BIISM Applied to Pollutant Source Tracking and Localization

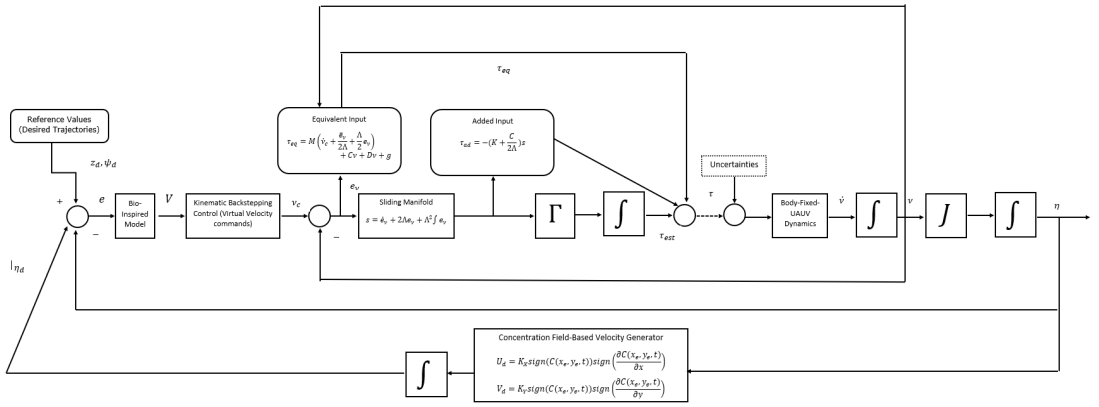

Figure B.3: BIISM Pollutant Source Tracking and Localization Control.

Bibliography

[1] Antonelli, G., Antonelli, G. (2014). Underwater robots (Vol. 3). Switzerland: Springer International Publishing.

[2] Fossen, T. I. (1999). Guidance and control of ocean vehicles. University of Trondheim, Norway, Printed by John Wiley Sons, Chichester, England, ISBN: 0 471 94113 1, Doctoral Thesis.

[3] Healey, A. J., Lienard, D. (1993). Multivariable sliding mode control for autonomous diving and steering of unmanned underwater vehicles. IEEE journal of Oceanic Engineering, 18(3), 327-339.

[4] Fossen, T. I. (2011). Handbook of marine craft hydrodynamics and motion control. John Wiley Sons.

[5] Triantafyllou, M. S., Franz, S. (2003). Hover. Maneuvering and control of marine vehicles. Lecture Notes, Department of Ocean Engineering Massachusetts Institute of Technology Cambridge, Massachusetts USA.

[6] Solowjow, E. (2019). Design, dynamics, and control of micro underwater vehicle systems for autonomous environmental exploration (Doctoral dissertation, Universitätsbibliothek der Technischen Universität Hamburg-Harburg).

[7] Li, B. (2016). Dynamics and Control of Autonomous Underwater Vehicles with Internal Actuators (Doctoral dissertation, Florida Atlantic University)

[8] Evans, J., Nahon, M. (2004). Dynamics modeling and performance evaluation of an autonomous underwater vehicle. Ocean Engineering, 31(14-15), 1835-1858.

[9] Duecker, D. A., Hackbarth, A., Johannink, T., Kreuzer, E., and Solowjow, E. (2018, May). Micro underwater vehicle hydrobatics: A submerged furuta pendulum. In IEEE International Conference on Robotics and Automation (ICRA) (pp. 7498-7503).

[10] Gruneisen, A., Henriet, Y. (2002). Monterey, California USA.3D Model of the Aries Autonomous Underwater Vehicle (AUV), Javadoc for Dynamics Software,AUV Mission-Visualization Workbench, and AUV Dynamics Control

Workbench in Matlab.Prepared for: Naval Postgraduate School, Monterey, CA and Ecole Nationale d'Ingénieurs de Tarbes, Tarbes Cedex, France.

[11] Brutzman, D., Healey, T., Marco, D., and McGhee, B. (1998). The Phoenix autonomous underwater vehicle. Artificial Intelligence and Mobile Robots: Case studies of successful robot systems, 323-360.

[12] Marco, David Healey, Anthony. (2000). Current developments in underwater vehicle control and navigation: The NPS ARIES AUV. Proc IEEE Oceans. 2. 1011 - 1016 vol.2. 10.1109/OCEANS.2000.881732.

[13] Hopkin, D., Den Hertog, V. (1993, August). The hydrodynamic testing and simulation of an autonomous underwater vehicle. In Proceedings of the Second Canadian Marine Dynamics Conference (pp. 274-281).

[14] D. E. Perrault, T. Curtis, N. Bose, S. O'Young and C. Williams, "C-SCOUT maneuverability-a study in sensitivity," MTS/IEEE Oceans 2001. An Ocean Odyssey. Conference Proceedings (IEEE Cat. No.01CH37295), Honolulu, HI, USA, 2001, pp. 436-443 vol.1, doi: 10.1109/OCEANS.2001.968764.

[15] Hackbarth, A., Kreuzer, E., Solowjow, E. (2015, September). HippoCampus: A micro underwater vehicle for swarm applications. In 2015 IEEE/RSJ International Conference on Intelligent Robots and Systems (IROS) (pp. 2258-2263).

[16] Duecker, D.A., Kreuzer, E., Maerker, G. and Solowjow, E. (2018), Parameter Identification for Micro Underwater Vehicles. Proc. Appl. Math. Mech., 18: e201800350.

[17] Lewis, E. V. (1988). Principles of naval architecture second revision. Jersey: Sname, 2.

[18] Newman, J. N. (1969). Marine Hydrodynamics. Massachusetts Institute of Technology, MIT, USA, Lecture Notes, Spring Term 1969.

[19] Ridley, P., Fontan, J., Corke, P. (2003). Submarine dynamic modelling. In Proceedings of the Australian Conference on Robotics and Automation (pp. 1-8). Australian Robotics and Automation Association.

[20] Wu, H. M., Karkoub, M. (2014, October). Hierarchical backstepping control for trajectory-tracking of autonomous underwater vehicles subject to uncertainties. In 14th International Conference on Control, Automation and Systems (ICCAS 2014) (pp. 1191-1196).

[21] Rojas, J. S. C. (2019). Vehículos Submarinos Autónomos. Pädi Boletín Científico de Ciencias Básicas e Ingenierías del ICBI, 7(Especial), 60-70.

[22] Cervantes, J., Yu, W., Salazar, S., Chairez, I., Lozano, R. (2016, July). Output based backstepping control for trajectory tracking of an autonomous underwater vehicle. In American Control Conference (ACC) (pp. 6423-6428).

[23] Rout, R., Subudhi, B. (2016). A backstepping approach for the formation control of multiple autonomous underwater vehicles using a leader–follower strategy. Journal of Marine Engineering Technology, 15(1), 38-46.

[24] Garcia, Delvis Jiménez, Yenier. (2013). Sistema de guiado para Vehículo Autónomo Sumergible. XV Convención y Feria Internacional Informática 2013. XI Simposio Internacional de Automatización La Habana, Cuba.

[25] Shen, C., Shi, Y., Buckham, B. (2017). Trajectory tracking control of an autonomous underwater vehicle using Lyapunov-based model predictive control. IEEE Transactions on Industrial Electronics, 65(7), 5796-5805.

[26] Khalaji, A. K., Zahedifar, R. (2020). Lyapunov-based formation control of underwater robots. Robotica, 38(6), 1105-1122.

[27] Shen, C., Shi, Y., Buckham, B. (2017, October). Lyapunov-based model predictive control for dynamic positioning of autonomous underwater vehicles. In IEEE International Conference on Unmanned Systems (ICUS) (pp. 588-593).

[28] Guerrero, J., Torres, J., Creuze, V., Chemori, A., Campos, E. (2019). Saturation based nonlinear PID control for underwater vehicles: Design, stability analysis and experiments. Mechatronics, 61, 96-105.

[29] Do, K. D., Pan, J. (2009). Control of ships and underwater vehicles: design for underactuated and nonlinear marine systems. Springer Science Business Media.

[30] Roghani, S. E. S., Koyuncu, E., Uzun, M. (2019, March). Trajectory Generation and Regeneration for Constrained Differentially Flat Control Systems. In IEEE Aerospace Conference (pp. 1-9).

[31] Luukkonen, T. (2011). Modelling and control of quadcopter. Independent research project in applied mathematics.Aalto University, Espoo, 22, 22.

[32] Das, L. C. S. Mathematical Modeling and Understanding Roll Motion of A Ship.

[33] Bykanova, A. Y., Storozhenko, V. A., Tolstonogov, A. Y. (2019, June). The compact remotely operated underwater vehicle with the variable restoring moment. In IOP Conference Series: Earth and Environmental Science (Vol. 272, No. 2, p. 022199). IOP Publishing.

[34] Sun, B., Zhu, D., Li, W. (2012, September). An integrated backstepping and sliding mode tracking control algorithm for unmanned underwater vehicles. In Proceedings of UKACC International Conference on Control (pp. 644-649).

[35] Jha, S., Raman, V., Sadigh, D., Seshia, S. A. (2018). Safe autonomy under perception uncertainty using chance-constrained temporal logic. Journal of Automated Reasoning, 60(1), 43-62.

[36] Khalil, H. K. (2014). Nonlinear control. Pearson Higher Ed.

[37] Drouot, A., Richard, E., Boutayeb, M. (2014). Hierarchical backstepping-based control of a Gun Launched MAV in crosswinds: Theory and experiment. Control Engineering Practice, 25, 16-25.

[38] Soylu, S., Buckham, B. J., Podhorodeski, R. P. (2008). A chattering-free sliding-mode controller for underwater vehicles with fault-tolerant infinity-norm thrust allocation. Ocean Engineering, 35(16), 1647-1659.

[39] Qiu, B., Wang, G., Fan, Y., Mu, D., Sun, X. (2019). Adaptive sliding mode trajectory tracking control for unmanned surface vehicle with modeling uncertainties and input saturation. Applied Sciences, 9(6), 1240.

[40] Lin, X., Jiang, H., Nie, J., Jiao, Y. (2018, August). Adaptive-sliding-mode trajectory tracking control for underactuated surface vessels based on NDO. In IEEE International Conference on Mechatronics and Automation (ICMA) (pp. 1043-1049).

[41] LIANG, K., Jiaoyan, A. I., Zengqiang, L. E. I., Gang, L. I. U. (2017, July). Sliding-mode trajectory tracking control of autonomous surface vessel. In International Conference on Electronic Industry and Automation (EIA 2017). Atlantis Press.

[42] Li, J. H., Lee, P. M., Jun, B. H. (2004). A neural network adaptive controller for autonomous diving control of an autonomous underwater vehicle. International Journal of Control, Automation, and Systems, 2(3), 374-383.

[43] Sun, B., Zhu, D., Ding, F., Yang, S. X. (2013). A novel tracking control approach for unmanned underwater vehicles based on bio-inspired neurodynamics. Journal of marine science and technology, 18(1), 63-74.

[44] Grossberg, S. (1988). Nonlinear neural networks: Principles, mechanisms, and architectures. Neural networks, 1(1), 17-61.

[45] A. L. Hodgkin and A. F. Huxley, A quantitative description of membrane current and its application to conduction and excitation in nerve, J. Physiol., vol. 117, no. 4, pp. 500-544, 1952.

[46] Tian, X., Demetriou, M. A., Gatsonis, N. A. (2020). Domain Decomposition for a Hybrid State Estimation of a Plume Field with a Moving Sensor. In AIAA Scitech 2020 Forum (p. 0394).

[47] Egorova, T., Gatsonis, N. A., Demetriou, M. A. (2016). Estimation of gaseous plume concentration with an unmanned aerial vehicle. Journal of guidance, control, and dynamics, 39(6), 1314-1324.

[48] Fischer, H. B., List, J. E., Koh, C. R., Imberger, J., Brooks, N. H. (1979). Mixing in inland and coastal waters. Academic press.

[49] Anderson, J. D., Wendt, J. (1995). Computational fluid dynamics (Vol. 206, p. 332). New York: McGraw-Hill.

[50] Socolofsky, S. A., Jirka, G. H. (2005). Special topics in mixing and transport processes in the environment. Engineering–Lectures. 5th Edition. Texas AM University, 1-93.

[51] Saqib, M., Hasnain, S., Mashat, D. S. (2017). Computational solutions of three-dimensional advection-diffusion equation using fourth order time efficient alternating direction implicit scheme. AIP Advances, 7(8), 085306.

[52] Tkalich, P. (2006). A CFD solution of oil spill problems. Environmental Modelling Software, 21(2), 271-282.

[53] Kumar, A., Jaiswal, D. K., Kumar, N. (2010). Analytical solutions to one-dimensional advection–diffusion equation with variable coefficients in semi-infinite media. Journal of Hydrology, 380(3-4), 330-337.

[54] Dehghan, M. (2004). Numerical solution of the three-dimensional advection–diffusion equation. Applied Mathematics and Computation, 150(1), 5-19.

[55] Guerrero-Aconcha, U. E. (2009). The Diffusion Coefficient of Liquid and Gaseous Solvents in Heavy Oil and Bitumen (Doctoral dissertation, UNIVERSITY OF CALGARY).

[56] Ahmed, N., Shah, N. A., Vieru, D. (2019). Two-dimensional advection–diffusion process with memory and concentrated source. Symmetry, 11(7), 879.

[57] Appadu, A. R. (2013). Numerical Solution of the 1D Advection-Diffusion Equation Using Standard and Nonstandard Finite Difference Schemes. Journal of Applied Mathematics, 2013, 1-14.

[58] Nagheeby, M., Kolahdoozan, M. (2010). Numerical modeling of two-phase fluid flow and oil slick transport in estuarine water. International Journal of Environmental Science Technology, 7(4), 771-784.

[59] Zadeh, E. S., Hejazi, K. (2012). Eulerian Oil Spills Model Using Finite-Volume Method with Moving Boundary and Wet-Dry Fronts. Modelling and Simulation in Engineering, 2012, 244-250.

[60] Zhang, Z., Schaefer, T., Kress, M. E. (2020, January). The Lattice Boltzmann Method for Ocean Oil Spill Propagation Modeling and Simulation—A Comparison Study of the Navier–Stokes Model and the Advection Diffusion Model. In 100th American Meteorological Society Annual Meeting.

[61] Zadeh, E. S., Hejazi, K. (2012). Eulerian oil spills model using finite-volume method with moving boundary and wet-dry fronts. Modelling and Simulation in Engineering, 2012.

[62] Bodin, J. (2015). From analytical solutions of solute transport equations to multidimensional time-domain random walk (TDRW) algorithms. Water Resources Research, 51(3), 1860-1871.

[63] Anderson, J. D., Wendt, J. (1995). Computational fluid dynamics (Vol. 206, p. 332). New York: McGraw-Hill.

[64] Seinfeld, J. H., Pandis, S. N. (2016). Atmospheric chemistry and physics: from air pollution to climate change. John Wiley & Sons.

[65] Massabó, M., Cianci, R., Paladino, O. (2011). An analytical solution of the advection dispersion equation in a bounded domain and its application to laboratory experiments. Journal of Applied Mathematics, 2011.

[66] Fedi, A., Massabò, M., Paladino, O., Cianci, R. (2010). A new analytical solution for the 2D advection-dispersion equation in semi-infinite and laterally bounded domain. Applied Mathematical Sciences, 4(75), 3733-3747.

[67] Sankaranarayanan, S., Shankar, N. J., Cheong, H. F. (1998). Three-dimensional finite difference model for transport of conservative pollutants. Ocean Engineering, 25(6), 425-442.

[68] Demetriou, M. A. (2010). Guidance of mobile actuator-plus-sensor networks for improved control and estimation of distributed parameter systems. IEEE Transactions on Automatic Control, 55(7), 1570-1584.

[69] Axelsson, O., Barker, V. A. (1984). Finite Element Solution of Boundary Value Problems: Theory and Computation (Vol. 35). SIAM.

[70] Hu, W., Demetriou, M. A. (2019, June). Domain decomposition methods for the state estimation of parabolic PDEs in 2D rectangular domains: well-posedness and convergence. In 2019 18th European Control Conference (ECC) (pp. 1920-1925).

[71] Calvo, M. P., De Frutos, J., Novo, J. (2001). Linearly implicit Runge–Kutta methods for advection–reaction–diffusion equations. Applied Numerical Mathematics, 37(4), 535-549.

[72] Zhu, L., Yuan, G. and Du, Q., 2010. An efficient explicit/implicit domain decomposition method for convection-diffusion equations. Numerical Methods for Partial Differential Equations: An International Journal, 26(4), pp.852-873.

[73] Demetriou, M.A., Gatsonis, N.A. and Court, J.R., 2013. Coupled controls-computational fluids approach for the estimation of the concentration from a moving gaseous source in a 2-D domain with a Lyapunov-guided sensing aerial vehicle. IEEE Transactions on Control Systems Technology, 22(3), pp.853-867.

[74] Sari, M., Gürarslan, G., Zeytinoğlu, A. (2010). High-order finite difference schemes for solving the advection-diffusion equation. Mathematical and Computational Applications, 15(3), 449-460.

[75] Chen, H., An, W., You, Y., Lei, F., Zhao, Y., Li, J. (2015). Numerical study of underwater fate of oil spilled from deepwater blowout. Ocean Engineering, 110, 227-243.

[76] Yapa, P. D., Li, Z. (1997). Simulation of oil spills from underwater accidents I: Model development. Journal of Hydraulic Research, 35(5), 673-688.

[77] Yang, Z., Yu, J., Li, Z., Chen, H., Jiang, M., Chen, X. (2018). Application of computational fluid dynamics simulation for submarine oil spill. Acta Oceanologica Sinica, 37(11), 104-115.

[78] Wang, S. D., Shen, Y. M., Guo, Y. K., Tang, J. (2008). Three-dimensional numerical simulation for transport of oil spills in seas. Ocean Engineering, 35(5-6), 503-510.

[79] Wang, S. D., Shen, Y. M., Zheng, Y. H. (2005). Two-dimensional numerical simulation for transport and fate of oil spills in seas. Ocean Engineering, 32(13), 1556-1571.

[80] Kanoğlu, M., Çengel, Y. A., Cimbala, J. M. (2020). Fundamentals and Applications of Renewable Energy. McGraw-Hill Education.

[81] Thomazella, R., Castanho, J. E. C., Franchin, M. N., Algarve, R. J., Dotto, F. R. L., Fiocchi, A. A., ... Nunes, M. (2015, September). System diagnostics and monitoring applied in flaws of the structure systems in HPSs by using image processing. In 2015 18th International Conference on Intelligent System Application to Power Systems (ISAP) (pp. 1-6).

[82] "Outland Technology: Products - ROV Model 1000." [Online]. Available: http://www.outlandtech.com/rov100.php. [Accessed: 26-Apr2012].

[83] Yang, C, "Modular Modelling and Control for Autonomous Vehicle (AUV)". Master Thesis of Engineering, 2007, Department of Mechanical Engineering National University of Singapore.

[84] Britannica, The Editors of Encyclopaedia. "naval architecture". Encyclopedia Britannica, 19 Apr. 2018, https://www.britannica.com/technology/naval-architecture. Accessed 29 June 2021.